

Durham E-Theses

The Modified Function of a Stem Cell Regulator in Monocots and Dicots

BROWN, CATHERINE,MARGARET

How to cite:

BROWN, CATHERINE,MARGARET (2023) *The Modified Function of a Stem Cell Regulator in Monocots and Dicots*, Durham theses, Durham University. Available at Durham E-Theses Online: <http://etheses.dur.ac.uk/15522/>

Use policy

The full-text may be used and/or reproduced, and given to third parties in any format or medium, without prior permission or charge, for personal research or study, educational, or not-for-profit purposes provided that:

- a full bibliographic reference is made to the original source
- a [link](#) is made to the metadata record in Durham E-Theses
- the full-text is not changed in any way

The full-text must not be sold in any format or medium without the formal permission of the copyright holders.

Please consult the [full Durham E-Theses policy](#) for further details.

The Modified Function of a Stem Cell Regulator in Monocots and Dicots

by

Catherine Margaret Brown

A Doctoral Thesis

Submitted to the Department of Biosciences

Durham University

In Fulfilment of the Requirements for a PhD in Plant Genetics

September 2023

Acknowledgements

This endeavour would not have been possible without Dr Peter Etchells, who has been a phenomenal supervisor throughout this process. I would like to thank him for his guidance, feedback and expertise, which have been vital throughout this project. I would also like to thank Professor Natalio Krasnogor, who generously provided knowledge I lacked.

I am deeply indebted to the BBSRC, and by extension the UKRI, for funding this research.

Many thanks go to my academic advisors, Dr Miguel de Lucas and Professor Ari Sadanandom, for providing valuable insights throughout this process. Special thanks also go to Dr Wenbin Wei and Dr Adrian Brennan for their guidance and assistance on this project.

I would like to mention my lab mates, who I thank for their advice and camaraderie throughout my degree. I am grateful to my friends for their moral support throughout this project, in particular Paul Reynolds, who provided endless encouragement. I would be remiss in not mentioning my family - without their belief in me, I may never have embarked upon this path.

Finally, I would also like to thank my fish, for bringing entertainment and levity during the final stretch of my degree.

Contents

- Introduction – page 8
 - Differences in Monocot and Dicot Development – page 8
 - Figure 1: An image from depicting some key differences between monocots and dicots – page 8
 - Secondary Growth and the Genetic Mechanisms of Vascular Development – page 11
 - Figure 2: An image depicting the orientation of cells and tissues within a woody stem – page 12
 - Figure 3: A cartoon depicting the vascular organisation of seedlings – page 13
 - Figure 4: A model showing *BIN2* interactions that control vascular development – page 16
 - Figure 5: Vascular bundle sections of *A. thaliana* – page 17
 - Similar Mechanisms of Development – page 18
 - Figure 6: A depiction of a feed forward loop – page 20
 - Monocot Development and Importance – page 22
 - Figure 7: Stem cross-sections illustrating the different cell types and arrangements between monocots and dicots – page 24
 - Figure 8: A depiction of barley development throughout the crop cycle – page 27
- Chapter 1: Establishing the Evolutionary Background – page 29
 - Identification of *PXY* and *CLE41* homologues – page 29
 - Figure 9: A dendrogram depicting the sequence similarities between *PXY* orthologues of various species – page 32
 - Figure 10: A dendrogram depicting the sequence similarities between *CLE41* orthologues of various species – page 35
 - *HvPXY* and *HvTDIF* Mimic the Function of their *A. thaliana* Homologues – page 37
 - Figure 11: Phenotypes of WT, *pxy*, *pxy AtPXY::HvPXY* and *35S::HvTDIF A. thaliana* seedlings – page 38

- Figure 12: Vascular bundle and hypocotyl sections of various *A. thaliana* genotypes – page 39
- Chapter 2: Do HvPXY and HvTDIF Regulate Vascular Development in *H. vulgare*? – page 43
 - Generation of Gene-Edited *H. vulgare* – page 43
 - Table 1: Guide RNA sequences for generating PXY alleles – page 45
 - Figure 13: A depiction of the locations of both *Hvpxy-1* and *Hvpxy-2* within the *HvPXY* gene – page 45
 - Vascular and Gross Morphological Traits in *pxy H. vulgare* – page 46
 - Figure 14: Radial sections of *H. vulgare* – page 47
 - Figure 15: A diagram depicting vascular bundle distribution in *H. vulgare* to demonstrate vascular bundle classifications used – page 48
 - Table 2: *H. vulgare* vascular trait ANOVA P-values, averages and standard deviations – page 49
 - Figure 16: Violin and box plots of vascular areas in wild type and *pxy* mutant *H. vulgare* – page 51
 - Figure 17: Violin and box plots of vascular cell numbers in wild type and *pxy* mutant *H. vulgare* – page 52
 - Table 3: *H. vulgare* gross morphological trait T-test results – page 53
 - Figure 18: Violin and box plots of the tiller width and height of wild type and *pxy* mutant *H. vulgare* – page 54
 - Figure 19: Violin and box plots of various gross morphological traits of wild type and *pxy* mutant *H. vulgare* – page 55
 - The Impacts of Drought Stress – page 58
 - Table 4: *H. vulgare* drought gross morphological trait ANOVA P-values – page 60
 - Table 5: *H. vulgare* drought gross morphological trait overview – page 60
 - Figure 20: Violin and box plots of the tiller width and length of wild type and *pxy* mutant *H. vulgare* in drought and non-drought conditions – page 61
 - Figure 21: Violin and box plots of the tiller and internode number of wild type and *pxy* mutant *H. vulgare* in drought and non-drought conditions – page 62

- What Are the Impacts of *HvPXY* Mutation? – page 65
- Chapter 3: Differences in Gene Expression – page 67
 - RNA Expression Analysis – page 67
 - Figure 22: Volcano plot showing the fold change in gene expression between *pxy* and WT samples – page 68
 - Figure 23: A figure showing the overall results of FPKM cluster analysis – page 69
 - Figure 24: A scatter plot depicting the 20 most significantly enriched GO categories – page 71
 - Figure 25: A scatter plot depicting the 20 most significantly enriched KEGG categories – page 72
 - Table 6: Enrichnet output for the additional dataset – page 76
- Chapter 4: Longitudinal Cell Divisions – page 79
 - Analysis of Longitudinal Sections – page 79
 - Figure 26: A depiction of the *H. vulgare* phytomer – page 79
 - Table 7: Average cell lengths and standard deviations of wild type and *pxy H. vulgare* node-adjacent and internode cells – page 80
 - Figure 27: Longitudinal sections of *H. vulgare* node tissue – page 81
 - Figure 28: Longitudinal sections of *H. vulgare* internode tissue – page 81
 - Figure 29: Violin and box plots depicting the cell lengths of wild type and *pxy* mutant plants – page 82
 - *In Situ* Hybridisation – page 84
 - Figure 30: *In situ* staining indicating expression of genes in *Zea mays* intercalary meristems – page 85
 - Figure 31: *In situ* hybridisation sections of 1-week old barley shoot apical meristems – page 87
- Discussion – page 88
 - Figure 32: A figure depicting ICM development – page 91
- Methods – page 99

- Creation of Dendrograms – page 99
- DNA Extraction – page 100
- Cloning of HvTDIF and HvPXY for Complementation Experiments in *A. thaliana* – page 101
 - Table 8: Primers used in this method – page 101
- Ampure Bead PCR Clean-Up – page 104
- Transformation of *E. coli* – page 105
- Transformation of *A. thaliana* – page 106
- Embedding and Sectioning in JB-4® – page 107
- *H. vulgare* Mutant Generation – page 109
- Barley Plant Growth – page 110
- Lithograph X – page 111
- Gross Morphological Measurements – page 112
- Water Restriction – page 113
- RNA Extraction – page 114
- RNA Sequencing and Analysis – page 116
- Enrichnet Analysis – page 118
- Embedding and Sectioning in Wax – page 119
- *In situ* Probe Synthesis – page 121
- *In situ* Hybridisation – page 124
- Appendices – page 126
 - Appendix A: PXY dendrogram with bootstrap values – page 126
 - Appendix B: CLE dendrogram with bootstrap values – page 127
 - Appendix C: Sequences and alignment of *HvPXY*, *Hvpxy-1* and *Hvpxy-2* – page 128
 - Appendix D: R code for dendrogram construction – page 135
 - Appendix E: enrichnet_stat.R – page 137
 - Appendix F: R code for using enrichnet with gene sets of interest – page 145
 - Appendix G: The genomic locations of identified *H. vulgare* genes, and the primers generated for them – page 146
 - Appendix H: An overview of the data production quality during RNA sequencing – page 147

- Appendix I: An overview of mapping status – page 148
- Appendix J: The percentage of reads from each sample which mapped to exonic, intergenic and intronic regions – page 150
- Appendix K: FPKM intervals for the reads of each sample, and example expression levels of specific genes – page 151
- Appendix L: A violin plot depicting the FPKM distribution of each sample – page 152
- Appendix M: Example differential gene analysis – page 153
- Appendix N: *In situ* images using sense and antisense probes – page 154
- References – page 155

Introduction

Differences in Monocot and Dicot Development

Within the angiosperms, there are two distinct clades – the monocots and the dicots. These clades are estimated to have diverged approximately 200 million years ago, and the differences between them are therefore distinct and numerous (Wolfe et al., 1989). In this thesis, I shall focus on the differences specific to vascular development and structure, however it is important that the breadth of the differences seen between these clades across multiple traits is first noted. This will provide context for the extent of the deviation between the two clades, and highlight that differences in development can be seen across their multiple organs and mechanisms (Figure 1).

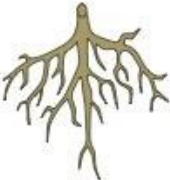
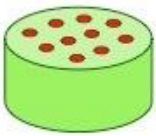
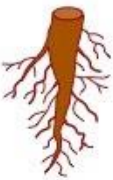
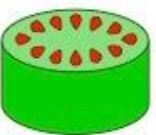
	Seed	Root	Vascular	Leaf	Flower
Monocot					
	One cotyledon	Fibrous roots	Scattered	Parallel veins	Multiples of 3
Dicot					
	Two cotyledon	Tap roots	Ringed	Net-like veins	4 or 5

Figure 1: An image from <https://old-ib.bioninja.com.au/higher-level/topic-9-plant-biology/untitled-3/monocots-versus-dicots.html>, depicting some key differences between monocots and dicots.

As the name implies, the number of cotyledons formed by a species is one of the key ways to separate between monocots and dicots. Cotyledons are one of the first organs to emerge during germination, and many mutants in cotyledon formation have been used to learn about the mechanisms behind embryogenesis. Gymnosperms, a sister group to the angiosperms, also have two cotyledons, though these lack the flowering traits of the monocot and dicot angiosperms (Chandler, 2008).

Whilst on the topic of flowering, another difference is the arrangement of the floral organs. Monocot flowers typically have three planes of bilateral symmetry, generating the floral organs in multiples of three, whereas dicots only have one such plane, leading to their floral organs comprising of multiples of four or five. A notable exception to the typical 3 planes of symmetry in monocots are the orchids, some species of which display secondary bilateral symmetry (Davenport & Kohanzadeh, 1982). There is also frequently little difference between the sepals and petals in monocots, in contrast to the dicots, leading to the terms inner and outer tepals to refer to the structures (Rudall & Bateman, 2004).

Differences also exist in the leaf architecture of monocots and dicots. Monocots form narrow, elongated leaves, with veins running parallel along the leaf. Dicots, however, tend to form rounder leaves, with reticulate vein organisation. This difference occurs despite certain similarities in their manner of leaf development, where both clades follow similar temporal and spatial changes – initially, cell division occurs throughout the length of the developing leaf, and gradually those cells at the tip stop dividing whilst those at the base continue. Eventually, all cells reach maturity, and the leaf reaches its finished shape and size, and so growth ceases (Nelissen et al., 2016).

There are also differences in root morphology. In dicots, the root system is comprised of a central primary or tap root accompanied by several lateral roots which branch outwards. In monocots, however, the roots are comprised of several different types, formed at different developmental stages. For example, in a *Zea mays* seedling, three types of roots can be shown to form - primary, seminal, and crown roots. There are also several differences in the individual root formation, for example that lateral roots form at xylem poles in dicots such as *Arabidopsis thaliana*, but at phloem poles in monocots such as *Oryza sativa* or *Z. mays*. Dicot roots are also much more regular, with one being able to predict which epidermal cells will form root hairs, and also being able to trace the cell fate of a root cell to an initial – neither of these can be done in monocots (Hochholdinger & Zimmerman, 2008).

Both the dicots and monocots produce shoot apical meristems (SAMs), however whilst the dicots form the SAM between two cotyledons, the monocots generate theirs laterally, at the base of a single cotyledon (Barton, 2010). The SAM in dicots such as *A. thaliana* produce all above-ground parts of the plant, and it is therefore a key component in apical growth regulation. In monocots however, the intercalary meristem (ICM) is predominantly responsible for apical growth, and is a unique feature of monocot development. The ICM is a key component in the growth and development of monocot phytomers, which consist of a node, internode, axillary bud and leaf. The ICM initialises the process of apical growth via cell divisions, until the internode is several millimetres long, after which cell elongation begins and leads to growth of the phytomer (Evans, 1968; S. Zhang et al., 2005).

Secondary Growth and the Genetic Mechanisms of Vascular Development

As has been made clear, both monocots and dicots undergo primary growth. However, differences lie in secondary growth, which describes the radial expansion of a plant during development and is often also associated with wood development (Groover & Robischon, 2006). In dicots, secondary growth occurs first through the development of primary vasculature and the tissue types therein – the xylem, responsible for water transport, the phloem, responsible for nutrient transport, and the vascular cambium, a key population of meristematic stem cells which exists as a layer between the xylem and phloem, giving rise to both (Figure 2). These tissues exist in isolated vascular bundles, which merge together through the developmental process to form unbroken concentric rings of tissue types (Figure 3). In monocots, due to the differences in vascular bundle arrangement, secondary growth is typically absent, though some exceptions to this will be described later in this thesis. It should be noted that differences in vascular bundle organisation can exist from the standard arrangement seen in dicots depending on a species' method of photosynthesis, such as the difference between C3 and C4 plants. C4 plants have evolved a particular vascular organisation known as Kranz anatomy in response to heat stress, in order to avoid photorespiration, which wastes some of the energy produced in photosynthesis. Kranz anatomy achieves this through alternative structural organisation to facilitate the localisation of the enzyme Rubisco and high concentrations of CO₂, via a wreath like organisation comprising an outer layer of mesophyll containing the components necessary for initial carboxylation, and inner layers near or within the vascular bundle containing the Rubisco and Calvin cycle components. The evolution of C4 anatomy has occurred over 45

times, with some variations between each instance, and whilst some versions developed in dicots, the majority of species displaying C4 organisation are monocots (Sage, 2003, 2016).

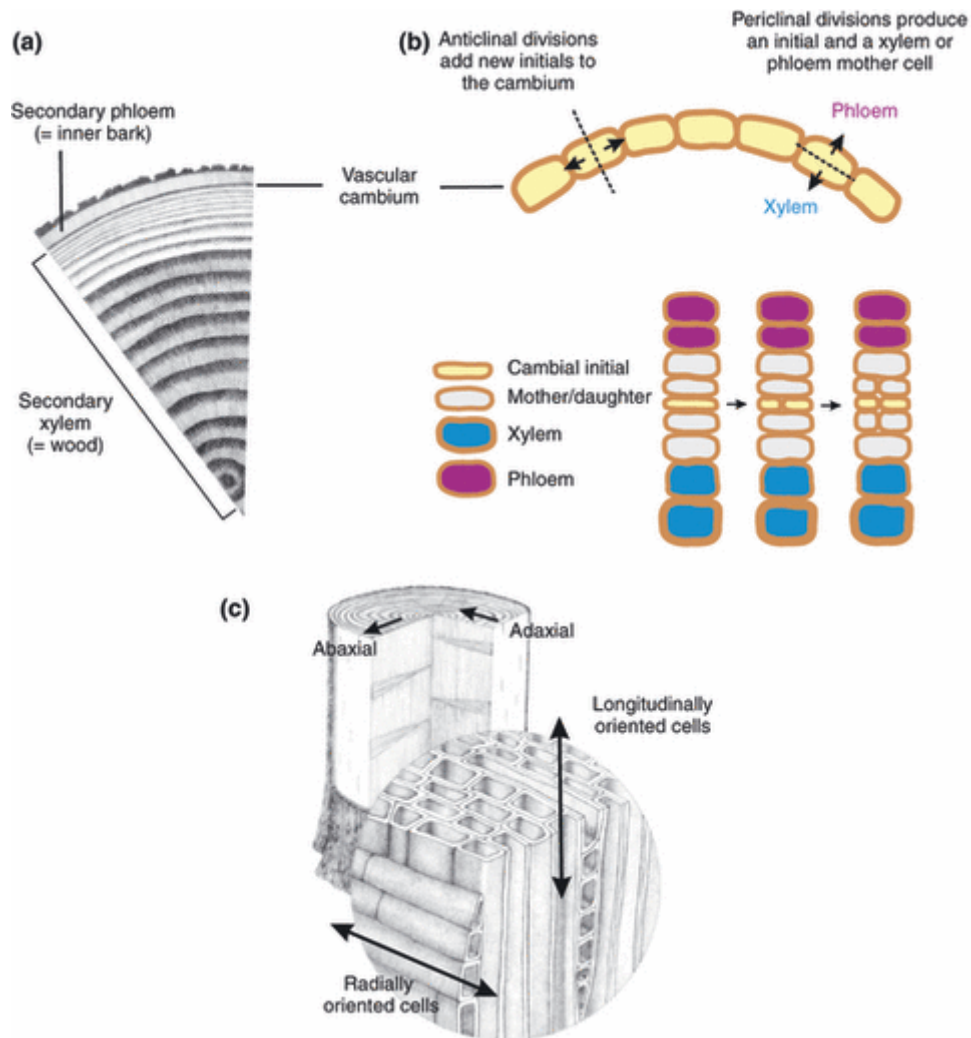


Figure 2: An image from Spicer & Groover, 2010 depicting the orientation of cells and tissues within a woody stem. (a) A depiction of the layout of xylem, phloem and cambium in a woody stem. (b) A depiction of how the vascular cambium divides to produce vascular tissues. (c) An image showing the resulting longitudinal and radial cell growth.

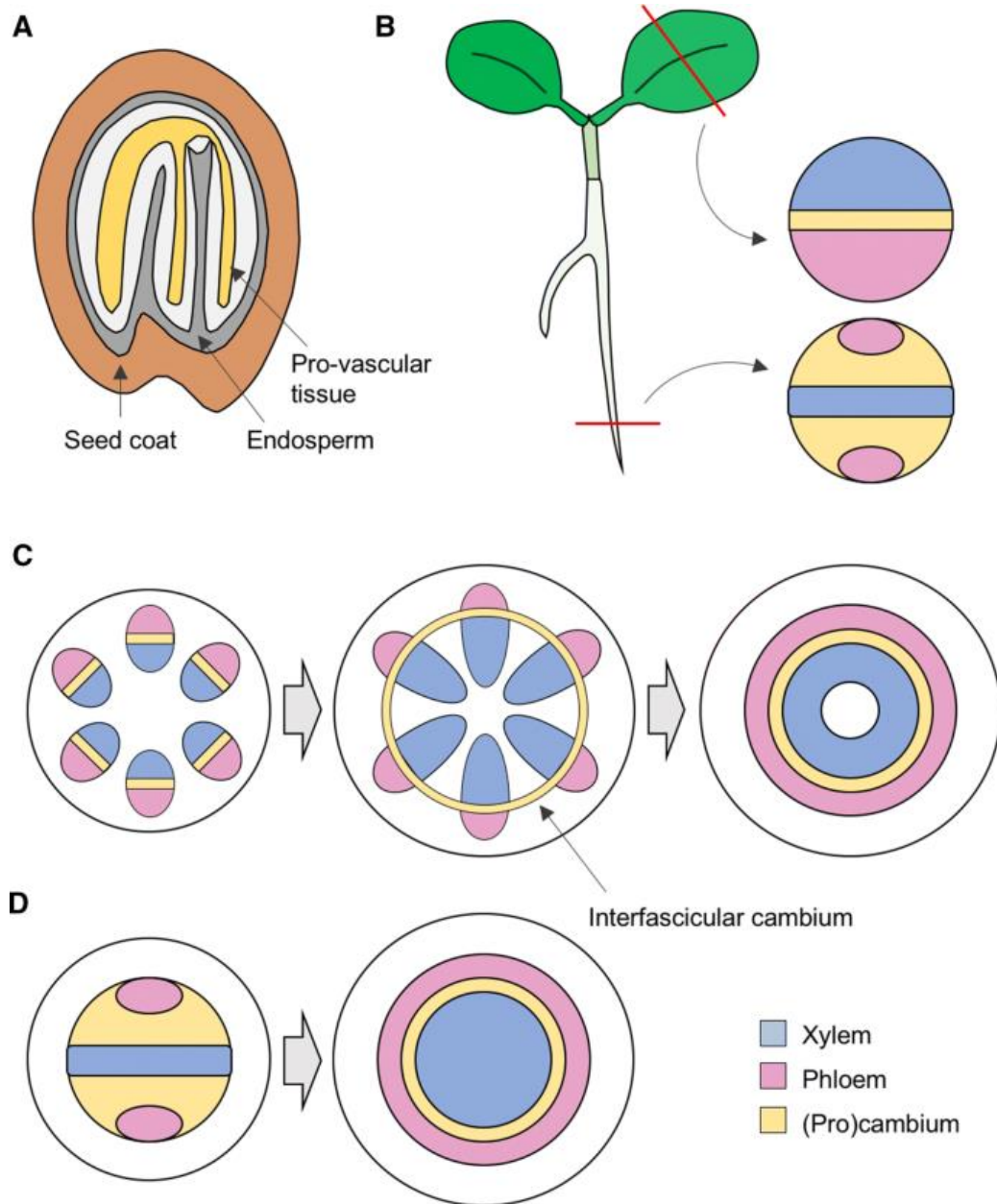


Figure 3: A cartoon depicting the vascular organisation of seedlings, sourced from Agustí & Blázquez, 2020. (a)

The appearance of the provascular tissue at the end of embryo development. (b) Localization of the procambial, phloem and xylem tissues within primary vasculature in veins and in the root of young seedlings. (c) Secondary growth in stems. In Arabidopsis (and other dicotyledonous plants), primary vasculature appears in bundles with the phloem facing outwards and the xylem inwards, separated by a layer of procambial cells. Secondary growth requires the sequential formation of a cambial ring between bundles and the stimulation of periclinal cell divisions. (d) Secondary growth in roots also involves expansion of xylem at the expense of the cambium.

Secondary growth is in part facilitated by considerable radial expansion of these vascular tissues, driven by cambial divisions and differentiation. For example, in the dicot species *A. thaliana* and *Populus tremula* x *P. tremuloides*, significant studies have been performed to understand the underlying mechanisms controlling secondary growth. These include the genetic components responsible for controlling both the cell divisions of the vascular cambium and the differentiation of the cells produced, and for regulating the balance between these two processes (Laxmi, 2016). Should these processes no longer be correctly maintained, defects in stem size and vascular organisation can be the result.

An important example of this is when defects arise in the gene *PHLOEM INTERCALATED WITH XYLEM (PXY)*, a leucine rich repeat receptor-like kinase expressed on the cell surface membrane of cambial cells. This receptor responds to the short dodecapeptide TDIF, or TRACHEARY ELEMENT DIFFERENTIATION INHIBITORY FACTOR, encoded by specific genes from the *CLE (CLAVATA3/EMBRYO SURROUNDING REGION)* family (Figure 4). One such gene, *CLE41*, is expressed in the phloem cells – this specific spatial expression of both *CLE41* and *PXY* is vital for the regulation of cambium cell activity, and therefore for vascular organisation as a whole. As the name suggests, *pxy* mutant plants show significant intercalation of the phloem and xylem tissues, showing significant loss of organisation, as well as reductions in vascular bundle size and cambium cell population size. Use of genetically modified lines containing the 35S promoter, a gene promoter originating from the Cauliflower Mosaic Virus, can provide insights into the roles of certain genes, including *CLE41* and *PXY*. The 35S promoter generates constitutive expression of genes within plants, and therefore creates lines which overexpress a gene of interest, allowing for the resulting line to be studied to determine differences to the wild type and inform future study into the

role of said gene (Amack & Antunes, 2020). For instance, *35S::CLE41* phenotypes can often instead show a near lack of differentiation at all, instead displaying a significant over-proliferation of cells, and the vascular bundles can often show significant ectopic expression of phloem cells within areas usually restricted to xylem cells (Figure 5). Additionally, mutations in *PXY* lead to decreases in hypocotyl diameter, whilst overexpression of *CLE41* produces increased radial thickening (Bagdassarian et al., 2022; Etchells et al., 2016; Etchells & Turner, 2010).

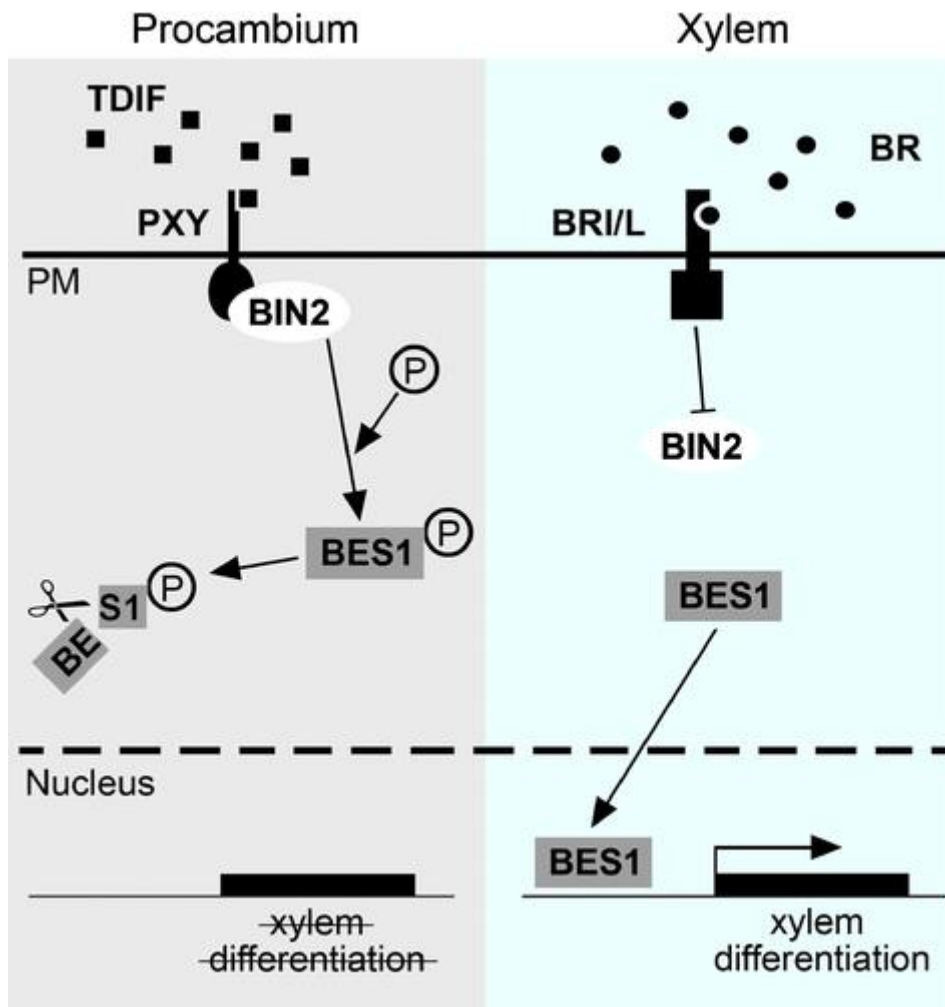


Figure 4: A model showing BRASSINOSTEROID INSENSITIVE 2 (BIN2) interactions that control vascular development, sourced from Etchells et al., 2016. In the procambium (left panel), TRACHEARY ELEMENT DIFFERENTIATION INHIBITORY FACTOR (TDIF) ligand binds to PHLOEM INTERCALATED WITH XYLEM (PXY) receptor resulting in an interaction between PXY and BIN2, which in turn results in phosphorylation and proteolysis of the transcription factor BRI1-EMS-SUPPRESSOR 1 (BES1). By contrast, in the xylem (right panel), brassinosteroid (BR) binding to BRASSINOSTEROID INSENSITIVE (BRI) receptors negatively regulates BIN2, preventing its phosphorylation. BES1 is therefore free to move to the nucleus and promote xylem differentiation. PM = plasma membrane.

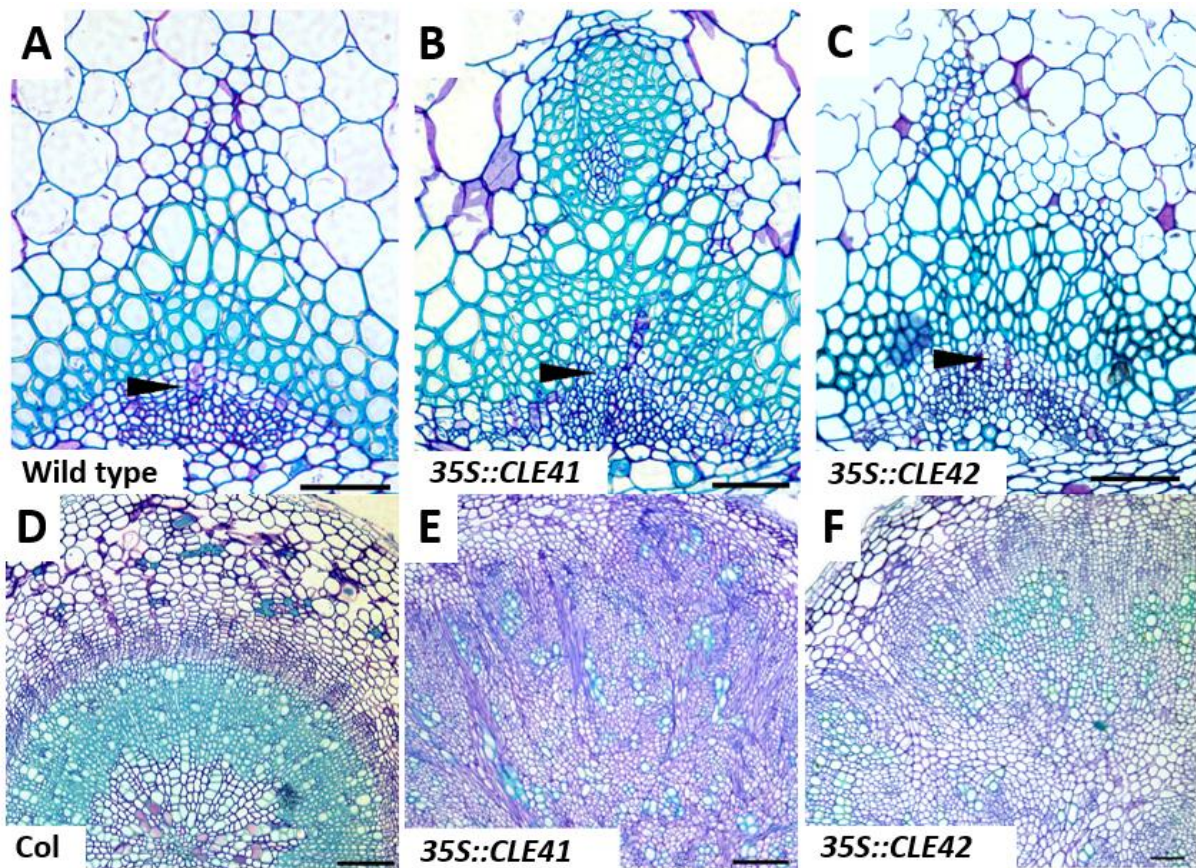


Figure 5: (A-C) Vascular bundle sections of *A. thaliana*. (D-F) Hypocotyl sections of *A. thaliana*. Images obtained from Etchells & Turner, 2010. Black arrows indicate cell divisions. Scale bars for A-C represent 50µm, bars for D-E represent 100µm, the bar for F represents 50µm.

The *PXY* signalling pathway, like many pathways found in living organisms, does not act in isolation, and is known to interact with key genes in the brassinosteroid signalling pathway. Brassinosteroids are one of several categories of plant hormone, known for their function in a wide range of processes which include regulating plant development, cell division, and cell elongation, as well as various stress response mechanics. These hormones are present throughout various plant organs, and play a role in vascular development (Manghwar et al., 2022). In the presence of TDIF, PXY binds to BRASSINOSTEROID INSENSITIVE 2 (BIN2), leading to the phosphorylation and eventual degradation of BRI1-EMS-SUPPRESSOR 1 (BES1). In TDIF's absence, this does not occur, and BRASSINOSTEROID INSENSITIVE (BRI)

receptors will instead bind to brassinosteroids, leading to the repression of BIN2, at which point BES1 remains unphosphorylated and enters the nucleus to bind to and promote genes leading to xylem differentiation (Etchells et al., 2016). Studies on key brassinosteroid signalling genes have shown that they have clear impacts on vascular development, for example BES1 and BZR1 are known to act redundantly to promote both xylem and phloem differentiation (Saito et al., 2018). Thus PXY excludes these differentiation-promoting factors from the cambium.

Having now covered vascular development in dicots, and the physical, genetic and hormonal components therein, this thesis now moves to cover other similar mechanisms of other developmental processes, and the mechanisms of vascular development seen in other species. This is important for gaining a full understanding of the background feeding into this work, as this will provide greater insight into that which is conserved within and between clades, and therefore provide some reasoning as to why this work was performed.

Similar Mechanisms of Development

The PXY signalling pathway is similar to other receptor-ligand pairs found in other meristematic tissues, for example the *CLAVATA1 (CLV1)* pathway in the shoot apical meristem, which regulates the cell divisions within the SAM and plays a vital role in floral organ development. This pathway features both a receptor-like kinase, *CLV1*, and a small signalling ligand encoded by the gene *CLAVATA3* (Hazak & Hardtke, 2016). *WUSCHEL* also plays a key part in this pathway, and is a homeodomain transcription factor also vital for SAM integrity (Jha et al., 2020). Another similar trio of genes are *CLE40*, which encodes a short signalling peptide, *ACT DOMAIN REPEAT 4 (ACR4)*, a receptor kinase, and *WUSCHEL*

RELATED HOMEODOMAIN TRANSCRIPTION FACTOR 5 (WOX5), a homeodomain transcription factor, all of which together were hypothesised to regulate the root apical meristem (RAM), though this is under some debate (Berckmans et al., 2020; Stahl et al., 2009). This arrangement of 3 genes playing pivotal roles in the regulation of stem cell populations is present in the vascular cambium of *A. thaliana*, with the receptor kinase in this case being *PXY*, the gene encoding a signalling factor being *CLE41*, and the homeodomain transcription factor being *WUSCHEL LIKE HOMEODOMAIN TRANSCRIPTION FACTOR 4 (WOX4)* (Qiang et al., 2013). *WUSCHEL* and *WOX* genes are known for their impacts on stem cell fate and regulation of stem cell initials, and inhibiting *WOX4* activity via RNAi is shown to reduce apical growth, vascular bundle size, and the differentiation of xylem and phloem cells. The function of *WOX4* is also conserved between *A. thaliana* and *Solanum lycopersicum* (Ji et al., 2010).

In addition to this, previous work indicates that *PXY* and *TDIF* interact to regulate a key set of genes involved in vascular bundle development – *TARGET OF MONOPTEROS 6 (TMO6)*, *WOX14*, and *LOB-DOMAIN CONTAINING PROTEIN 4 (LOB4)*. These three genes interact in *A. thaliana* to generate a feed-forward loop, a network motif where genes X and Y both positively regulate gene Z expression, and where gene X also positively regulates gene Y expression, as depicted in Figure 6 (Shen-Orr et al., 2002; Smit et al., 2020). Such motifs allow for a network to limit responses to small variations in input, but remain responsive to more persistent changes. *TMO6* and *WOX14* bind to and regulate the transcription factor *LBD4*, with *WOX14* also acting to regulate the expression of *TMO6* in turn. Mutant lines of *A. thaliana* showed a reduction in vascular cell proliferation and changes to vascular bundle shape when any one of these genes were knocked out, with the changes greater and more significant when multiple genes in the loop were knocked out, particularly where these

were one or both of *LBD4* or *TMO6*. *PXY* and *TDIF* were shown to regulate this loop, with *pxy/pxl1/pxl2* (*pxyf*) and *tdif* lines showing reduced expression of *TMO6* and *LBD4*, and thereby impact the regulation of cell divisions in vascular bundles. This again highlights the importance of *PXY* on the regulation of genes relating to vascular development in *A. thaliana*, and the ability for its role in this to interact and integrate with other systems within an organism performing similar functions.

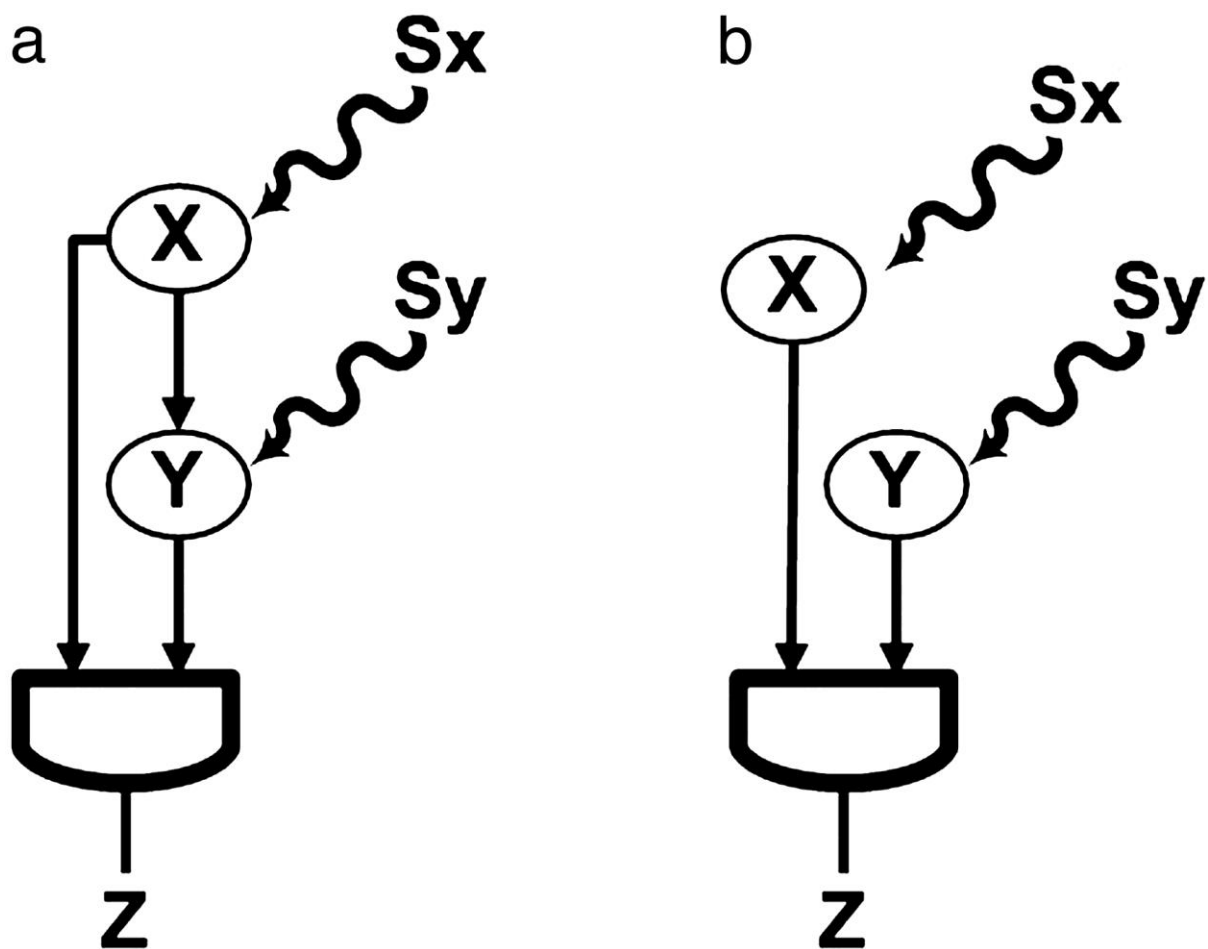


Figure 6: A depiction of a feed forward loop, from Mangan & Alon, 2003. (a) Transcription factor X regulates transcription factor Y, and both jointly regulate Z. S_x and S_y are the inducers of X and Y, respectively. The action of X and Y is integrated at the Z promoter with a cis-regulatory input function. (b) Simple regulation of Z by X and Y.

There are two *PXY* paralogues within *A. thaliana*, known as *PXY-LIKE 1* and *PXY-LIKE 2* (*PXL1* and *PXL2*). The *PXL1* and *PXL2* genes provide some redundancy with *PXY* with regards to vascular development, with mutations in all three leading to a more dramatic vascular bundle phenotype than mutation in *PXY* alone. Interestingly however, mutation in only *PXL1* or *PXL2* does not produce an obvious phenotype, indicating that whilst the genes do play a role in development, they are not as vital to maintenance of the vasculature as *PXY* itself, and thus are not sufficient or indeed necessary for vascular development (Mou et al., 2017; H. Zhang, Lin, Han, Wang, et al., 2016). *PXY*, *PXL1* and *PXL2* are also known to be required for pollen development, with *PXL1* in particular known to act alongside *SOMATIC EMBRYOGENESIS RECEPTOR-LIKE KINASEs* (*SERKs*) to bind with *CLE19* for this process, and *PXL2* known to also interact with *SERK2* in the presence of *CLE42* (Mou et al., 2017; Y. Yu et al., 2023).

Another *CLE* family gene, *CLE44*, can also encode the small signalling TDIF peptide, and *CLE42* encodes a dodecapeptide differing by only one amino acid, with the second amino acid in the chain being glycine instead of glutamic acid (Etchells & Turner, 2010). Mutations in all three of these *CLE* genes has been shown to inhibit xylem differentiation, and overexpression of both *CLE41* and *CLE44* displays similar levels of heightened cell division as is seen through exogenous application of the TDIF peptide (Qiang et al., 2013). Mutations in both *CLE42* and *CLE44* have been noted to produce a more bush-like gross morphology, with reduced apical dominance, and the *cle41 cle44* double mutant was shown to have a more severe vascular phenotype than either alone, showing that as there is redundancy amongst *PXY*, *PXL1* and *PXL2*, redundancy also exists between these three *CLE* genes (Hirakawa et al., 2010; Yamaguchi et al., 2017).

The importance of *CLE* and *PXY* homologues can even be seen in non-vascular plants. In *Marchantia polymorpha*, only two *CLE* genes exist, *MpCLE1* which produces a small peptide homologous with TDIF, and *MpCLE2* which is homologous with CLV3. The small signalling peptides encoded by these genes bind to the receptors *MpTDIF RECEPTOR (MpTDR)*, homologous with *PXY*, and *MpCLV*, homologous with *CLV1*, respectively. *MpTDR* and *MpCLE1* act in the *M. polymorpha* shoot apex to negatively regulate cell division, highlighting that whilst there is obviously no vascular regulation in this species, PXY-TDIF signalling is an ancient mechanism for the regulation of key stem cell populations within plants (Hirakawa et al., 2019; Takahashi et al., 2021). *CLAVATA* genes are also noted for their roles in the regulation of 3D growth transition, axis orientation, and cell proliferation in non-vascular plants such as *Physcomitrella patens*. For example, application of *P. patens* CLE peptides or *A. thaliana* CLV3 in *P. patens* gametophores is shown to lead to a reduction in overall size and leaf development, indicating a conserved role in cell proliferation for these genes in vascular and non-vascular species (C. D. Whitewoods et al., 2018).

Monocot Development and Importance

In monocots, the vascular structure is quite different to that of dicots, as can be seen in Figure 7 (Scarpella & Meijer, 2004). Monocot vascular bundles remain distinct and scattered throughout the tissue, whereas in dicots the tissue begins to form cohesive concentric rings at the hypocotyl. The xylem vessels are fewer and larger than in dicot counterparts, and exist at the inner poles of the vascular bundles. This is opposed to the phloem, which sit at the outer poles of the vascular bundles, and differ from dicots in that they contain two distinct sieve tube types, only one of which is associated with companion cells (Botha, 2005). There are also the parenchyma cells, which cluster near the xylem vessels and can

function as storage cells, as well as potentially aiding in stem growth by exerting pressure. The sclerenchyma, which clusters near the phloem poles, comes in two forms, those which provide further support to the stem through lignification, and those which conduct (Lopez & Barclay, 2017). The vascular bundles in monocots are also surrounded by a layer, or occasionally two layers, of bundle sheath cells. These cells do not perform a role in apical-basal transport, but instead act as a barrier between the vascular cells and the mesophyll which separates the vascular bundles, and can act as a buffer area for transport of both water and photosynthates between the vascular bundles and mesophyll (Leegood, 2008).

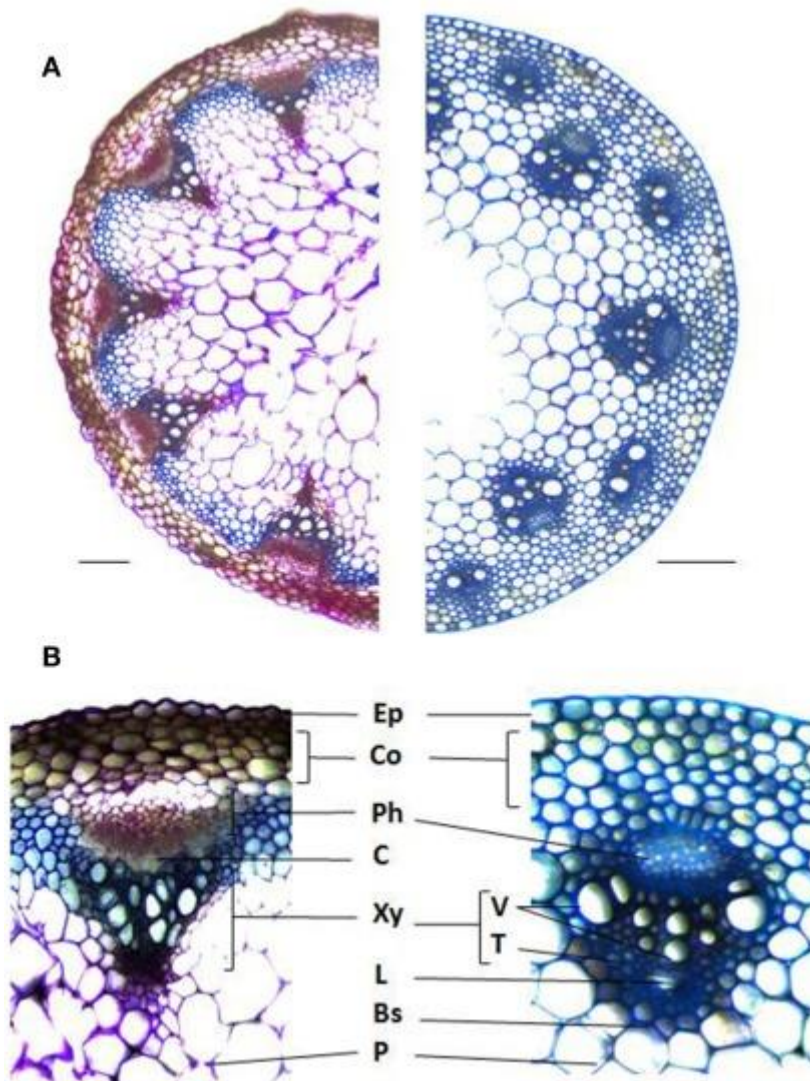


Figure 7: Stem cross sections illustrating the different cell types and arrangements between dicots and monocots, sourced from Handakumbura & Hazen, 2012. (a) *Arabidopsis thaliana* (left) and *Brachypodium distachyon* (right) stained with Toluidine blue. (b) Vascular bundle anatomy of *A. thaliana* (left) and *B. distachyon* (right). Ep, Epidermis; Co, Cortex; Ph, Phloem; C, Cambium; Xy, Xylem; V, Vessels; T, Tracheads; L, Lacuna; Bs, Bundle Sheath; P, Pith. Bars = 0.1 mm.

In all plants, the vascular tissues are initially derived from procambium cells. In dicots, the procambium gives rise to the vascular cambium, which leads to secondary growth.

Monocots, however, intriguingly lack a vascular cambium – a small number of woody monocots, such as those in the genera *Yucca*, *Aloe* and *Agave*, produce an unusual cambium

derived from the pericycle, which produces tissue on the inner side of the cambium tissue which differentiates into secondary vascular bundles and parenchyma and generates secondary growth, however this is a rare monocot trait (Barkley, 1924; Zinkgraf et al., 2017). Due to this, monocot species rarely undergo secondary growth, and the few which undergo significant radial thickening do so via the division and expansion of ground tissue parenchyma cells (Scarpella & Meijer, 2004). Due to the lack of a vascular cambium, the nature of how the xylem and phloem originate within the monocots remains elusive.

One monocot of particular interest is *Hordeum vulgare*. More commonly known as barley, this is a vital crop grown across the world, used for food for both humans and livestock, and also used in malting and beer production. In 2010, it was the 4th most grown cereal crop worldwide in terms of quantity produced and area of cultivation, highlighting its global importance (Zhou, 2010). This is in part due to its ability to adapt to environments where alternative cereals such as maize or rice would struggle, and in part due to the health benefits it provides. For example having some of the highest concentrations of beta-glucan of any cereal, which are known for their beneficial impact in obesity (El Khoury et al., 2012; Sullivan et al., 2013). For the UK specifically, barley production has increased over recent years – yield has increased from 5.7 tonnes per hectare in 2018 to 6.9 tonnes per hectare in 2019 (a 21.1% increase), and production has increased from 6510 thousand tonnes in 2018 to 8048 thousand tonnes in 2019 (a 23.6% increase) (DEFRA, 2019). These increases in yield were thought to be in part due to the increased growth of more promising varieties, such as the winter barley variety Funky, noted as one of the best conventional 6-row varieties by Scotland's Rural College in 2019 (Cunningham, 2019; Hoad, 2019). In addition to its importance as a crop, barley is also an excellent target for genetic studies of monocots, due

to its diploid nature increasing ease of research in comparison to more genetically complex alternatives such as the hexaploid *Triticum aestivum*. It is also amenable to transformation, allowing for a range of genome editing-based experimentation which is not possible with some other monocots (Bartlett et al., 2008). It also has a fully sequenced and annotated genome, which is vital for developing an in depth understanding of the varied genetic pathways and processes within an organism (Beier et al., 2017).

H. vulgare development occurs in 3 major stages (Figure 8). The first, the vegetative stage, runs from sowing to floral initiation, and is predominantly involving leaf development. The second, the reproductive phase, runs from then until the beginning of grain filling, and includes spikelet and tiller development. The third and final phase is the grain filling phase, and runs until harvest. As with most species, the exact timings for each stage will differ depending on both genetic and environmental factors. *H. vulgare* cultivars are 2-row or 6-row, with the variety Golden Promise being 2-row. Golden Promise is a semi-dwarf variety of spring barley, and was predominantly grown in the 1970s and 1980s as a grain for malting and whisky production. It is often now used in research due to the ease with which it can be genetically transformed, including via CRISPR-Cas9 techniques, and is therefore the variety used in the work outlined in this thesis (Schreiber et al., 2020).

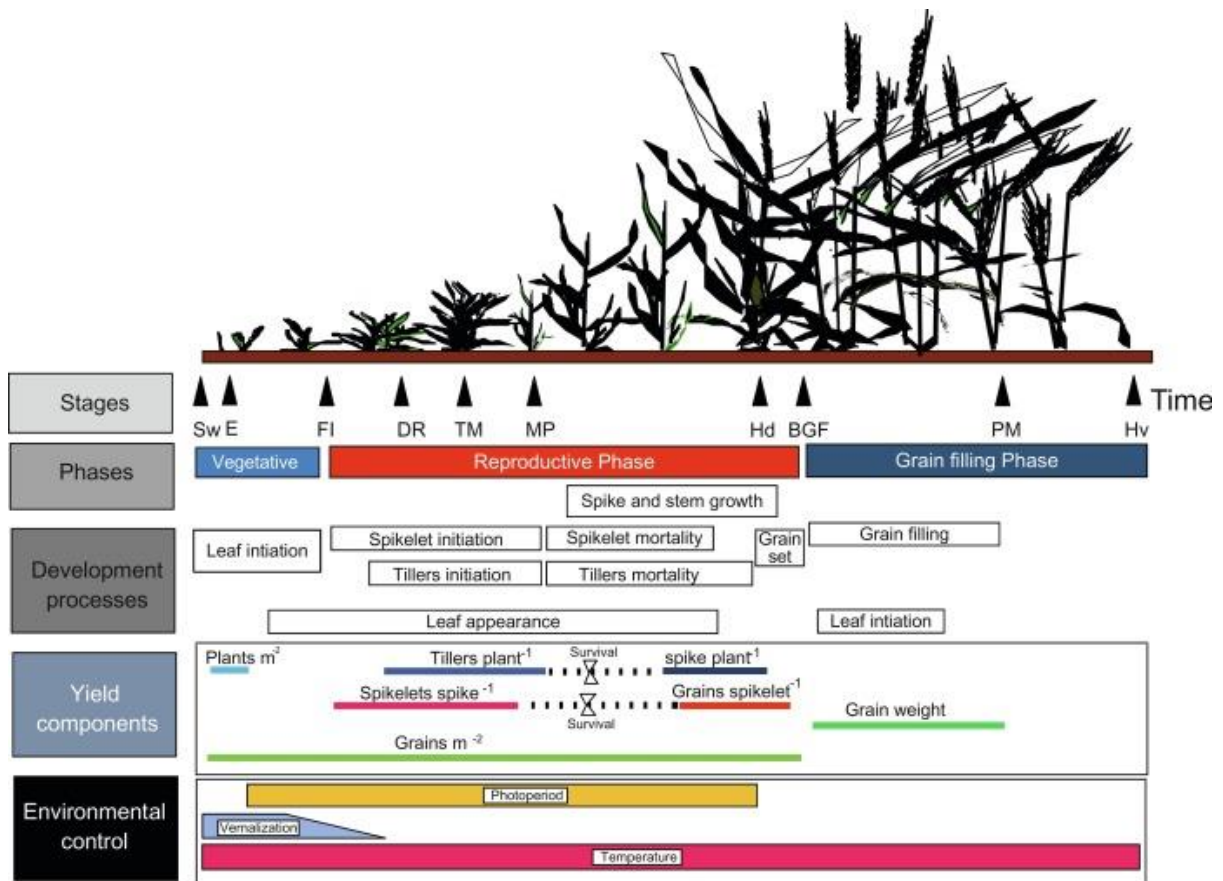


Figure 8: A depiction of barley development throughout the crop cycle, sourced from Miralles et al., 2021, p. 4.

Sowing (Sw), seedling emergence (E), floral initiation or ‘collar’ stage (FI), double ridge (DR), triple mound (TM), maximum number of total primordia initiated in the apex (MP), heading (Hd), beginning of grain-filling period (BGF), physiological maturity (PM), and harvest (Hv). Boxes indicate different phases, developmental processes, and yield components formation. Environmental factors that control the length of different phases are also indicated.

Every year, cereal crop yield is lost due to lodging – a process where the crop bends at the base of the stem or at the root, near the soil surface, causing reduced yield via both the lodged crop producing less and lower quality yield, but also due to an increase in the difficulty and cost of harvesting (Q. Li et al., 2022; Shah et al., 2019). Lodging can be caused by one or both of two key factors - by insufficient strength in the stem for the crop to stand upright, and by external conditions such as intense weather, poor soil quality, or field

topography. With increases in extreme weather predicted due to global warming, this will likely lead to an increase in crop lodging, and therefore a decrease in yield, and this combined with the increasing global population could contribute to food shortages in future (Coumou & Rahmstorf, 2012; Tilman et al., 2011).

With this in mind, it follows that methods for improving crop lodging tolerance should be investigated, and a good place to start is by looking at stem structure and vascular development. *PXY* has already proven a promising candidate for genetic manipulation in other areas, for example in *Populus tremula* x *P. tremuloides*. It has been shown that manipulation of the *PXY* pathway can generate increases in radial growth, which could lead to the generation and usage of genetically modified tree species with increased wood production (Etchells et al., 2015). Whilst monocots such as *H. vulgare* do not experience secondary growth like a dicot, as *PXY* is such a key genetic component to dicot vascular development, it seems an excellent starting point for investigation to begin to deepen our understanding of monocot vascular development on a genetic level.

The project outlined in this thesis therefore aimed to investigate the role of a homologue of *A. thaliana PXY* in *H. vulgare*, with the hypothesis that *HvPXY* plays a role in the regulation of *H. vulgare* vascular development. Given the lack of a cambium or procambium in monocots, the project also aimed to discover the location of expression of this gene. These goals were approached through a range of gross morphological, vascular and genetic investigations, including comparisons of gross morphological and vascular traits, RNAseq analysis, and *in situ* hybridisation. As is described later, this project shows that *H. vulgare* contains a homologue of *AtPXY*, that this gene likely plays a role in longitudinal cell divisions rather than radial, and that it is expressed in the intercalary meristem.

Chapter 1: Establishing the Evolutionary Background

Identification of *PXY* and *CLE41* homologues

To begin to address the question of whether the function of *PXY* and *CLE41* remains consistent between *A. thaliana* and *H. vulgare*, homologues needed to first be identified. To ensure that the correct sequences had been identified for *PXY* and *CLE41* in *H. vulgare*, it was determined that a broad-scale approach would provide beneficial context. By determining that the sequences found were both similar to the corresponding *A. thaliana* sequence, and also to others of similar evolutionary origins (i.e. monocots), greater confidence could be had that the correct sequences had been identified. The approach would also provide some additional insight into the evolution of the genes, and where key differences in function may arise, if any.

Protein IDs and sequences for AtPXY and HvPXY were found on Uniprot, and the IDs were subsequently entered into the PANTHER database to obtain the IDs for homologues from a range of species. Homologues were also identified via the TAIR entries for both proteins, and through use of the BLAST function of the Phytozome website. Several species were included for specific purposes, such as *Nicotiana tabacum* and *Populus trichocarpa*, which show similarities in both secondary growth patterning and regulation to *A. thaliana*, indicating some conserved mechanisms may exist between these species and therefore providing an interesting comparison (Groover & Robischon, 2006; Liu et al., 2016; Xu et al., 2023). In contrast, species such as *Selaginella moellendorffii* and *Physcomitrella patens* were included as representative early vascular and non-vascular species respectively. These two species often act as model organisms for comparative genomics, plant evolution, physiology, and development (Ferrari et al., 2020; Rensing et al., 2020). *Marchantia polymorpha* was also

included, due to the aforementioned literature discussing the role and function of MpTDR and MpCLE1. Additionally, species such as *Zea mays*, *Triticum aestivum* and *Oryza sativa* were included as comparable crop monocots to *H. vulgare* (Haberer et al., 2016). Sequences for each of the IDs were again obtained from Uniprot or Phytozome, and all the sequences identified were then aligned using the T-Coffee multiple sequence aligner, alongside one additional sequence in each set for a similar gene to root an eventual dendrogram to. Where multiple potential homologues were found in a species, further investigation of known function was performed to attempt to guard against the inclusion of paralogues or genes otherwise not of interest for this comparison. Some species continued to contain multiple potential homologues even after this screening, thus all were included for completeness. For the PXY alignment, the *H. vulgare* ERECTA sequence was chosen, as it is also a leucine rich repeat receptor-like kinase and so serves as a similar sequence for comparison, whilst containing a distinct enough sequence and function to act as a baseline without risk of being too similar to the sequences to be aligned. For the CLE41 alignment the *A. thaliana* CLAVATA3 sequence was used, a small peptide ligand similar in role to CLE41, but in a different developmental pathway, thus similar logic applies here to the reasons for using ERECTA.

Multiple sequence alignment is a method of aligning three or more sequences for the purposes of comparison – in this case, to determine the sequence similarity between the homologues of specific genes between different species, and potentially also deduce evolutionary relationships between them. Several alignment methods were tested, and the alignment method which provided the most useful result for each protein set was determined – M-Coffee for the PXY sequences, and Expresso for the CLE41 sequences. M-Coffee is a T-Coffee aligning tool which combines the outputs of multiple popular aligners to

obtain more rounded results, rather than using the T-Coffee default alone, thus it likely provided more robust information. Espresso is another T-Coffee tool which instead aligns protein sequences using structural information, something which is beneficial for a short peptide like TDIF where much of the encoding genetic sequence is not directly related to the eventual protein structure, and as such it provides rationale for Espresso providing the clearest results for those sequences. Following this, dendrograms were created from these alignments using R studio, using the packages phangorn, treeio, ggplot2 and ggtree. These packages were selected to create the desired appearance for the dendrogram, and to test multiple maximum likelihood models to obtain the best fit for the alignment data (Schliep, 2011; L.-G. Wang et al., 2020; Wilkinson, 2011; G. Yu et al., 2016). Versions of the dendrograms created with bootstrap values visible can be found in Appendices A and B.

For PXY alignments, sequences from the dicots and monocots separated into distinct and expected clades, as well as non-vascular plants remaining separate (Figure 9), with none of the resulting sequence placements yielding any unexpected results. AtPXY showed the greatest similarity to sequences from *Brassica napus* and *Populus trichocarpa*, whilst HvPXY was most similar to *Triticum aestivum* sequences. Sequences for PXL1 and PXL2 had also been included for comparison purposes, and it is interesting to note that the PXY homologues within many of the non-vascular plants represented show greater similarity to these genes than to PXY itself, for example *Marchantia polymorpha*'s MpTDR. This may indicate that PXL1 and PXL2 retain functions or sequence structures that are more similar to an ancestral version of PXY, and that these proteins therefore perform functions which are less specific to the needs of angiosperm development than PXY.

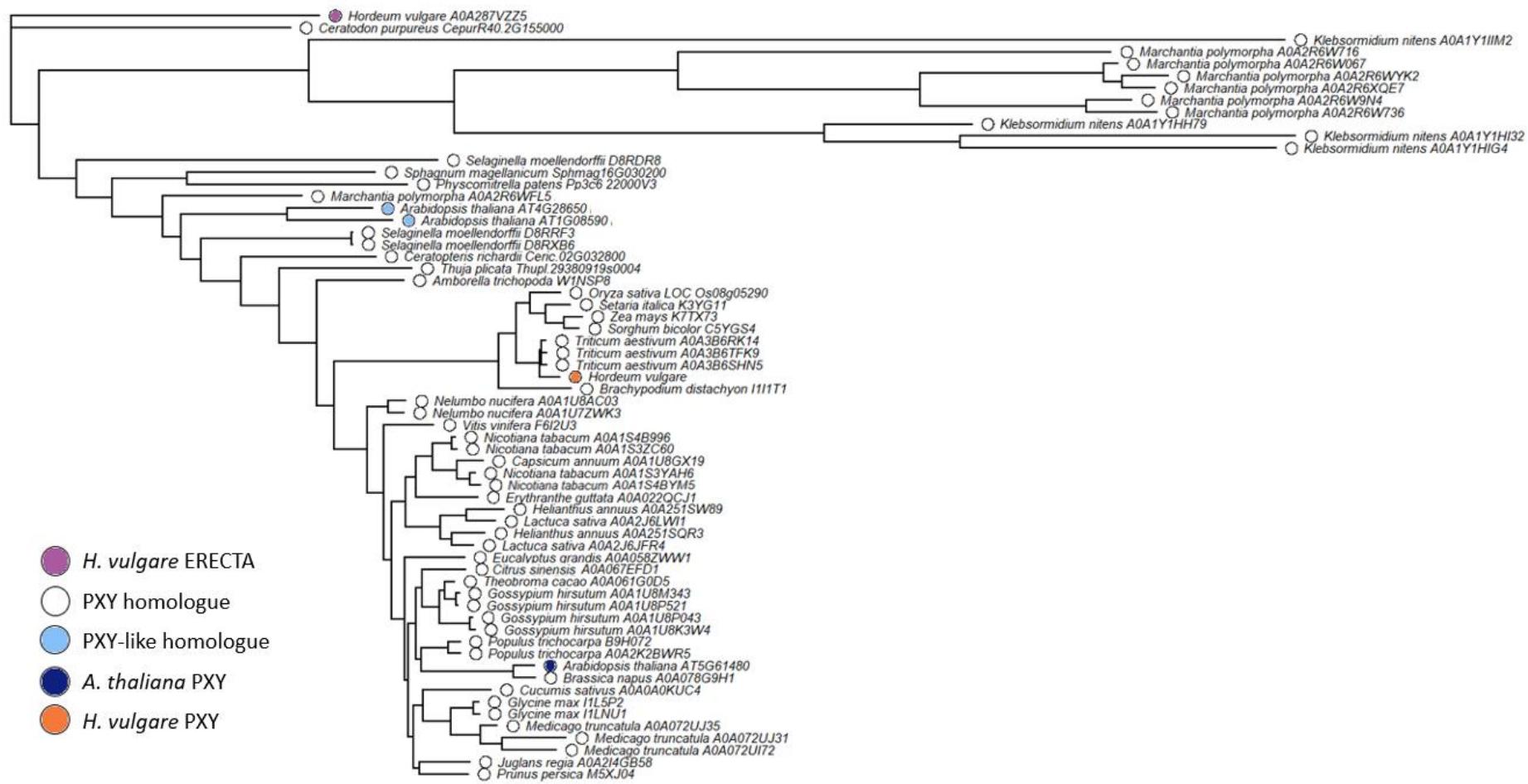


Figure 9: A dendrogram depicting the sequence similarities between PXY homologues of various species. Codes next to species names are the Uniprot IDs for each sequence, or the name of the gene encoding the protein.

For certain sequences, such as the PXY sequences from the algal *Klebsormidium nitens*, there may be questions around the accuracy of the comparisons made between these sequences and those from *A. thaliana* and *H. vulgare*. All of the *K. nitens* sequences on UniProt (bar A0A1Y1HH79) have AlphaFold predictions available for their structures, which show similar structures to that of the *A. thaliana* PXY protein. However, the accuracy of some of these models is lower than desired in some areas, so whilst they remain likely orthologues, comparisons to some non-flowering plants should be treated with some caution.

When CLE sequences were analysed (Figure 10), the separation of clades was not as visibly clear, however the bootstrap values for many of these branches fell below 50 (Appendix B), therefore this dendrogram provides less reliable information. This is to be expected in some ways – due to the short sequence of CLE41, small changes in sequence will have a far larger impact on resulting alignments, and therefore comparisons of these short sequences will naturally result in a more confused result. Additionally, it was somewhat difficult to obtain sequences for non-angiosperms which were identified as CLE homologues via both PANTHER and Phytozome, as CLE peptides are shorter than typical proteins in length and consequently are sometimes not annotated. This resulted in fewer sequences which could be included in the alignment, which perhaps contributed to a less robust result than the PXY dendrogram. The lack of CLE41 homologues in non-angiosperm species which could be identified may also indicate that its emergence was in some ways linked to the development of vascular structures, and may not have been present in these earlier lineages. Alternatively, it may be that other proteins filled the niche of CLE41 in these species, for example proteins more similar to CLV3, which as mentioned previously performs a similar function in angiosperms

to CLE41 as a small signalling peptide involved in stem cell fate regulation in the shoot apical meristem.

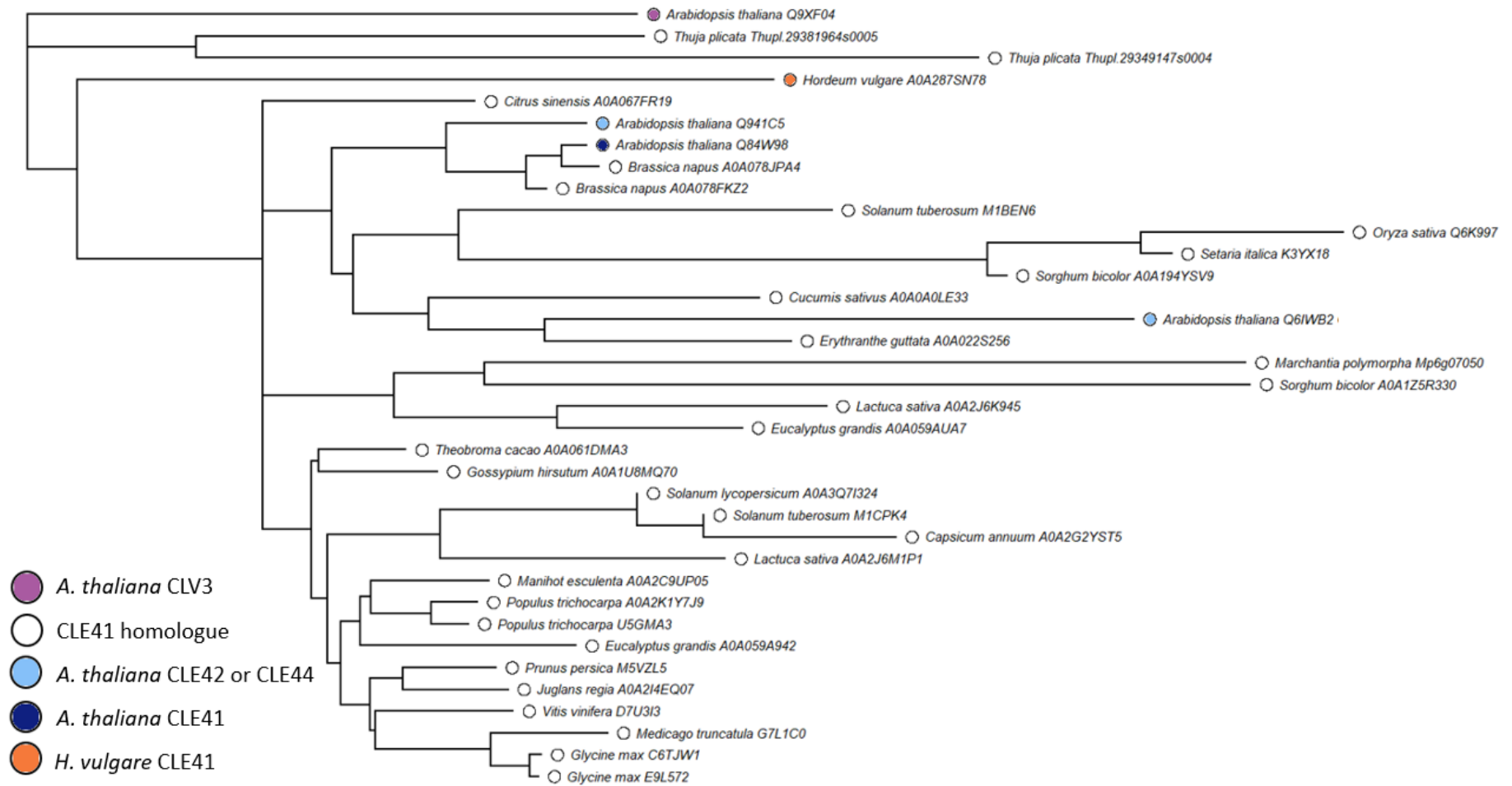


Figure 10: A dendrogram depicting the sequence similarities between CLE41 homologues of various species. Codes next to species names are the Uniprot IDs for each sequence, or the name of the gene encoding the protein.

Another interesting note is that certain CLE homologues showed greater similarity to AtCLE42 than AtCLE41, such as *Cucumis sativus* and *Erythranthe guttata*. It is known that AtCLE42 is expressed in the shoot apical meristem of *A. thaliana* rather than in the phloem (Mou et al., 2017; Yaginuma et al., 2011), though it does still have a role in the regulation of cell division like AtCLE41, so whilst a difference in function is possible for these homologues, they may retain enough similarities to AtCLE41 to perform this protein's functions. It is also worth reiterating that due to the short peptides being compared, and the low bootstrap values resulting from this alignment, this may not have as much weight as could otherwise be expected.

HvPXY and HvTDIF Mimic the Function of their *A. thaliana* Homologues

Once homologues of both AtPXY and AtCLE41 had been confidently identified, the next step was determining if those *H. vulgare* homologues perform a similar function to their *A. thaliana* counterparts. This initial analysis was performed in *A. thaliana* for multiple reasons – the rapid growth of the species enabling a swift experimental process, and the far more well characterised nature of its vascular development. As the processes underpinning vascular development are so well known, and the phenotypes of various mutants relating to vascular development shown in multiple studies, analysing the role of the *H. vulgare* homologues within this species provided the best opportunity for clear comparison between wild type plants, *A. thaliana* vascular gene mutants, and the constructs containing *H. vulgare* genes outlined below.

Constructs for *AtPXYpro::HvPXY* and *35S::HvTDIF* were created for this analysis in order to determine two different functions – whether *HvPXY* could allow an *A. thaliana pxy* mutant to recover and present more like the wild type, and whether an overexpression of *HvTDIF* mimics the phenotype seen in *AtCLE41* overexpressors. For the first, the *AtPXY* promoter was used to ensure localisation and promotion of expression of the *HvPXY* gene was akin to it, to better assess whether *HvPXY* would be able to recover the *pxy* phenotype. For the second, the 35S promoter was used, which drives constitutive gene expression (Amack & Antunes, 2020). This was used as localisation of a mobile ligand was not deemed as important in comparison to ensuring higher expression levels of the HvTDIF peptide. Wild type *A. thaliana* plants were transformed with the *35S::HvTDIF* construct using an *Agrobacterium tumefaciens*-based method, whilst *pxy A. thaliana* was transformed with the *AtPXYpro::HvPXY* construct. At approximately 6 weeks old, hypocotyls and stems from these

plants, alongside untransformed wild type and *pxy* mutant *A. thaliana*, were fixed with formaldehyde alcohol acetic acid (FAA), embedded in JB-4[®] resin, sectioned via microtome, and stained with toluidine blue prior to imaging with QCapture software. 6 weeks was chosen as it ensured that the plants would have reached a developmental stage where vascular structures of interest were developed, and were of large enough size for ease of dissection. Hypocotyl tissues were examined to view impacts on the concentric rings of vascular tissue typical of this tissue type. Stem tissues were taken from the main stem, avoiding branches or areas where branching occurred to seek greater consistency in comparison between samples, in order to examine impacts on vascular bundles. Of the lines generated, 3 per genotype were selected for this analysis.

In initial visual analysis the gross morphology of the transformants indicated that the homologues may perform similar functions. The *pxy AtPXYpro::HvPXY* individuals (Figure 11B) were visually indistinguishable from the wild type (Figure 11A), which would not be seen if the *HvPXY* gene did not perform a similar function to *AtPXY* to compensate for these individuals' mutations. The *35S::HvTDIF* (Figure 11C), on the other hand, showed a phenotype akin to that of *35S::AtCLE41*, being shorter than the wild type and more prone to branching in later development. The leaf-shape also appeared to be more rounded in these transformants, which was observed from an early stage.



Figure 11: 15 day old *A. thaliana* seedlings. (A) Wild type. (B) *pxy AtPXYpro::HvPXY*. (C) *35S::HvTDIF*.

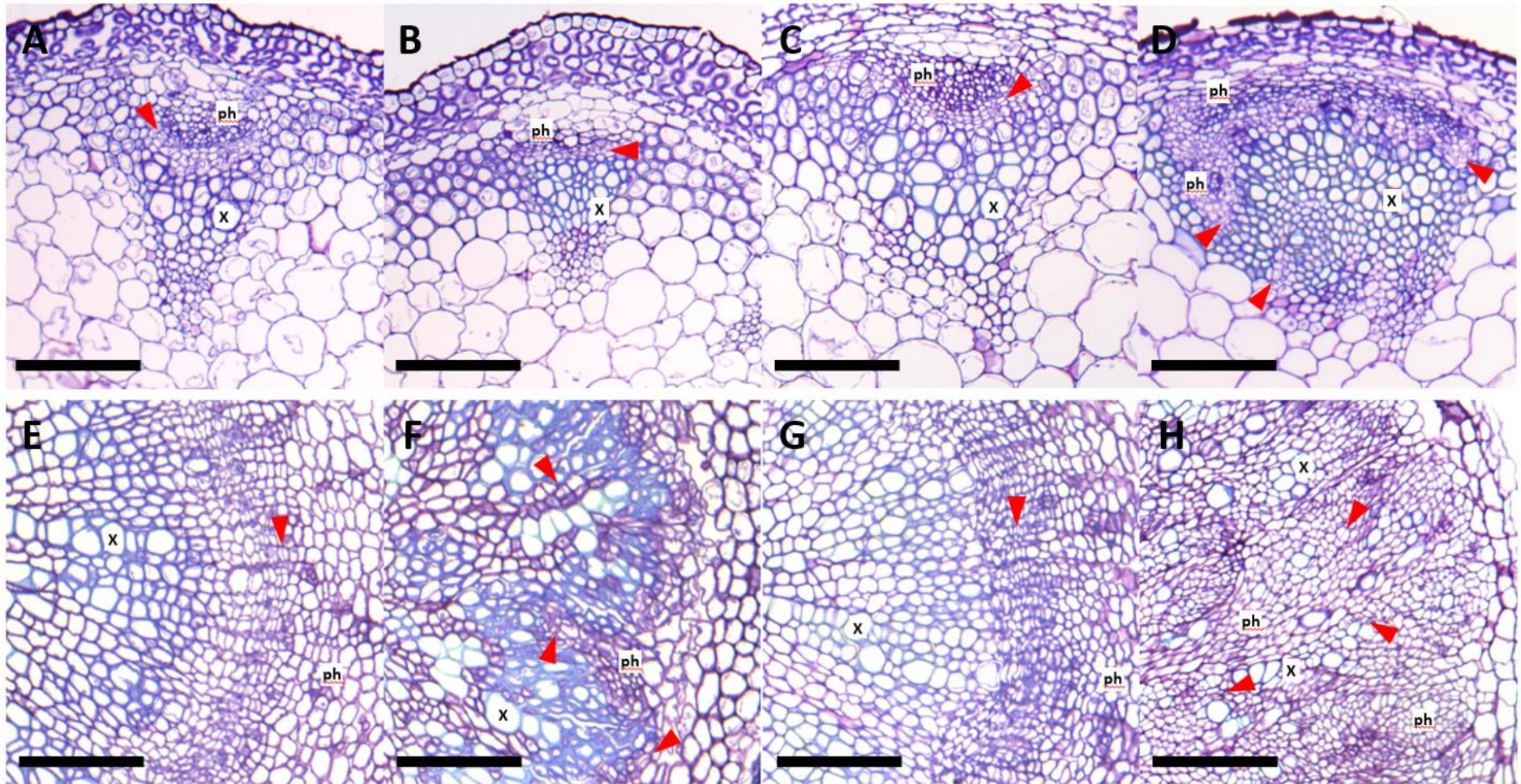


Figure 12: (A-D) Vascular bundle sections of *A. thaliana* seedlings. (A) Wild type. (B) *pxy*. (C) *pxy AtPXYpro::HvPXY*. (D) *35S::HvTDIF*. (E-H) Hypocotyl sections of *A. thaliana* seedlings. (E) Wild type. (F) *pxy*. (G) *pxy AtPXYpro::HvPXY*. (H) *35S::HvTDIF*. X = xylem, ph = phloem, red arrows indicate cell divisions (and therefore the area of vascular cambium), scale bars represent 100μm.

Upon investigating the vasculature of these transformants in thin sections, it was found that the *pxy AtPXYpro::HvPXY* vascular bundles were able to develop an organised vascular structure comparable to the wild type, with a clear cambium layer separating the phloem and xylem, and no intercalation of tissues (Figure 12 A-C). The phloem also formed a distinct, rounded mass of cells, which was similar to wild type controls, as opposed to the flattened phloem phenotype caused by fewer layers of phloem cells along the radial axis, displayed by *pxy* mutants. In the hypocotyl sections, distinct areas of xylem, phloem and cambium were again seen, mimicking the phenotype of the wild type and again lacking the intercalation of the *pxy* mutant (Figure 12 E-G). This, alongside the gross morphology, indicates that the *HvPXY* gene can perform a similar function to its *A. thaliana* counterpart within *A. thaliana* tissue, as it is able to recover the *pxy* phenotype to that more akin to the wild type.

The *35S::HvTDIF* vascular bundles, on the other hand, showed clear disruption to the vascular organisation (Figure 12D). The bundles were often found to be much wider than that of the wild type, with a flattened appearance to the phloem cell distribution, and patches of ectopic phloem in areas where xylem is typically expected. Divisions could also be seen in various locations within bundles, as opposed to being restricted to typical cambial divisions. The phenotype was more dramatic in the hypocotyl (Figure 12H), where no trace of vascular organisation remained, and development of phloem and xylem appeared throughout the tissue. Further unusual division placements could also be seen here. These phenotypes are incredibly similar to that seen in *35S::AtCLE41*, albeit are somewhat more severe than phenotypes observed for *35S::AtCLE42* (Figure 5; Etchells & Turner, 2010). This genotype does display vascular disorganisation within the hypocotyl, but it did not show the same level of disruption in the vascular bundles. This could be for a number of reasons –

potentially there could be a difference in function which leads to these slight differences in phenotype severity, however it could also be possible that the two overexpression lines exhibited differing degrees of overexpression, so it is unknown whether these differences are due to a significant difference in the role of these two genes. Expression levels were not specifically investigated for this thesis, as the purpose of this experiment was to gain an initial glimpse into whether these *H. vulgare* genes could perform similar functions in *A. thaliana* and thus gain some understanding of their potential function in *H. vulgare* itself, however this would be intriguing to test at a later date.

That these constructs were able to replicate known similar genotypes was intriguing, but not wholly unanticipated. As was discussed in the introduction, *PXY* and *CLE* genes can be found across many species and clades, with evidence of them retaining their role in stem cell population regulation throughout. This experiment fits nicely within that context, and shows that *H. vulgare* *PXY* and *CLE* homologues retain that ancestral function. It is also known that the sequences involved in PXY-CLE41 binding in *A. thaliana* are highly conserved within similar leucine rich receptor-like kinases in *A. thaliana*, and thus these may also see similar levels of conservation between species (H. Zhang, Lin, Han, Qu, et al., 2016). Had the constructs failed to produce similar phenotypes to *Atpxy* and to *AtCLE41* overexpression lines, this could have indicated fundamental differences in the sequences of the *A. thaliana* and *H. vulgare* homologues, which may have prevented ligand-receptor binding and thus resulted in little change. As this was not the case, one can assume that the structures of the *H. vulgare* proteins are similar enough to perform the roles of the *A. thaliana* proteins.

Collectively, the results shown above demonstrate that the identified barley genes are sufficient to mimic the functions of *PXY* and *CLE41* genes in *Arabidopsis*.

Chapter 2: Do HvTDIF and HvPXY regulate vascular development in *H. vulgare*?

Generation of Gene-Edited *H. vulgare*

The evidence presented in Chapter 1 has shown that both *HvPXY* and *HvTDIF* are homologues of known genes which act to regulate vascular development, such as those in *A. thaliana* and *P. trichocarpa* which have been well studied in vascular development (Smit et al., 2020; J. Zhang et al., 2015). Additionally, the phenotypes of *A. thaliana* plants harbouring these *H. vulgare* genes clearly indicated that both perform a similar function to their *A. thaliana* homologues, as both had a clear impact on vascular organisation when expressed in *A. thaliana*. This raised the hypothesis that *HvPXY* and *HvTDIF* may both also function in *H. vulgare* vascular development, and as such, the next step was to begin to analyse the effects of *HvPXY* mutation within *H. vulgare* itself, to investigate this.

To investigate the role of *PXY* in barley development, loss-of-function alleles were generated using the CRISPR/Cas9 system. Genome editing constructs were generated and barley transformation was performed at the John Innes Centre crop transformation facility, as detailed in the methods. The variety used was Golden Promise, as is mentioned in the introduction. Pairs of guide RNAs were included in the construct (Table 1) with the aim of deleting sections of the *PXY* coding sequence. Transformants were transferred to Durham for further analysis, and T1 plants were screened using PCR to identify band size polymorphisms that would indicate a deletion in the *HvPXY* open reading frame between the two guide RNA recognition sites. A deletion mutant with a 139 base pair deletion in the LRR domain that also resulted in a frame-shift and a premature stop codon was identified and referred to as *Hvpxy-1*. A second mutant which resulted in the deletion of a leucine rich repeat (LRR)

was also identified and referred to as *Hvpxy-2* (Figure 13). Both lines were otherwise in-frame. Deletions were detected by size polymorphism, then a PCR product which spanned the deletion was sequenced. Protein sequences of each mutant, as well as an alignment of both the gene and protein sequences, can be found in Appendix C. Initial visual analysis of the two mutant genotypes found them to be indistinguishable, and as such throughout this thesis *Hvpxy-1* was used.

Table 1: Guide RNA sequences for generating PXY alleles.

BRACT line	<i>Hvpxy</i> allele	Guide RNA1	Guide RNA2
1971-02-01 G2	<i>pxy-1</i>	GGTAATGCCGTCGGGGAAGG	GGTTGAGGTGCTCGAGTCTG
1972-03-01 H2	<i>pxy-2</i>	GTTGCTGTAGGCGTCGAGGA	GGGCGTCCCAGCGAGGTGC



Figure 13: A depiction of the locations of both *Hvpxy-1* and *Hvpxy-2* within the *HvPXY* gene. Light green = LRR domain, dark green = individual repeats, red = transmembrane domain, purple = kinase domain. A blue background is used to show the full length of the protein. Asterisks show the locations of CRISPR-induced lesions.

Vascular and Gross Morphological Traits in *pxy H. vulgare*

An initial assessment of differences between wild type and mutant *H. vulgare* was made by growing both genotypes to maturity, then obtaining and fixing stem samples from which transverse sections could be made. These sections were compared to analyse differences in vascular organisation between the two genotypes. Tissue samples were taken when the plants were approximately 3 months old. Tissue for sections was obtained from the primary tillers of the plants, just above the 1st internode.

No clear differences were noted between the two genotypes upon initial examination of the slides (Figure 14), however measurements were taken to confirm this. The measurements to determine potential differences in vascular organisation and morphology included size and number of xylem cells per bundle, size and number of phloem cells per bundle, the total number of cells per bundle, and the overall vascular bundle size. Measurements for cell and bundle sizes were performed using Lithograph X.

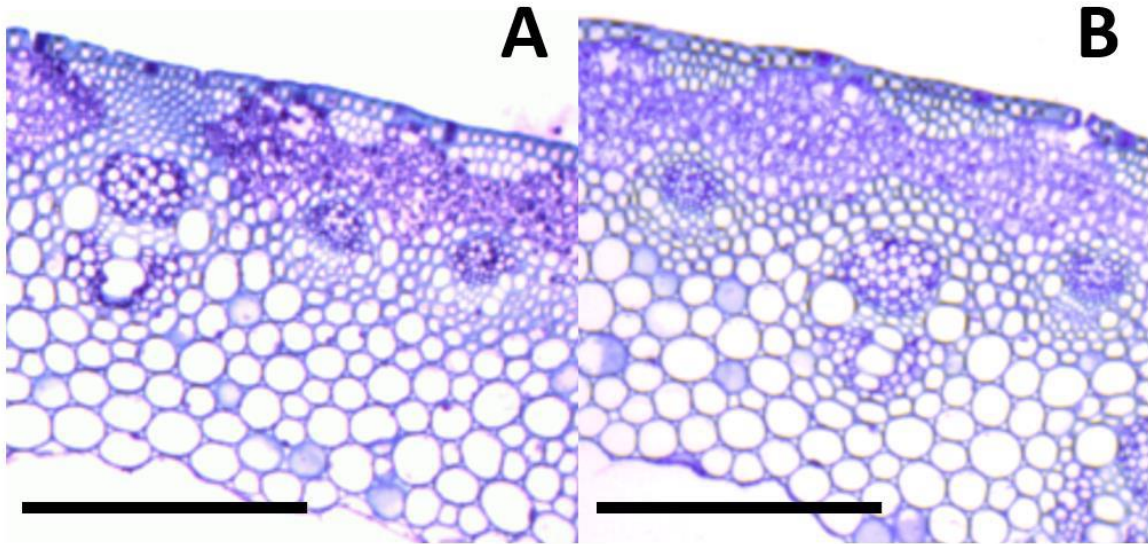


Figure 14: Radial sections of *H. vulgare*. (A) Wild type. (B) *pxy*. Scale bars represent 100µm.

Statistical analyses of these traits were done via one-way ANOVA, where each bundle was grouped into an external, middle or internal category to account for differences in bundle and cell size due to radial position within the stem (Figure 15). This method was chosen in case additional comparisons between bundle categories would prove informative, however this did not prove to be the case. Through this method, it was determined that there were no significant differences in the number of xylem or phloem cells per vascular bundle, nor in the total number of cells per bundle, the size of the xylem cells, the size of the phloem cells, or the size of the bundle (Table 2, Figures 16 and 17).

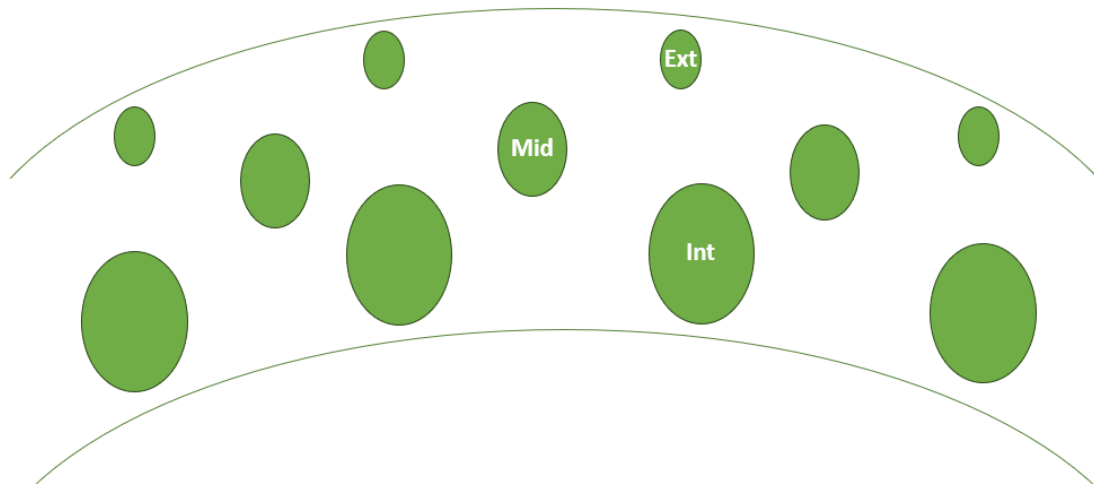


Figure 15: A diagram depicting vascular bundle distribution in *H. vulgare* to demonstrate vascular bundle classifications used. Ext = external, Mid = middle, Int = internal.

Table 2: *H. vulgare* vascular trait ANOVA P-values, averages and standard deviations.

		External Bundle	Middle Bundle	Internal Bundle
Phloem Cell Number	ANOVA P-Value	1.000	0.964	0.195
	WT Average	14.133	16.133	26.667
	WT Standard Deviation	3.335	4.438	8.209
	<i>pxy</i> Average	13.933	17.867	21.733
	<i>pxy</i> Standard Deviation	3.990	4.809	8.066
Xylem Cell Number	ANOVA P-Value	0.916	1.000	0.955
	WT Average	3.733	3.800	4.200
	WT Standard Deviation	0.704	1.521	1.014
	<i>pxy</i> Average	4.200	3.733	4.600
	<i>pxy</i> Standard Deviation	1.612	0.884	1.595
Total Cell Number	ANOVA P-Value	1.000	0.560	0.762
	WT Average	71.000	70.800	130.267
	WT Standard Deviation	8.115	21.578	38.016
	<i>pxy</i> Average	68.867	86.933	117.267

	<i>pxy</i> Standard Deviation	16.780	13.008	42.500
Phloem Cell Size	ANOVA P-Value	0.998	0.652	0.171
	WT Average	6305.359	10317.983	18390.894
	WT Standard Deviation	2070.744	4160.919	5117.601
	<i>pxy</i> Average	5758.434	12315.751	15248.104
	<i>pxy</i> Standard Deviation	1927.102	3368.799	3841.585
Xylem Cell Size	ANOVA P-Value	0.999	0.867	0.845
	WT Average	23963.868	44056.633	64129.106
	WT Standard Deviation	7830.681	12992.083	12164.744
	<i>pxy</i> Average	22487.503	48465.931	59528.608
	<i>pxy</i> Standard Deviation	10668.337	10318.010	9244.555
Total Bundle Size	ANOVA P-Value	0.985	0.830	0.843
	WT Average	80479.809	114887.835	183567.077
	WT Standard Deviation	19566.000	39140.605	43253.533
	<i>pxy</i> Average	71380.277	131421.477	167378.141
	<i>pxy</i> Standard Deviation	30465.715	27000.433	54308.510

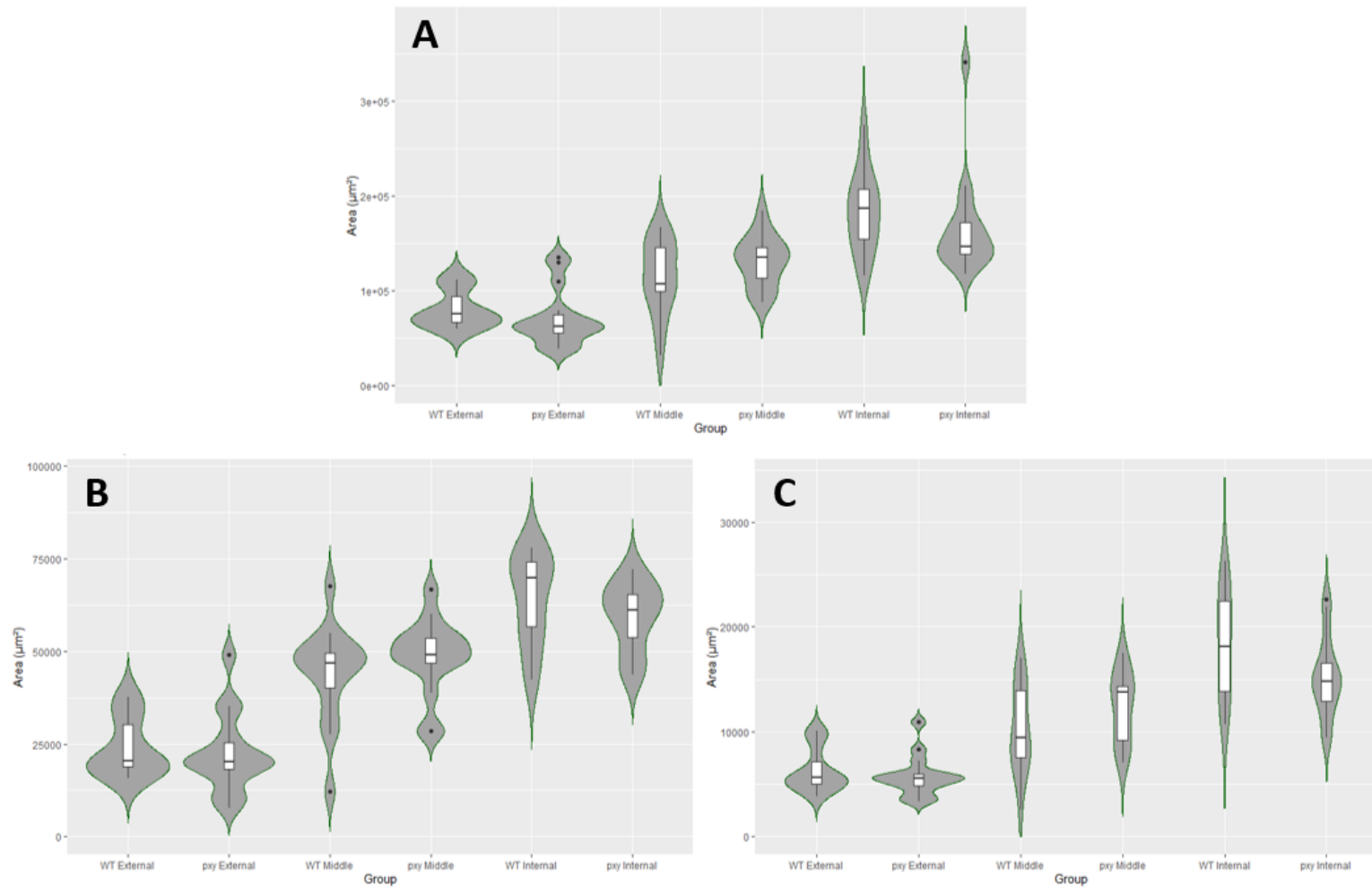


Figure 16: Violin and box plots of vascular traits in wild type and *pxy* mutant *H. vulgare*, showing (A) the area of the vascular bundles, (B) the area of the xylem cells, and (C) the area of the phloem cells. Black dots represent outliers identified by R Studio. N = 15 per genotype.

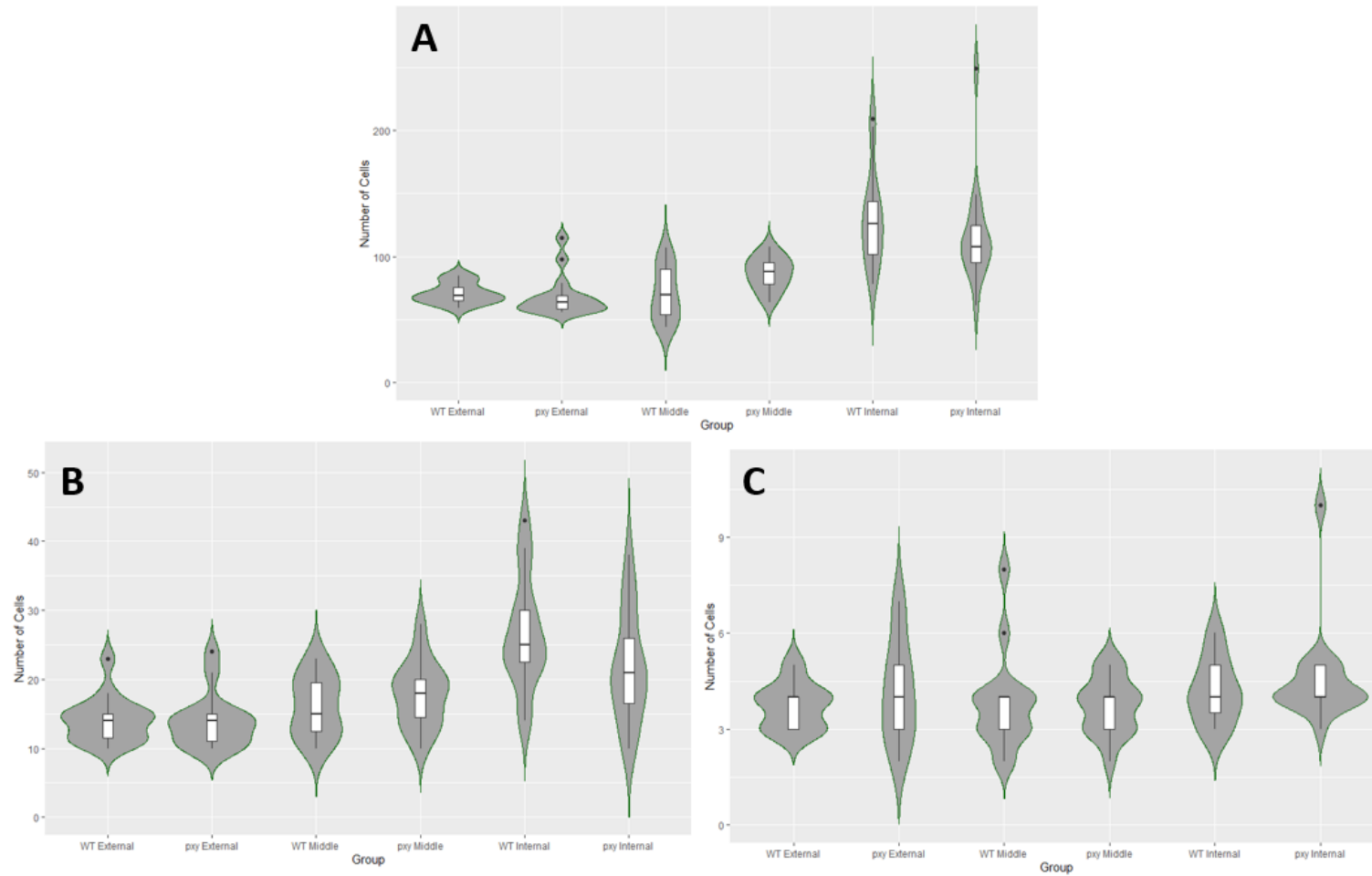


Figure 17: Violin and box plots of vascular traits in wild type and *pxy* mutant *H. vulgare*, showing (A) the number of cells per vascular bundle, (B) the number of xylem cells per vascular bundle, and (C) the number of phloem cells per vascular bundle. Black dots represent outliers identified by R Studio. N = 15 per genotype.

Given the function of *HvPXY* and *HvTDIF* when expressed in *A. thaliana*, these findings were contrary to what was expected, therefore it was decided that an investigation into the gross morphology of wild type and *pxy* mutant *H. vulgare* might provide some insight into the potential function of these genes within this species.

At maturity, approximately 3 months old, the following traits were measured – the height of primary tillers, width of primary tillers above the 1st node, number of tillers, number of nodes per tiller, and above-ground dry weight. These were analysed via T-test, as unlike in the vascular bundle trait analysis, only two groups were to be compared, thus an ANOVA was not deemed to be necessary. All traits bar the number of tillers were statistically significantly different between the two genotypes ($P < 0.05$), though some differences were small (Table 3, Figures 18 and 19). *pxy* mutant tillers were on average 2.631cm shorter and 0.136mm thinner than their wild type counterparts, with 0.219 fewer internodes per tiller. Additionally, *pxy* mutant plants had an above ground dry weight which was on average 4.293g lighter than the wild type.

Table 3: *H. vulgare* gross morphological trait T-test results. SD = standard deviation.

	WT Mean	WT SD	<i>pxy</i> Mean	<i>pxy</i> SD	P-Value
Tiller Number	18.429	2.573	21.714	11.206	0.464
Tiller Height (cm)	47.609	6.938	44.978	7.759	0.003
Tiller Width (mm)	1.331	0.619	1.195	0.517	0.046
Number of Internodes per Tiller	6.258	0.786	6.039	0.853	0.028
Dry Weight (g)	25.614	4.147	21.321	2.465	0.036

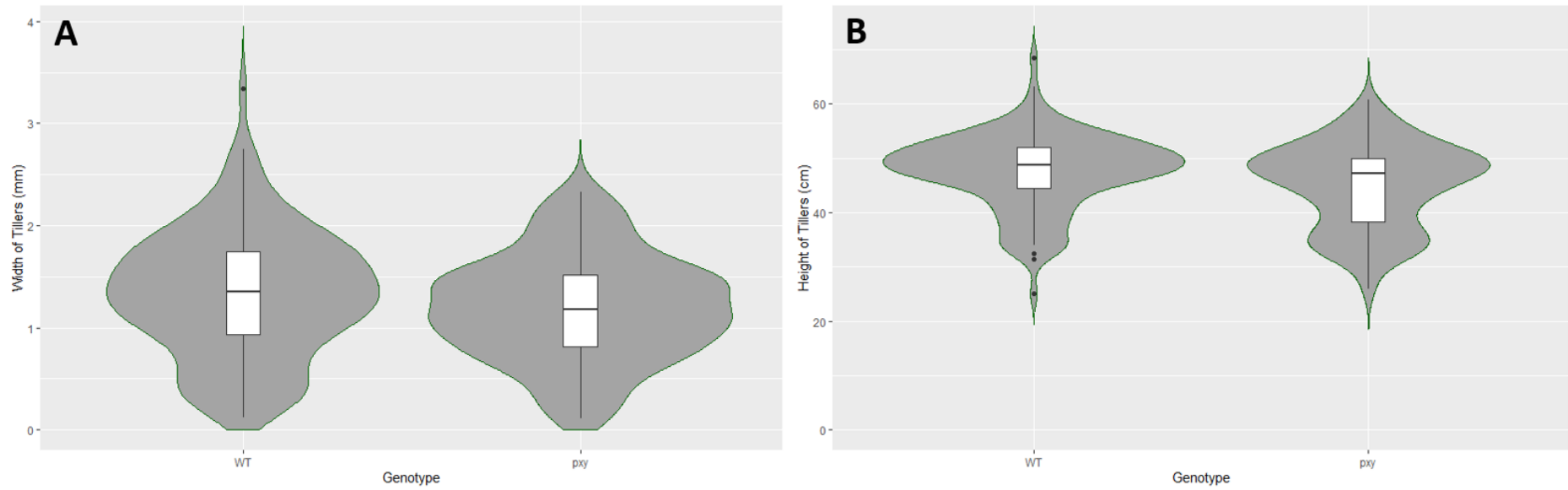


Figure 18: Violin and box plots of the gross morphological traits of wild type and *pxy* mutant *H. vulgare*, showing (A) the tiller width, and (B) the tiller height. Black dots represent outliers identified by R Studio. N = 128 for wild type, and N = 152 for *pxy*.

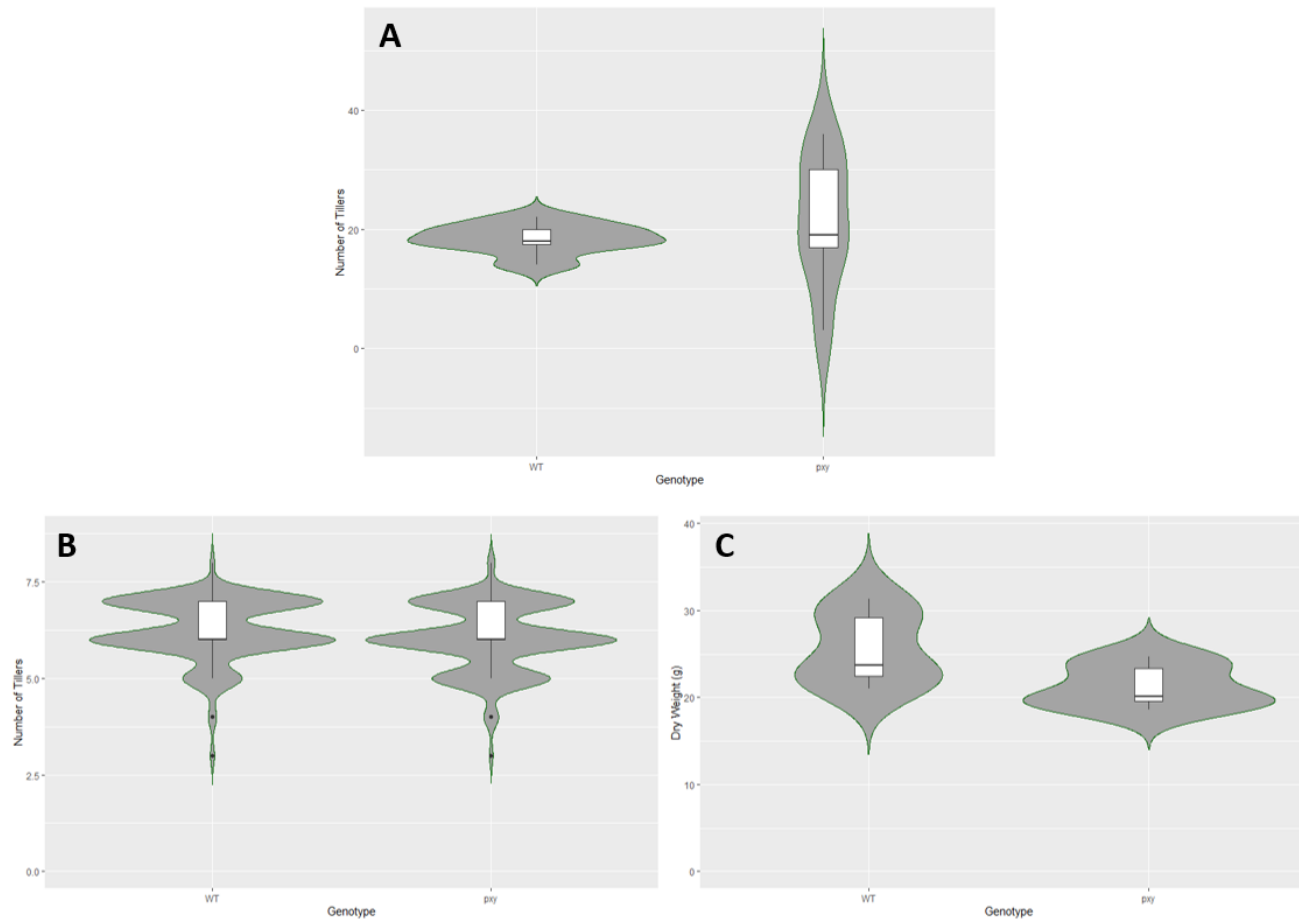


Figure 19: Violin and box plots of the gross morphological traits of wild type and *pxy* mutant *H. vulgare*, showing (A) the number of internodes per tiller, (B) the number of tillers per plant, and (C) the above-ground dry weight. Black dots represent outliers identified by R Studio. For (A), N = 128 for wild type, and N = 152 for *pxy*. For (B) and (C),

N = 7 per genotype.

This, in combination with the lack of significant difference seen in the vascular traits of wild type and *pxy* mutant *H. vulgare*, raised further questions regarding the role of *HvPXY* and *HvTDIF* in development. Whilst gross morphological differences were significant, they were often small differences in traits, and this lack of strong impact is in stark contrast to the differences seen in *A. thaliana pxy* mutants, which display significant vascular disruption and growth impairment (Etchells et al., 2013). Given the known function of *AtPXY* and *AtTDIF* in vascular development, the lack of impact on the vascular development was particularly perplexing. The dendrogram in Figure 9 indicates that there is distinct separation in the similarity between the monocot and dicot *PXY* homologues, and it is possible that in that separation lies a difference in function. Monocot homologues also showed greater similarity to non-vascular plant homologues than dicots, which may be an indication of a reduced role for *PXY* in monocot vascular organisation. It may also be possible that *HvPXY* exhibits some redundancy with another *H. vulgare* gene in this developmental process, as *AtPXY* does with *AtPXL1* and *AtPXL2*, however if this is the case the lack of impact of *HvPXY* mutation would indicate the redundancy may be greater.

Due to the role of plant vasculature in water transport, it was then hypothesised that some differences may become more apparent between the WT and *pxy* mutant *H. vulgare* should the plants experience drought conditions. If *HvPXY* plays a role in vascular development, as does its *A. thaliana* homologue, then any defects in this process would theoretically exacerbate the consequences of drought. In addition to this, it is known that *AtPXY* has some involvement in stress responses in *A. thaliana*, such as abscisic acid (ABA) signalling. ABA induces induction of defence genes in various organs, via binding to PYR1-like (PYL) receptors and causing them to also bind to protein phosphatase 2Cs (PP2Cs), freeing sucrose

nonfermenting-1-related protein kinase 2s (SnRK2s) from inhibition. PXY proteins are known to negatively regulate ABA signalling through inhibition of PYL proteins (K. Chen et al., 2019; Z. Yu et al., 2019). Similar genes, such as *PXL1*, have also been shown to play roles in stress responses such as the response to cold or heat stress, as do various other LRR-RLKs (Jose et al., 2020). Later work in this thesis also confirmed a link between *HvPXY* and stress response. Due to this reasoning, the decision to perform an analysis of wild type and *pxy* mutant *H. vulgare* traits under drought and non-drought conditions was made.

The Impacts of Drought Stress

A subsequent experiment to analyse the gross morphological and vascular traits was then set up which was near identical to the previous, however the wild type and *pxy* plants were split into non-drought and drought groups, and placed under water restrictions accordingly as described in the methods. This resulted in four groups, hereafter referred to as WT4L, *pxy*4L, WT2L, and *pxy*2L, where both 2L groups experienced water-restricted (termed “drought” henceforth as shorthand) conditions and both 4L groups did not. 2 litres of water were added twice per week compared to 4 litres in the control group. The higher value was chosen based on the approximate amount of water given to *H. vulgare* plants in other experiments contained in this thesis, with drought conditions then considered to be half of this. As before, plants were grown to maturity and measurements were taken for tiller height, tiller width, number of internodes per tiller, and number of tillers. Stem sections from each group were also been taken, using JB-4[®] resin embedding as before.

Visual examination of the sections from the drought experiment showed no visible differences in cell or bundle size or proportion, and thus this was not taken further. As before, tissue samples were taken when the plants were approximately 3 months old, and the tissue was taken from the primary tillers, just above the first node. Samples were taken from individuals excluded from the gross morphology analysis.

For the gross morphological analysis, results were analysed via a balanced two-way ANOVA in R to assess the impact of genotype and water restriction both alone and in combination, with Tukey tests used to delve further into specific comparisons where the combination of water and genotype was significant. A balanced test was used as the groupings were similar

enough in size to not require an unbalanced analysis. For both number of tillers and tiller width, the combination of water and genotype was not shown to be significant, thus neither was investigated further. For both tiller length and number of internodes per tiller, both factors together were shown to have significant impacts ($P < 0.05$). When investigating further into specific comparisons between each category, the *pxy2L* was shown to significantly differ from each other group regarding tiller length and number of internodes per tiller ($P < 0.05$). No other significant differences between groups were found (Table 4). With regards to the differences themselves, the *pxy2L* group had tillers which were approximately 4cm shorter than the other groups, with approximately 0.5 fewer internodes per tiller (Table 5, Figures 20 and 21). Consequently, *HvPXY* contributes to robust growth under drought conditions likely through a role in the regulation of tiller length and number of internodes, but not through impacts on tiller width or number of tillers.

Table 4: *H. vulgare* drought gross morphological trait ANOVA P-values. Where no comparison was performed, the box has been left blank.

	ANOVA			Tukey					
	Genotype	Water	Genotype :Water	WT2L: pxy2L	pxy4L: pxy2L	WT4L: pxy2L	pxy4L: WT2L	WT4L: WT2L	WT4L: pxy4L
Number of Tillers	0.294	0.085	0.741						
Tiller Length	0.165	0.067	0.001	0.004	0.002	0.078	0.997	0.574	0.606
Tiller Width	0.299	0.327	0.156						
Number of Internodes per Tiller	0.070	0.077	0.019	0.019	0.021	0.044	0.985	0.949	0.996

Table 5: *H. vulgare* drought gross morphological trait overview.

Trait		WT4L	pxy4L	WT2L	pxy2L
Number of Tillers	Mean	19.400	21.400	13.600	17.400
	Standard Deviation	4.037	5.505	6.309	7.503
Tiller Length (cm)	Mean	37.994	39.586	39.863	34.729
	Standard Deviation	9.510	8.055	9.404	9.994
Tiller Width (mm)	Mean	1.613	1.628	1.650	1.481
	Standard Deviation	0.647	0.611	0.608	0.517
Number of Internodes per Tiller	Mean	6.144	6.187	6.265	5.598
	Standard Deviation	1.429	1.200	1.561	1.500

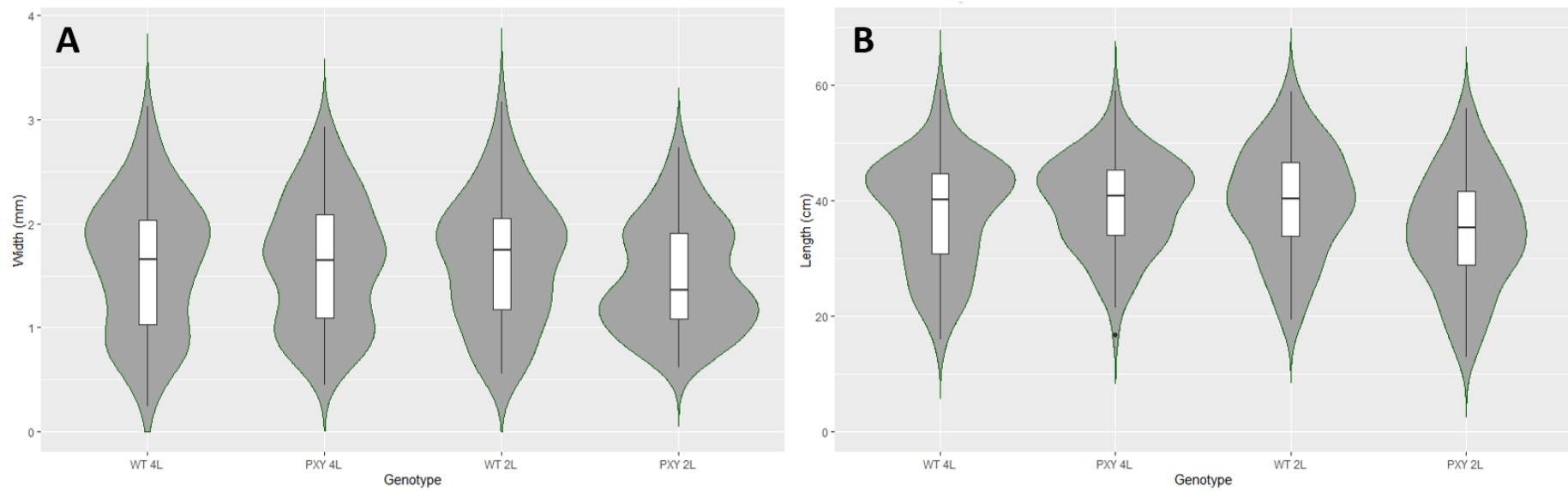


Figure 20: Violin and box plots of the gross morphological traits of wild type and *pxy* mutant *H. vulgare* in drought and non-drought conditions, showing (A) the tiller width, and (B) the tiller height. Black dots represent anomalous results identified by R Studio. N = 97 for WT4L, N = 107 for *pxy*4L, N = 68 for WT2L, and N = 87 for *pxy*2L.

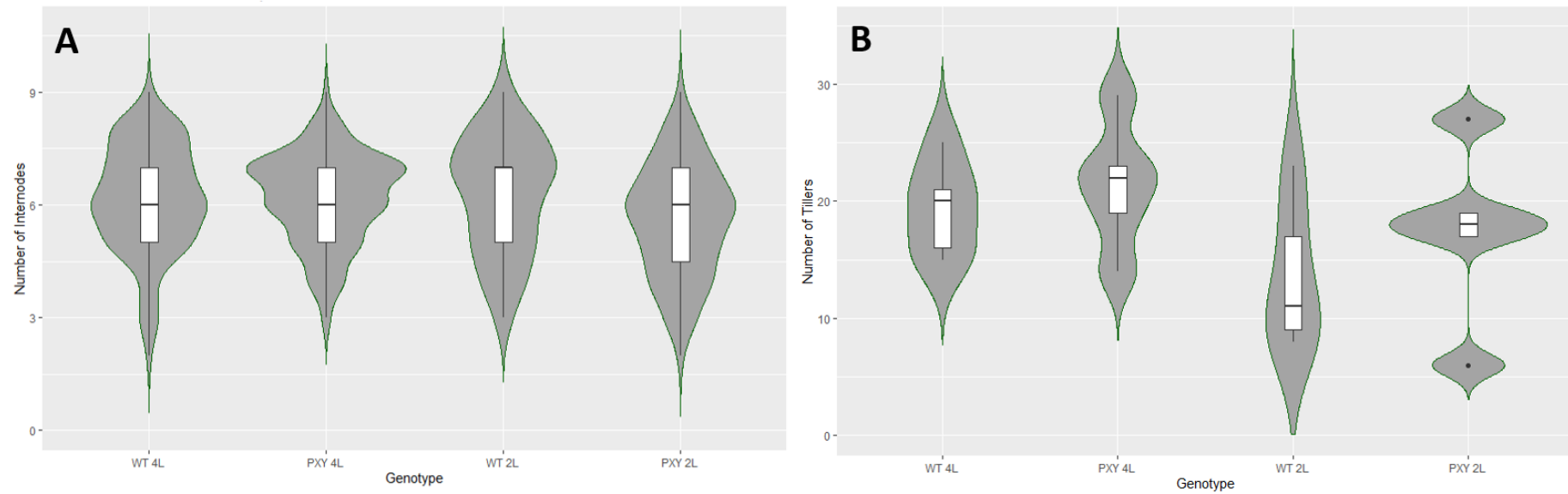


Figure 21: Violin and box plots of the gross morphological traits of wild type and *pxy* mutant *H. vulgare* in drought and non-drought conditions, showing (A) the number of internodes per tiller, and (B) the number of tillers per plant. Black dots represent anomalous results identified by R Studio. For (A), N = 97 for WT4L, N = 107 for *pxy*4L, N = 68 for WT2L, and N = 87 for *pxy*2L. For (B), N = 5 per genotype.

These results were perplexing – whilst no difference had been found again in the vascular bundles of *H. vulgare*, the drought experiment showed that *pxy* mutants do have a reduced ability to withstand drought compared to the wild type. However, the drought tolerance experiment also showed no difference between the WT4L and *pxy*4L groups, which did not experience drought conditions, which contradicts the differences found in the previous experiment on gross morphology in Chapter 2. This could be due to environmental conditions differing between the two experiments, as whilst the area in which they are grown is kept to the same temperature and light conditions as far as possible, factors such as weather will have led to changes in light levels and temperature fluctuation. It may also be a difference in the plants within both experiments, and thus may simply be chance that a significant difference was noted in one experiment and not in another – the first experiment's P values would imply that this is unlikely, but not impossible, and the differences seen in that experiment were small. The length of the tillers seen between both experiments appear to differ to a sizable degree, and the previously seen trend for *pxy* plants to be smaller is not present in the drought experiment under standard conditions, which would lend credence to some unknown environmental factor at play, though not all traits differed to such an extent between the two experiments (Tables 4 and 5). Attempting to determine if these are significantly different through existing data alone would not be appropriate due to the potential differences in growth arrangement, therefore to understand the change seen between the two experiments both should be repeated in future, with larger sample sizes.

Based on the combination of evidence from the drought and non-drought experiments presented in this thesis, it was suspected that HvPXY does not specifically regulate vascular development and as such differs from its *Arabidopsis* counterpart.

What Are the Impacts of *HvPXY* Mutation?

On the gross morphological level, it is clear that *pxy* mutation has some impact on *H. vulgare*, due to *pxy* mutants faring worse than the wild type when exposed to drought conditions. However, due to the conflicting results between the initial comparison of gross morphology and the comparisons seen between the non-drought groups in the follow up experiment, whether there is a significant difference between the wild type and *pxy* mutant groups under normal conditions is ambiguous, and if present only results in small differences in gross morphology. Additionally, no difference in vascular bundle traits could be seen between the wild type and *pxy* mutants, even when placed under drought stress.

This is a large difference from the effects of *pxy* mutation seen in *A. thaliana*, so these findings were surprising. The impact only being seen in tiller length and internode number differences implies a role in apical growth for *HvPXY*, rather than a vascular organisational role or role in secondary growth. Both of these are expected to some degree – monocots do not typically exhibit secondary growth, and with no cambium present in *H. vulgare*'s vascular bundles a function in vascular organisation would be surprising if it manifested in a way similar to *AtPXY*'s. Knowing the wide range of functions of LRR-RLKs, and the evolutionary history of *PXY* across clades, it was possible that *HvPXY* performed a role as yet unanticipated, though potentially still linked to stem cell population regulation. As impacts to apical growth were noted, a role in this area of growth was plausible, but as yet undetermined.

In an attempt to discover any other unanticipated impacts *HvPXY* was having, it was determined that the next course of action would be to look for any changes in gene

expression caused by mutation in *HvPXY*. Results from this would assist in finding new avenues of experimental pursuit.

Chapter 3: Differences in Gene Expression

RNA Expression Analysis

As the data regarding physical traits provided unexpected results which suggested the *HvPXY* may not regulate vascular development, it was hypothesised that analysis of the wider gene expression impacts of *Hvpxy* mutation may provide greater insights into the true role of *HvPXY*. mRNA was extracted from the 2nd internode below the apex of the primary tiller at flag leaf stage, with tissue adjacent to the node being taken. 3-month old *H. vulgare* plants of both wild type and *pxy* mutant genotypes were used. mRNA was subjected to next generation sequencing to determine differences in the transcriptomes of wild type and *pxy*. Between *pxy* and WT samples, 510 genes were found to be significantly upregulated and 517 were found to be significantly downregulated (Figure 22). Fragments per kilobase of transcript per million reads mapped (FPKM) cluster analysis was used to analyse the similarities in gene expression profiles between the samples, with dendrograms depicting sample similarity on the x-axis and the similarity between individual genes analysed on the y-axis. This FPRM analysis showed similar patterns of expression within the *pxy* and WT groups (Figure 23), supporting the idea there were consistent differences between genotypes.

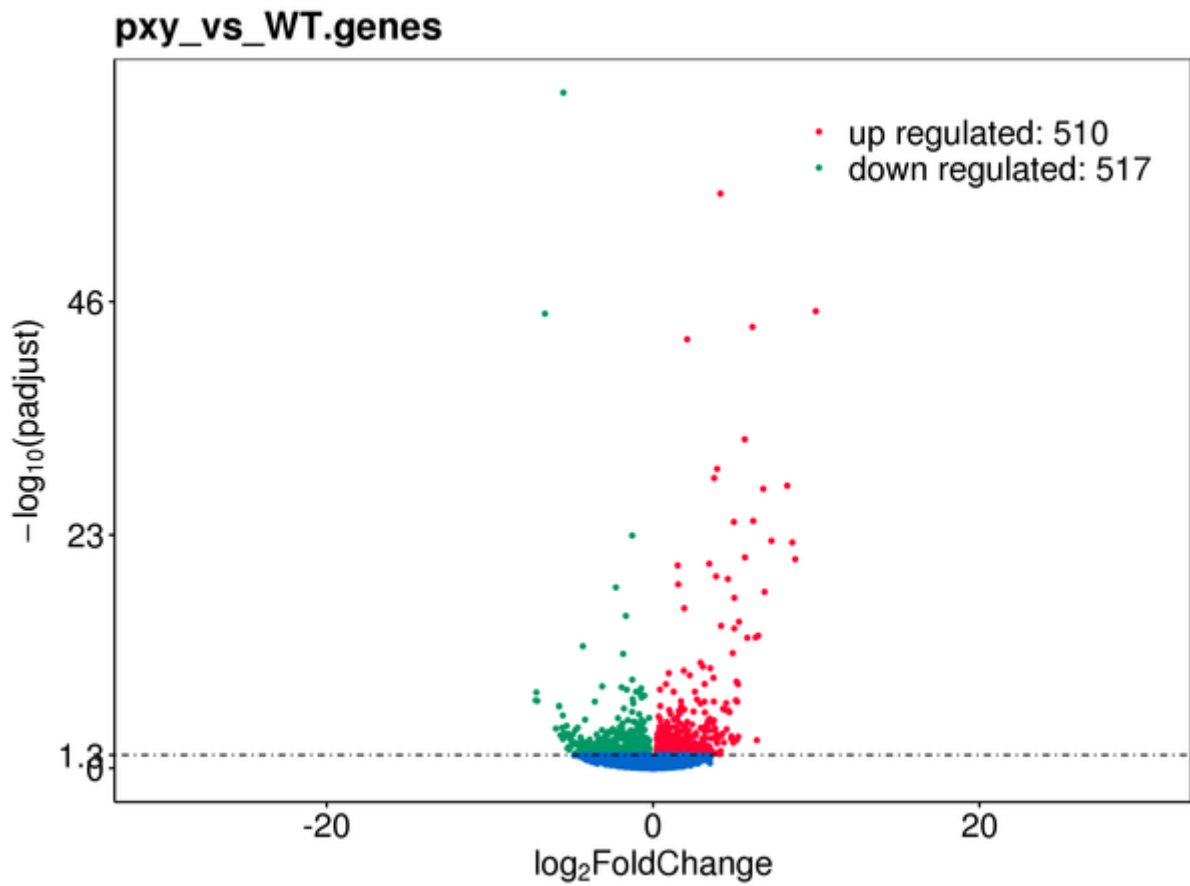


Figure 22: Volcano plot showing the fold change in gene expression between *pxy* and WT samples. Points shown in green are down regulated, points shown in red are up regulated, points shown in blue do not differ significantly between the two groups.

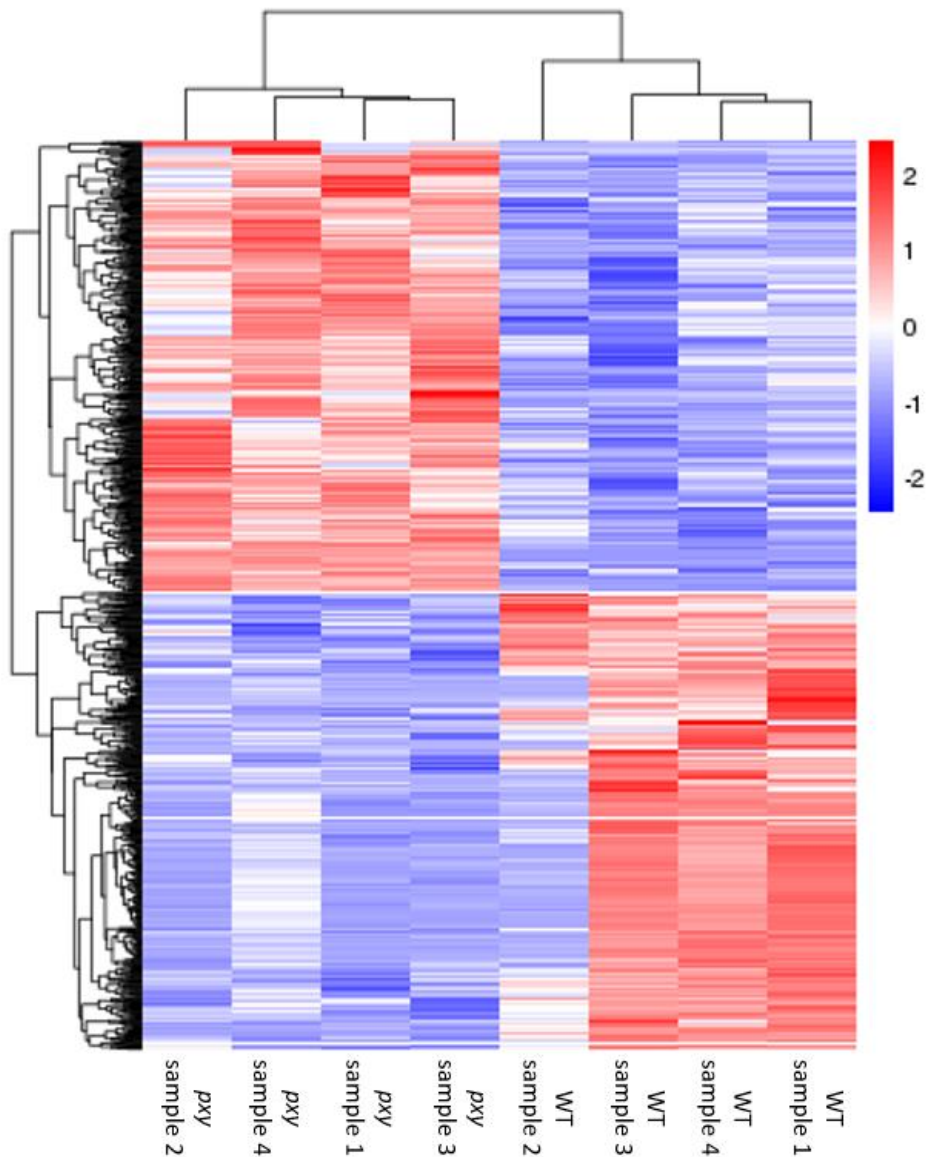


Figure 23: A figure showing the overall results of FPKM cluster analysis. Red denotes genes with high expression levels, blue denotes genes with low expression levels. The colour range from red to blue represents the $\log_{10}(\text{FPKM}+1)$ value from large to small.

To determine whether any biological processes were likely to be differentially regulated between the two genotypes, data was collated in order to identify differences in Gene Ontology (GO) category expression between the two. GO enrichment analysis was performed on all differentially expressed genes and revealed the top 20 GO categories which are differentially expressed between the two genotypes (Figures 24 and 25). This was

performed using the GOSeq R package, which also corrected gene length bias. Go terms with corrected P values of less than 0.05 were considered significantly enriched. Of these top 20 categories, several were of particular interest for this study, including “cell cycle”, “mitotic cell cycle”, and “cell division”. Given what is known of the function of AtPXY, the fact that several GO categories linked to cell division and related processes highlights the possibility that HvPXY also performs a similar role, despite evidence seen thus far. KEGG (Kyoto Encyclopaedia of Genes and Genomes) enrichment analysis was also performed – KEGG differs from GO analysis in that it looks at systems, genomic, chemical and health information, and can be used to analyse the pathways likely found in the gene set of interest. Of the enriched KEGG categories those which stood out were “homologous recombination” and “DNA replication”, both of which also indicate a role for HvPXY in cell division.

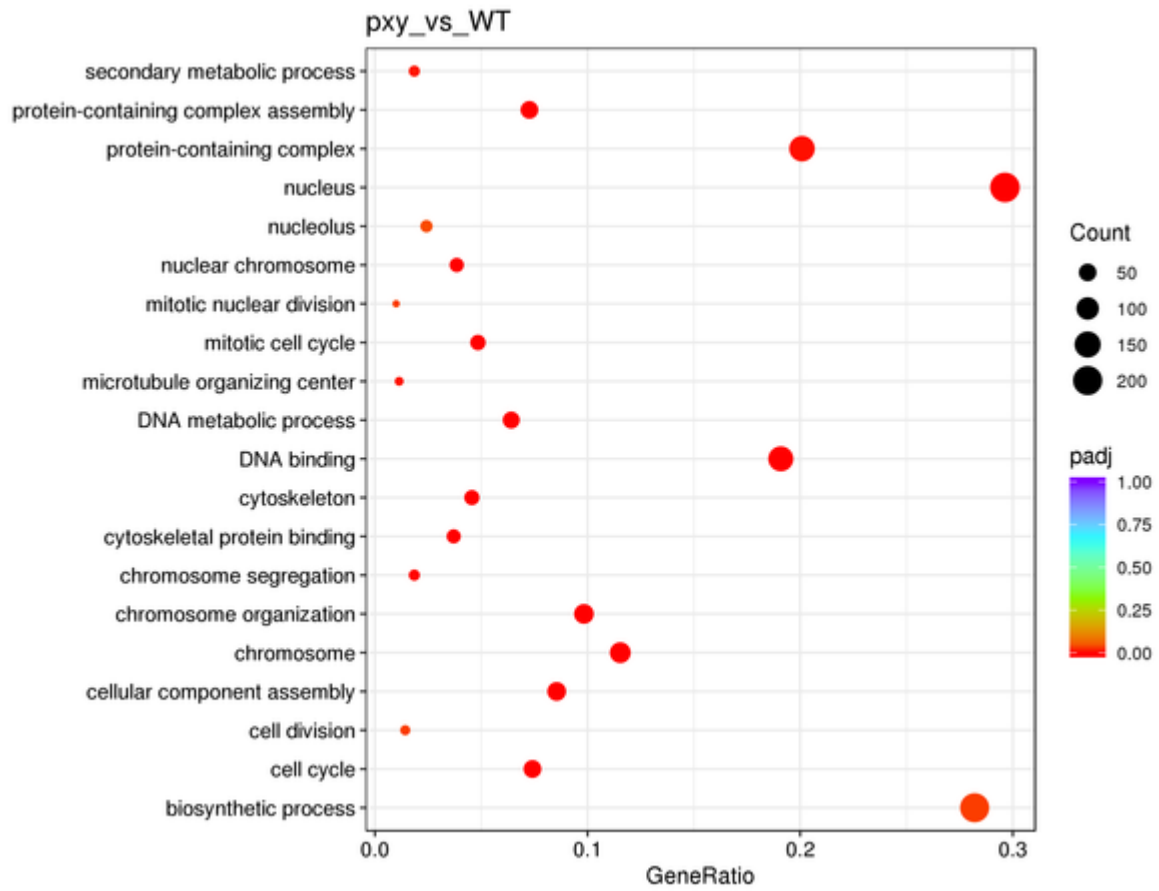


Figure 24: A scatter plot depicting the 20 most significantly enriched GO categories. The y-axis shows the name of the pathway and the x-axis shows the Rich factor. Dot size represents the number of different genes and the colour indicates the q-value.

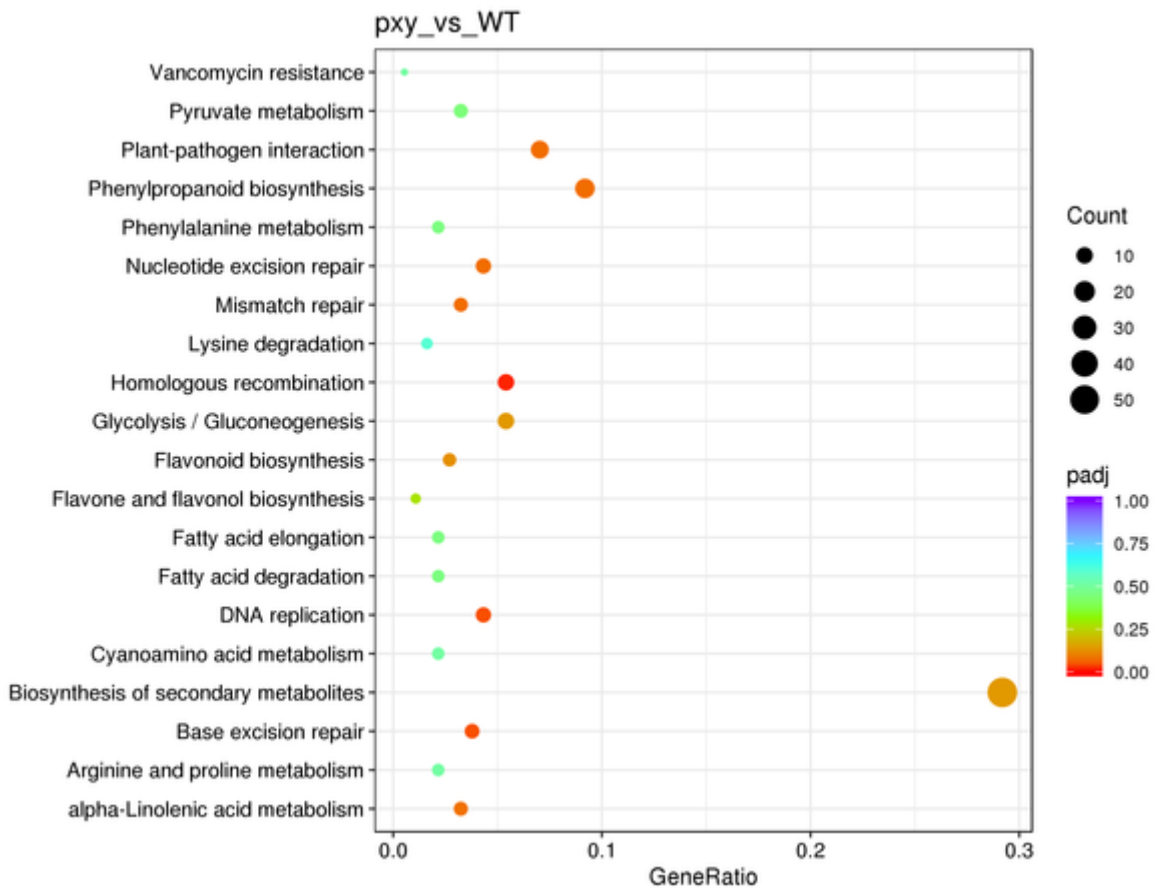


Figure 25: A scatter plot depicting the 20 most significantly enriched KEGG categories. The y-axis shows the name of the pathway and the x-axis shows the Rich factor. Dot size represents the number of different genes and the color indicates the q-value.

Of the differentially expressed genes, 70.1% had an identified *A. thaliana* homologue. Within the cell division category, several genes stood out, including *HORVU1Hr1G039250* and *HORVU5Hr1G064230*, identified as cellulose synthase-encoding genes, which were upregulated in *pxy* mutants with a 3.8 and 3.3 fold change respectively. The latter was specifically identified as a potential orthologue to *AT5G17420*, which encodes the protein IRREGULAR XYLEM 3 (IRX3, also known as CESA7), which is noted for its role in secondary cell wall synthesis in *A. thaliana* (Taylor et al., 1999). *HORVU5Hr1G068100*, also within this GO category, was instead downregulated in the *pxy* mutant (-487.5 fold change), and

identified as a potential orthologue to *AT1G46264*, which encodes HEAT SHOCK TRANSCRIPTION FACTOR B4 (HSFB4). Alongside their role in drought tolerance, HSFB4s are thought to play a role in stem cell fate in *A. thaliana*, specifically a role in root development when under non-drought conditions (Begum et al., 2013; Y. Zhang et al., 2022). Some of the genes which showed the highest degrees of downregulation in *pxy* included *HORVU6Hr1G008320* (-3200.4 fold change), a homologue of *AT3G46030*, and *HORVU1Hr1G007290* (-1748.9 fold change, a homologue of *AT4G15430*. *AT3G46030* is also known as *Histone Superfamily Protein 11 (HTB11)*, and *AT4G15430* is a gene in the Early Response to Dehydration stress (ERD) gene family specifically involved in osmotic stress (Wu et al., 2022; Yuan et al., 2014). Some of the genes displaying the highest degrees of upregulation in *pxy* included *HORVU5Hr1G062460* (431.3 fold change), a homologue of *AT4G03550*, and *HORVU7Hr1G006630* (18.6 fold change), a homologue to *AT1G71400*. *AT4G03550* is also known as *GLUCAN SYNTHASE-LIKE 5 (GSL5)*, a callose synthase, callose being a component of cell walls important in both development and stress response (X.-Y. Chen & Kim, 2009). *AT1G71400* is also known as *RECEPTOR-LIKE PROTEIN 12 (RLP12)*, a homologue itself to *CLAVATA2* known to complement it when expressed under the *CLAVATA2* promoter (G. Wang et al., 2010). These examples from the data highlight the wider impacts of *pxy* mutation on *H. vulgare* development, and indicate impacts which are not necessarily vascular specific, highlighting a role in stress response, cell wall production, and cell division.

A secondary gene analysis on another dataset was done to provide support for the findings of the GO and KEGG category analyses, using a modified version of Enrichnet. Enrichnet was initially designed to assess functional associations within a gene or protein set of interest, with some improvements compared to traditional techniques such as over-representation

analysis, gene set enrichment analysis, and integrative and modular enrichment analysis (i.e. those methods used above). It was originally designed to look at human cancer gene sets, and so had to be modified slightly to work with *H. vulgare* data through use of two new sets of information – a new set of pathways, obtained using the BioMart section of the EnsemblPlants website (<https://plants.ensembl.org/index.html>), and a new network obtained from the STRING database (<https://string-db.org/>).

The dataset analysed was a set of *H. vulgare* homologues of *A. thaliana* genes which were shown to be downregulated in *Hvpxy* and upregulated in *AtCLE41* overexpression lines, and was generated by Peter Etchells' Lab. This dataset was chosen to provide alternative insights into the role of *PXY* in *H. vulgare*, in order to either bolster the previous findings or to provide additional avenues of investigation, by analysing components which are likely downstream of *PXY*. *H. vulgare* homologues of *A. thaliana* genes were used to increase ease of comparison between the two studies. Several GO categories were revealed to be expressed to a significantly different degree from this analysis (Table 6), as can be seen by the XD scores which show the significance of the network distance distribution, highlighting the similarity of the gene set of interest to the mapped cellular pathways. Groups which were of interest from both datasets were “histone binding”, “protein heterodimerization activity”, “response to hormone”, “signal transduction”, “plant-type cell wall organisation”, “lignin catabolic process”, “actin filament organisation”, “cellulase activity”, and “cellulose catabolic process”. These GO categories support the evidence that HvPXY is involved in signalling pathways and changes to gene expression, and that it may well heterodimerize in a similar fashion to the way AtPXY does with proteins such as BAK1 (Yang et al., 2019). The XD values of these groups also imply again that HvPXY may have a similar role to AtPXY, as was shown in the RNA analysis earlier. In addition, the stress response-related GO category

“response to water deprivation” was also noteworthy, and was consistent with the findings of the drought tolerance experiment explained previously, continuing to indicate a role for HvPXY in *H. vulgare* development.

Table 6: Enrichnet output for the additional dataset, which had an upload size of 547 genes. The XD Score shows the measured similarity between the dataset of interest and the respective GO category pathway. The Pathway Size column shows the size of the respective GO category pathway, and the Overlap Size column shows the overlap between the dataset of interest and the respective GO category pathway.

GO Category Number	GO Category Description	XD Score	Pathway Size	Overlap Size
GO:0022625	Cytosolic large ribosomal subunit	2.492	10	3
GO:0031047	Gene silencing by RNA	2.417	24	7
GO:0000786	Nucleosome	2.192	15	4
GO:0042910	Xenobiotic transmembrane transporter activity	2.042	28	7
GO:0015297	Antiporter activity	1.974	33	8
GO:0009664	Plant-type cell wall organization	1.292	12	2
GO:0046274	Lignin catabolic process	1.292	18	3
GO:0052716	Hydroquinone:oxygen oxidoreductase activity	1.292	18	3
GO:0042393	Histone binding	1.176	13	2
GO:0046856	Phosphatidylinositol dephosphorylation	1.176	13	2
GO:0007015	Actin filament organization	0.992	15	2
GO:0009414	Response to water deprivation	0.992	15	2
GO:0043231	Intracellular membrane-bounded organelle	0.992	15	2
GO:0046982	Protein heterodimerization activity	0.917	32	4
GO:0003993	Acid phosphatase activity	0.739	19	2
GO:0009611	Response to wounding	0.692	10	1

GO:0043022	Ribosome binding	0.692	10	1
GO:0050790	Regulation of catalytic activity	0.692	10	1
GO:0005507	Copper ion binding	0.649	42	4
GO:0003779	Actin binding	0.610	33	3
GO:0008810	Cellulase activity	0.610	11	1
GO:0030245	Cellulose catabolic process	0.610	11	1
GO:0009725	Response to hormone	0.542	12	1
GO:0018024	Histone-lysine N-methyltransferase activity	0.542	12	1
GO:0004518	Nuclease activity	0.484	13	1
GO:0006289	Nucleotide-excision repair	0.484	13	1
GO:0016307	Phosphatidylinositol phosphate kinase activity	0.484	13	1
GO:0007165	Signal transduction	0.471	53	4
GO:0006073	Cellular glucan metabolic process	0.435	14	1

To summarise, the findings of these experiments corroborated evidence seen thus far in this thesis, highlighting roles for *HvPXY* in water deprivation, and again suggesting a role in cell division. Though this continued to be expected due to the role of *AtPXY*, the experiments thus far had not yet revealed where this function may occur, bar that it was unlikely to be in vascular cell divisions. In addition, it was striking that GO and KEGG categories such as Xylem histogenesis and others associated with vascular development appeared in neither GO analysis (which uses the Fisher's exact test statistic), nor Enrichnet (which makes use of the XD statistic). The rationale behind testing node adjacent tissue from internodes undergoing active elongation was that this would likely be a site of vascular deposition and/or expansion. However, the RNA-seq data may instead have captured differences in the intercalary meristem, a tissue type not found in dicots such as *A. thaliana*, but present in the tissue subjected to mRNA isolation.

Consequently, a new hypothesis was formed – that *HvPXY* regulates a different meristematic cell population. As such, the experiments here informed the next approaches, including to consider alternative areas in which the *HvPXY* gene could be exerting its influence. This began with an investigation into longitudinal cell divisions as opposed to radial, which would tie together the previously seen differences in tiller length between wild type and *pxy H. vulgare*, the lack of differences seen thus far in radial stem sections, and the role in cell division indicated in this GO analysis.

Chapter 4: Longitudinal Cell Divisions

Analysis of Longitudinal Sections

To address the hypothesis that *HvPXY* may influence cell divisions in the intercalary meristem, as was suggested by the RNAseq data, wild type and *pxy* mutant *H. vulgare* tissue samples were taken, both from node-adjacent and internodal tissue (Figure 26). Tissue was taken from 3 individuals per genotype. These were fixed, embedded, and sectioned via microtome longitudinally as opposed to in transverse to analyse potential differences in intercalary meristem cell divisions. Sections were stained with toluidine blue, photographed under microscope, and cell lengths were then measured using ImageJ software. 3 sections were analysed per individual, for a total of 9 sections per genotype for each tissue type.

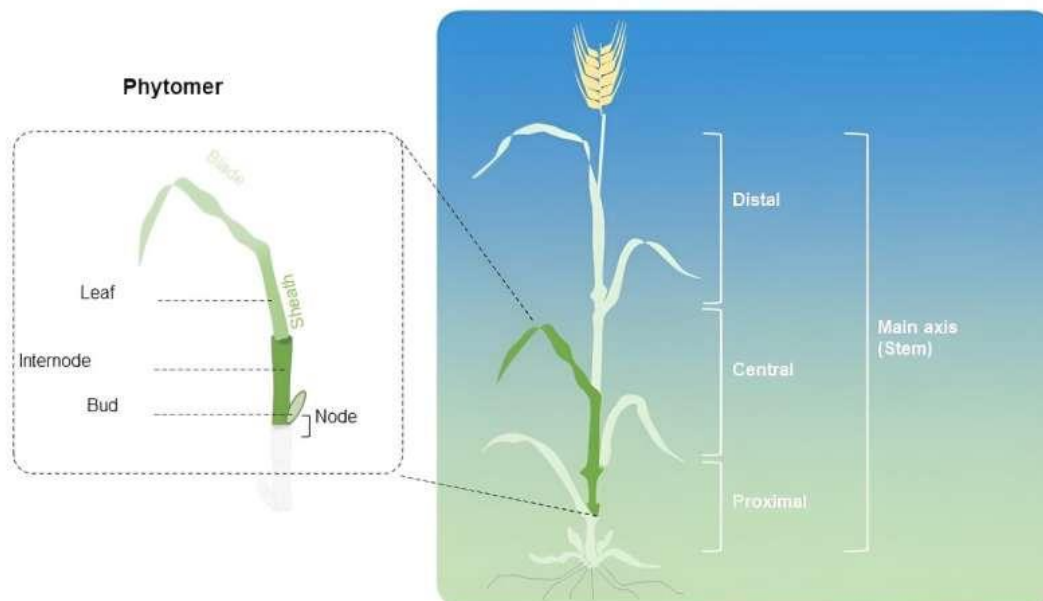


Figure 26: A depiction of the *H. vulgare* phytomer. Node-adjacent tissue was taken from the tissue immediately above the node. Image sourced from <https://scx1.b-cdn.net/csz/news/800a/2024/ipk-researchers-elucid.jpg>, and created by the Leibniz Institute of Plant Genetics and Crop Research.

Upon initial visual inspection of the tissue sections, no difference in cell length was thought to be seen in the node-adjacent cells (Figure 27), however internodal cells from *pxy* plants appeared to be longer than those of the wild type (Figure 28). A two-sample t-test confirmed that no significant difference in node-adjacent cell length was present between the two genotypes ($p = 0.12$), however there was a significant difference between the internodal cell lengths ($p < 0.01$), with the mean wild type internode cell length being $0.585\mu\text{m}$ and the *pxy* mutant mean length being $0.641\mu\text{m}$ (Table 7, Figure 29). As the violin plots revealed the data was not of a normal distribution, this was further confirmed by use of a Mann-Whitney U test, which also showed the difference in internodal cell length between the genotypes was significant ($p < 0.01$). This is a small yet important difference which should equate to *pxy* mutant plants having slightly taller tillers overall if all else were the same between the *pxy* and wild type plants, however experiments discussed previously showed that *pxy* mutant primary tillers were shorter than the wild type under standard conditions.

Table 7: Average cell lengths and standard deviations of wild type and *pxy H. vulgare* node-adjacent and internode cells.

Cell Type		Wild Type	<i>pxy</i>
Node	Average	0.155 μm	0.150 μm
	Standard Deviation	0.074 μm	0.073 μm
Internode	Average	0.585 μm	0.641 μm
	Standard Deviation	0.199 μm	0.231 μm

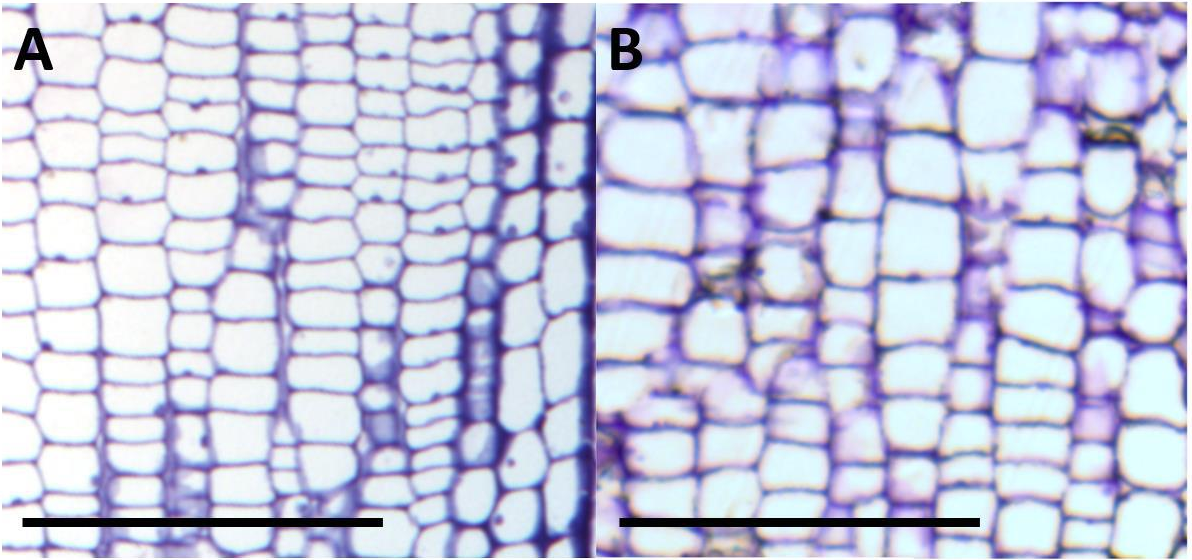


Figure 27: Longitudinal sections of *H. vulgare* node tissue. (A) Wild type. (B) *pxy*. Scale bar represents 100 μ m.

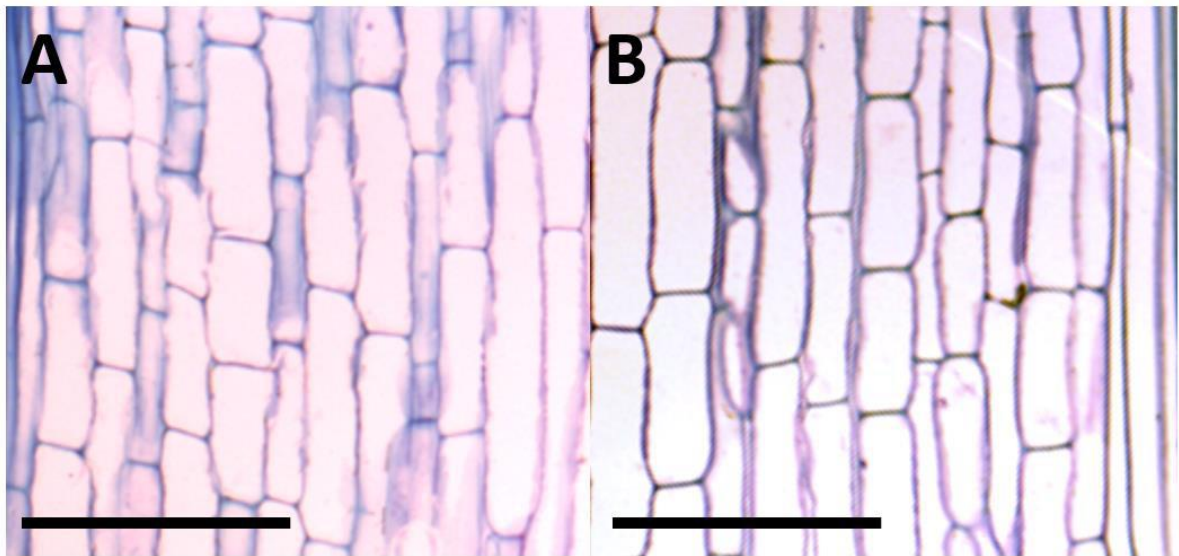


Figure 28: Longitudinal sections of *H. vulgare* internode tissue. A) Wild type. B) *pxy*. Scale bar represents 100 μ m.

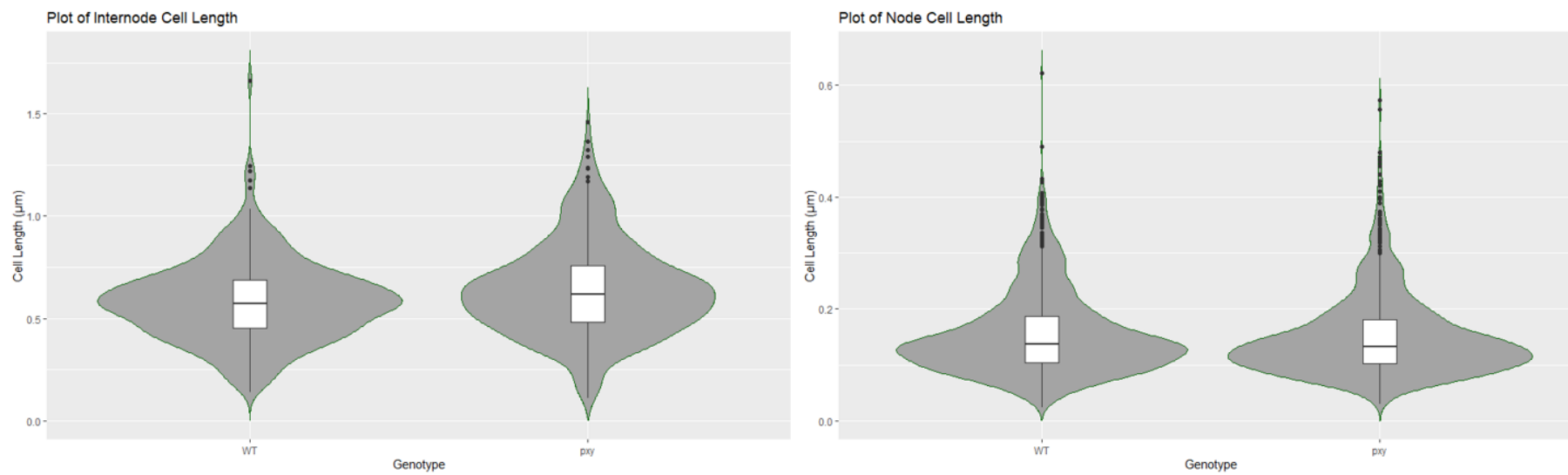


Figure 29: Violin and box plots depicting the cell lengths of wild type and *pxy* mutant plants. A) Plot depicting internode cell length, WT n = 324, *pxy* n = 375, B) Plot depicting node cell length, WT n = 1138, *pxy* n = 1147.

A way to explain this result would be to incorporate the evidence seen in the RNAseq experiment, which showed that *pxy* plants had lower expression of cell division-related genes than the wild type. If this difference in cell division is primarily linked to longitudinal cell divisions, this leads to the hypothesis that *pxy* plants possess both longer and fewer cells longitudinally, which could result in shorter tillers were the changes in cell length not sufficient to accommodate the difference in number of cell divisions.

Given all of this, it seemed possible that *HvPXY* may well be expressed in a meristematic region associated with apical growth. As such, an *in situ* hybridisation experiment was devised to analyse the expression of *HvPXY* in the beginnings of the intercalary meristems.

In Situ Hybridisation

In situ hybridisation was performed on 1 week old *H. vulgare* seedlings, using an antisense probe for *HvPXY* and using one for *HvHistoneH4* as a control (Appendix G). This age was chosen in order to find and section the shoot apical meristem (SAM), which is where it was hypothesised that the formative intercalary meristem may be found in *H. vulgare*, based on similar findings in other monocots, such as *Zea mays* (Figure 30, F. Wang et al., 2021). Sense and antisense probes were synthesised as per the methods, and targeted the mRNA of the relevant genes.

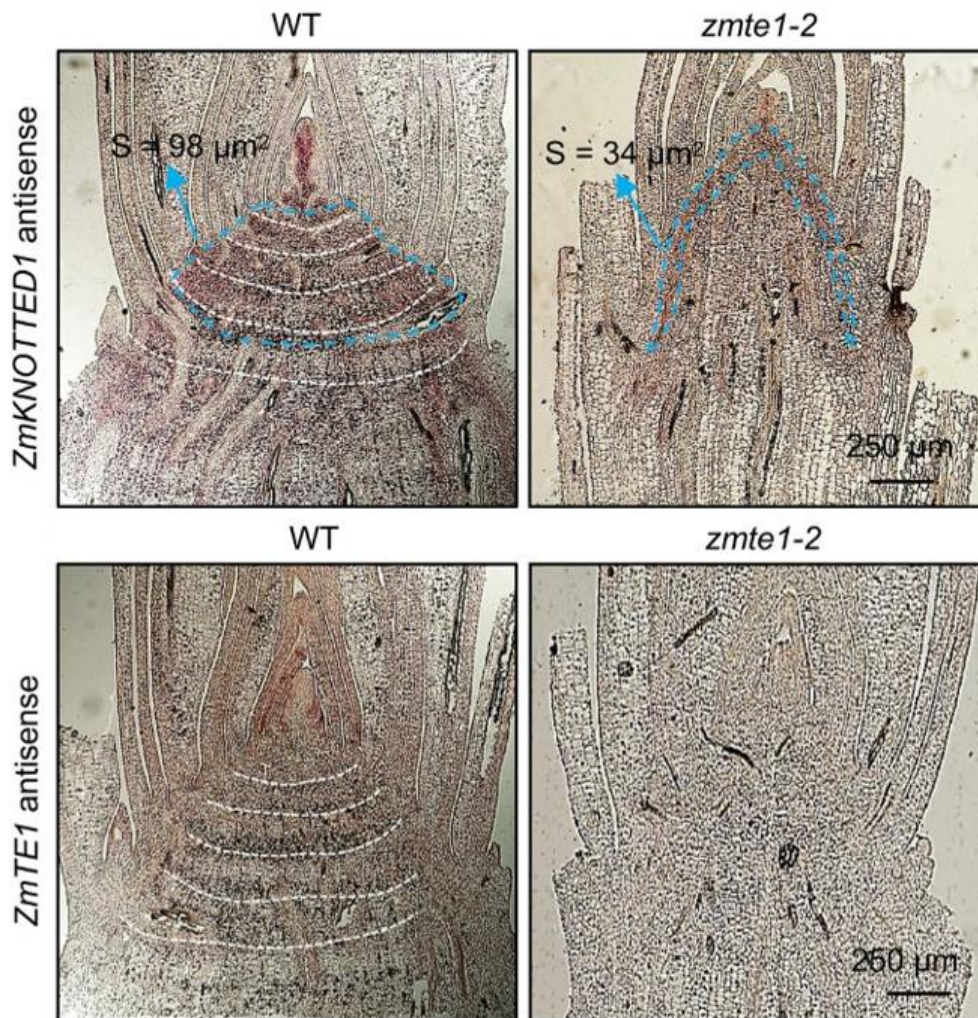


Figure 30: *In situ* staining indicating expression of *Zea mays* *KNOTTED1* (*ZmKNOTTED1*) and *TE1* (*ZmTE1*) in *Zea mays* intercalary meristems. Sections were taken from 4 week old specimens. Dotted white lines show banding of expression, indicating the formative intercalary meristems. Dotted blue lines represent meristem boundaries. Images sourced from Wang et al. 2021.

The staining pattern for *HvHistoneH4* was within expectation, with puncta visible in the image consistent with an expected, speckled expression pattern for histone H4 genes (Figure 31A). Staining for the antisense *HvPXY* probe appeared to show bands of expression across the stem tissue from the leaf bases (Figure 31B), albeit paler than the expression pattern seen in the *Zea mays* sections in Figure 30. This banded expression pattern may match that

of formative intercalary meristem, supporting the hypothesis that PXY regulates the intercalary meristem. To gain greater confidence in this result, this experiment should be repeated to see if more distinct banding can be seen – possibly, a range of plant ages should be used, as any expression may be greater at a different developmental stage. As the *Z. mays* specimens in Figure 30 were 4 weeks old, this may be a sensible age of plant to use for a repeat of this experiment.

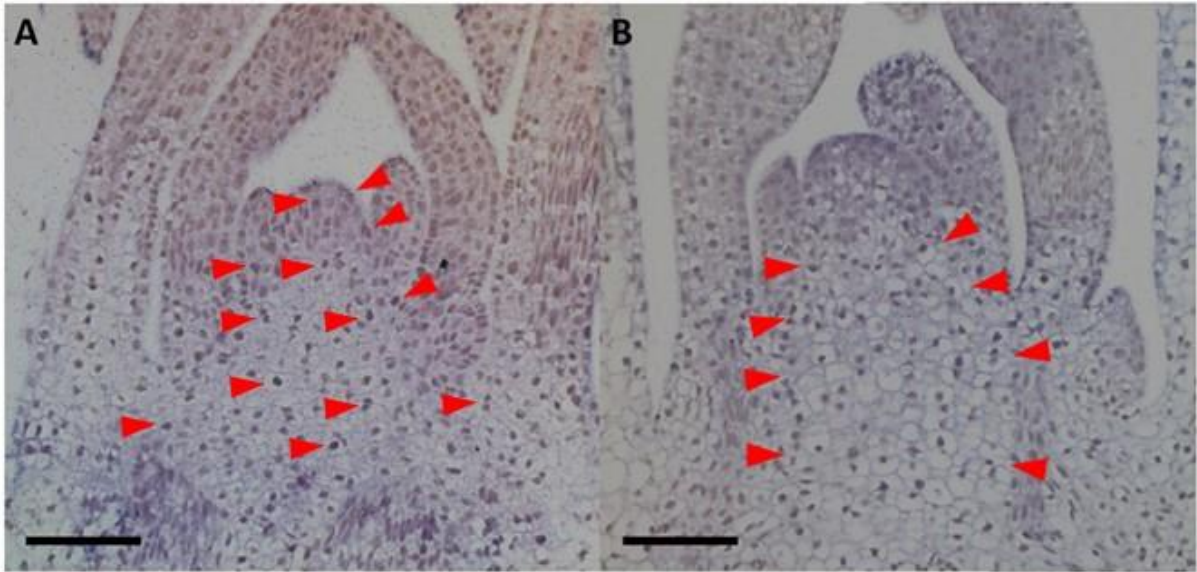


Figure 31: *In situ* hybridisation sections of 1-week old barley shoot apical meristems. A) *HvHistoneH4* probe, B) *HvPXY* probe. Red arrows in A highlight brighter nuclei to indicate the speckled expression pattern. Red arrows in B highlight where banded expression patterns can be seen, with each arrow showing the edge of a band.

Scale bars represent 100µm.

Discussion:

PXY genes in dicots are expressed within the vascular cambium, and are key regulators for cambium cell division and xylem differentiation. However, monocots typically lack a vascular cambium, causing the role *HvPXY* plays in *H. vulgare* to be unknown. This thesis investigated the role of *HvPXY* in *H. vulgare* development on a gross morphological, cellular and genetic level, its potential role in drought tolerance, and its location of expression.

From the evidence presented throughout this thesis, it can be concluded with relative certainty that *HvPXY* plays a role in the regulation of longitudinal cell divisions in *H. vulgare*. This fits what is known about *PXY* activity in dicots, specifically *A. thaliana*, in that the role in regulation of cell division appears to be conserved between *A. thaliana* and *H. vulgare*, though the area of expression and therefore direction of cell division regulated differs between the two. As there is no vascular cambium in which *HvPXY* could be expressed, it is logical that it is expressed in another stem cell population, and it appears likely that this population is the intercalary meristem (ICM).

This conclusion is brought about through the combination of varied pieces of evidence at the genetic, cellular and gross morphological levels. Starting with the cellular level, it was shown that *HvPXY* was able to complement the *pxy* mutant of *A. thaliana*, and *35S::HvTDIF* lines mimicked *AtCLE41* overexpression phenotypes, displaying the ability of these *H. vulgare* homologues to regulate cell division within the vascular cambium. Subsequent analyses of cell numbers and sizes in *H. vulgare* vascular bundles determined that *HvPXY* had no impact on the vascular bundle size or the number of cells per bundle, nor the size or number of individual cell types within the vascular bundles, which was understandable given

the lack of cambium cells in most monocots. However, differences were seen in the internode cell sizes longitudinally, with the *pxy* mutant plants possessing internodes cells approximately 10% longer than the wild type. Based on the cell lengths and tiller lengths measured previously, I would estimate that the number of cell divisions in *pxy H. vulgare* tillers were approximately 5% less than those in the wild type, however I would be hesitant to declare this figure to be accurate without further repeat experimentation.

The internodes are the areas of monocot stems where it would make sense to witness differences in cell divisions, as the intercalary meristems produce the internode cells in a role which is key to monocot apical growth (F. Wang et al., 2021). This leads to interesting conclusions when combined with the decrease in overall tiller length seen in *pxy* mutants under standard environmental conditions. It implies a far greater decrease in longitudinal cell number, and thus cell divisions, than either piece of evidence alone, and though the differences seen did not appear to drastically alter the health of the plants from casual observation, such a significant change in something as fundamental as plant growth and cell division should not go unnoticed. This made it clear that *HvPXY* plays a role in cell division, and it seemed likely that the divisions impacted were longitudinal rather than radial, as opposed to the radial divisions impacted by changes in *AtPXY*. From studies in various species, plant and otherwise, it is known that cell size is determined by the combination of cell growth and cell division (Jones et al., 2019). Cell size is vital for both maintaining the optimal size and shape on a gross morphological level, with mechanisms of compensation in leaf development found in various species such as *A. thaliana*, *O. sativa*, and *Antirrhinum majus*, whereby cells increase in size when cell division defects occur in order to maintain organ size and shape (Horiguchi & Tsukaya, 2011). As such, these changes in longitudinal cell

size in *H. vulgare* may be a similar method of compensation for decreased cell divisions, though it remains possible that it is merely a consequence of cell expansion without division.

The theory that *HvPXY* plays a role in cell division regulation was supported by the RNAseq data, which highlighted changes in key cell division and cell cycle GO categories in *hvpxy* mutants when compared to the wild type. These differences were seen even when utilising varying methods of analysis, both in terms of differing methods of performing GO category analysis, and also in terms of the evidence being seen in both GO category expression differences as well as KEGG category expression differences. The in situ hybridisation experiment seemed to also suggest a role in cell division, with distinct banding patterns displaying *HvPXY* expression within what is hypothesised to be the newly developing intercalary meristem (ICM). Each band may indicate the initial cells which will develop the ICMs, and therefore the internodes, within the tiller – this hypothesis complements literature which indicates internode formation in *H. vulgare* may begin in this banded manner, with cell layers constituting the ICMs present from an early stages, but each acting sequentially from the lowest upwards to generate cells and thus apical growth (Figure 32, McKim, 2020). This evidence and hypothesis combined with the differences in cell length could suggest that *HvPXY* plays a role in regulation of ICM cell divisions, and thus performs a function in cell division in more holistic manner than the vascular tissue specific *AtPXY*.

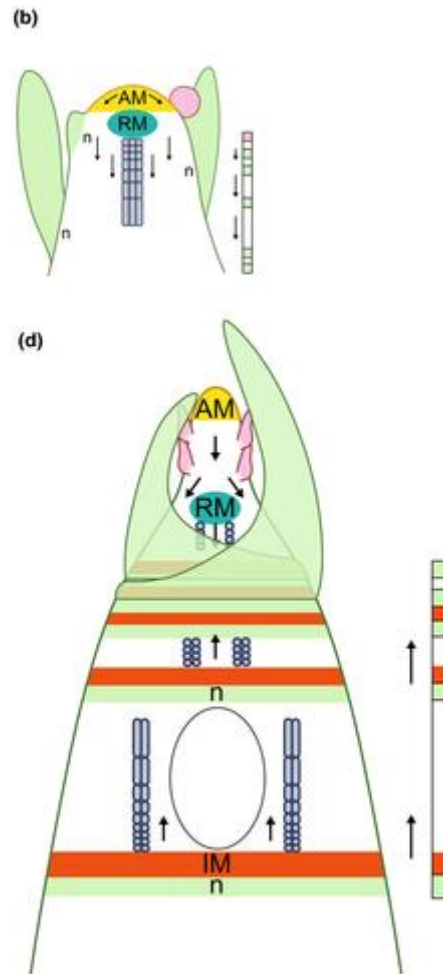


Figure 32: A figure depicting ICM development, obtained from McKim, 2020. (b) Model based on a flowering sticky mouse-eared chickweed rosette. Leaf primordia (green) and floral bud (pink) develop off the flanks of the apical meristem (yellow). Enhanced activity in the rib meristem (teal) drives increased internode elongation in internodes in a top-down developmental gradient. Bar on side shows alternating nodes (green) and internodes (white). (d) Model based on barley. Internodes elongate due to activation of intercalary meristems (orange) between vegetative nodes (green), elongating the internode from the bottom-up in an acropetal pattern as spikelets (pink) differentiate. Bars on side show alternating nodes (green), intercalary meristems (orange) and internodes (white). The youngest two leaves are shown; the rest are omitted for clarity. AM, apical meristem; RM, rib meristem; n, node.

Moving to the gross morphological results, it is evident that mutation of *HvPXY* leads to a decrease in tiller height and width, the number of nodes per tiller, and the above ground dry

weight of the plant. This all continues to point towards a difference in cell divisions, leading to a smaller stature and weight. The subsequent drought tolerance experiment, which showed that *pxy* mutant *H. vulgare* was more susceptible to drought stress than their wild type counterparts, also gave some credence to this. Several studies have highlighted that drought stress can negatively impact the rate of cell division in various plant tissues, for example in *Z. mays* endosperms and leaves (Avramova et al., 2015; Setter & Flannigan, 2001), and changes in cell turgor resulting from drought stress can impact the growth of cells (Ali et al., 2022). If both the WT and *pxy* mutants experienced an equal degree of perturbation in cell division and expansion due to drought stress, the resulting difference in overall plant size may be to do with a combinatorial effect of this and the cell division impacts *PXY* mutation alone has. It is also possible that the disruption caused by *PXY* mutation led to differences in water transport, and thereby restricted plant growth due to lack of water distribution, but this is not confirmed by data in this thesis. Confirming any of these theories would require repeat experiments, with particular focus on cell length variation under drought conditions. The drought tolerance experiment also, somewhat perplexingly, showed no difference between the WT and *pxy* mutant plants under standard conditions, however the overall difference seen across experiments indicated a difference between the two genotypes. Repeat experimentation can again confirm this. Due to these morphological differences, a role for *HvPXY* in growth and development seemed highly likely.

The findings of this thesis provide many questions regarding the evolutionary deviation in the role of *PXY* between monocots and dicots. Whilst the role in the regulation in cell division has been conserved, the difference in area of expression leads to questions about

how and when this change arose. Further investigation should be performed to fully confirm the location of both *HvPXY* and *HvTDIF* expression, at different developmental stages within *H. vulgare*, and investigation into the roles and locations of expression of *PXY* homologues in other monocot species would potentially provide valuable insights. Post-translational modifications may also be worth some exploration, as it is possible that the *HvPXY* protein is modified in ways in which differ from *AtPXY*, and that these differences lead to changes in both function and thus overall phenotype and impact in development. CLE peptides are known to be modified post-translationally, for example through the addition of arabinose sugar, and thus these would also be worth looking into (C. Whitewoods, 2021).

In addition to this, another perplexing element to the findings presented here is the unexpectedly mild phenotype presented by *pxy* mutant *H. vulgare*. When analysing mutations in the *PXY* pathway of *A. thaliana*, the changes in comparison to the wild type are unmistakable on both a cellular and gross morphological level, showing for example intercalation of xylem and phloem cells, or significant defects in overall growth and branching in the gross morphology (Fisher & Turner, 2007; N. Wang et al., 2019). Whilst the differences on both a gross morphological and cellular level are significant in *H. vulgare pxy* mutants, they are not as extreme as those seen in *A. thaliana*, and may in fact go unnoticed by the naked eye. This leads to questions about the significance of the role *HvPXY* plays in *H. vulgare* development in comparison to its *A. thaliana* counterpart. For example, it may be that *H. vulgare* contains other genes which contribute to vascular regulation, and that therefore the impacts of a mutating *HvPXY* alone produce limited results. For example, it is known that *KNOX* genes in play a role in cambium function within monocots which possess a vascular cambium (such as *Yucca*), as they do in dicots, and these may provide a promising

avenue for further investigation in *H. vulgare* to determine if these genes have shifted in function in a similar way to *HvPXY*. Other genes which may be similar candidates for future study would include *WOX* genes, some of which are also known to be expressed in monocot vascular cambium (Zinkgraf et al., 2017). There are also some genes involved in vascular development have been lost to monocots, but not necessarily in a manner which is consistent across the clade – for example, *E2FB* is known to be absent in *O. sativa* and *Setaria italica*, but not *H. vulgare*, and is a gene known to be important in the regulation of auxin-dependent cell division in *A. thaliana*. Genes such as these could be yet another route to consider in future work (Roodt et al., 2019).

Alternatively, it may be instead that the location of *HvPXY* expression, due to it necessarily being expressed in a different cell type to *AtPXY*, leads to the differences in the severity when *PXY* is mutated. The altered location will necessarily lead to differences in other genes and proteins connected to the function of *HvPXY*, and thus these additional factors may be the cause of the difference. *HvPXY* only seems to perform a role in vascular organisation when expressed in *A. thaliana* under the *AtPXY* promoter, and not in *H. vulgare* itself, which lends some credence to the idea that location contributes to the differences seen. Similar changes in key developmental genes when expressed in an alternative location can be seen in multiple organisms, perhaps most notably when considering the *HOX* genes in vertebrates. *HOX* genes play a vital role in the regulation of the animal body plan, and as high-level regulators of gross morphology, changes in their function have extreme impacts on phenotype. One example of a change in function of a *HOX* gene leading to alternate morphology would be the changes to *Ubx* and *AbdA* within the crustaceans, where changes in the regulation of those genes leads to their expression within a more posterior region of

the body, and causes the development of maxillipeds, a specialised type of feeding appendage (Averof & Patel, 1997). Outside of *HOX* genes, studies on butterflies have shown that mutations altering the areas of expression of the regulator *Distal-less* can alter the patterns which form on their wings. This again highlights the potential for key gene regulators to act in differing locations and then perform slightly altered functions (Brakefield & French, 1999). Other examples have already been discussed in this thesis which pertain to plants and to *PXY* and *CLE41*, which are the role a homologue of *PXY* itself plays within *M. polymorpha* as a regulator of cell division within the shoot apex, and the role of both *PXY* and *CLE* genes in the development of an altered cambium in woody monocots (Hirakawa et al., 2019; Takahashi et al., 2021; Zinkgraf et al., 2017). Each of these examples, and particularly the ones pertaining to altered *PXY* signalling, bolsters the idea that *HvPXY* maintains its function in cell division regulation, and that its altered area of expression in part leads to the differences seen between the roles of *HvPXY* and *AtPXY* within development. What this implies about the nature of the evolution of this gene pathway is unclear, and further investigation into the role of other monocot *PXY* genes may help to confirm whether this difference is linked to the monocot-dicot divergence specifically. It may also prove interesting to investigate other known regulators of stem cell division and organisation within plant species, to see if similar differences in function exist between monocot and dicot homologues.

To build on this, it would be worth considering the other elements involved in the *A. thaliana* *PXY* signalling pathway. As was discussed in the introduction, the pathway is interlinked with various hormone signalling pathways, such as the brassinosteroids. As such, investigating the role of homologues of genes in that pathway, such as *BAM1*, may provide

insights into the variation of role between the *AtPXY* and *HvPXY* pathways. Studies which look into the effects of exogenous hormone application on *H. vulgare* cell length and gross morphology may also be worthwhile, for hormones such as brassinosteroids, auxins and ethylene, all of which are known to be involved in the *A. thaliana* *PXY* pathway (Etchells et al., 2012; Kondo, 2022; Smit et al., 2020; Suer et al., 2011). *WOX4* and *WOX14* are known to act downstream of *PXY* in *A. thaliana* vascular development (Etchells et al., 2013), so it would therefore also be intriguing to investigate the presence and role of homologues of these genes in *H. vulgare*, to determine to what extent the genes involved in this process have diverged in function and location of expression. Additionally, genes such as *ERECTA*, which encodes an LRR-RLK, have also been known to mediate vascular cell divisions, and as such this gene and its paralogues (*ERL1* and *ERL2*) may also provide excellent candidates for future study, as would their peptide ligands derived from *EPFL* genes (Etchells et al., 2012; Uchida & Tasaka, 2013). *SERK* genes, which act as co-receptors to *PXY* in *A. thaliana*, may also be intriguing to investigate in future for similar reasons (H. Zhang, Lin, Han, Wang, et al., 2016).

PXY has been identified as part of leucine rich repeat receptor-like kinase (LRR-RLK) subfamily IX, one of the largest subfamilies of LRR-RLKs. It falls specifically into subgroup IX-a, alongside genes such as *CLAVATA 1* (*CLV1*), *BARELY ANY MERISTEM 1-3* (*BAM1-3*), *PXY-LIKE 1*, and *RGF RECEPTOR 1-5* (*RGFR1-5*), though other genes within the wider IX subfamily include *ERECTA*, *HAESA*, and *HAESA-LIKE 2* (*HSL2*). All genes within this subfamily are known for roles within development, plant growth, and stress response within *A. thaliana*, with evidence to support the roles are retained in *Solanum tuberosum*, indicating a high level of

conservation of function within the protein family as well as cross-species within the dicots (X. Li et al., 2018).

Other subfamilies of LRR-RLKs have been found to have conserved their function across multiple clades of plants, for example those in subfamily X relating to plant immunity or cysteine-rich peptides can be seen in the liverwort and moss lineages, with others showing more variability in terms of homologue presence such as those involved in brassinosteroid signalling, which become more consistently present in lineages such as angiosperms, gymnosperms, and ferns (Furumizu & Sawa, 2021). Genes encoding a receptor-ligand pair of PXY and CLE homologues are noted to be specifically absent in *P. patens*, yet not *M. polymorpha*, which indicates that this specific signalling pair is lost within the mosses (Bowman et al., 2017; Hirakawa et al., 2019). This highlights the likely role of PXY in the transition to vascular plants.

As mentioned elsewhere in this thesis, it is known that this signalling pair has been important for regulation of cell proliferation across the clades, however the specific clades it exists within may indicate that its function was important for the transition towards vascular plants specifically. In *A. thaliana*, it is known that the PXY signalling pathway is involved in more processes than cambial cell regulation, but also functions in lateral root and axillary bud formation. Noting the slight similarity in nodal stem structure between *H. vulgare* and *A. thaliana*, it may be that *HvCLE41* functions in a manner similar to the axillary bud role, and thus so too may *HvPXY*, however work on this is limited and so future studies in both this species and *A. thaliana* would be required to gain confidence in this hypothesis (Kondo & Fukuda, 2015). It may also be that PXY is conserved in *H. vulgare* for its role in maintaining

polarity of cell division, which is part of the role that the *A. thaliana* homologue plays (Sieburth, 2007).

The evidence and conjectures presented in this thesis should hopefully allow further work to be done investigating the genetic components of *H. vulgare* development, and in turn lead to potential insights into routes towards generating improved crop lines through genetic modification or selective breeding. Through a theoretical network of genes and their known functions, it may be possible to create crops better resistant to lodging, drought, and as the GO category expression results showed, possibly also cold. As global warming continues to create a less predictable and more hostile climate, hardier crops will be vital to ensuring food remains plentiful for all. This work may go some way towards that goal, and may also provide the beginnings to similar work in other vital monocot crop species.

Methods:

Creation of Dendrograms

Protein IDs and sequences for AtPXY and HvPXY were found on Uniprot, and the IDs were entered into the PANTHER database to obtain the IDs for homologues from a range of species. Homologues were also identified via the TAIR entries for both proteins, and through use of the BLAST function of the Phytozome website. Sequences for each of the IDs were again obtained from Uniprot or Phytozome, and all the sequences identified were then aligned using the T-Coffee multiple sequence aligner, alongside one additional sequence in each set for a similar gene to root an eventual dendrogram to (*H. vulgare* ERECTA for PXY, *A. thaliana* CLAVATA3 for CLE41). Where multiple potential homologues were found in a species, further investigation of known function was performed to attempt to guard against the inclusion of paralogues or genes otherwise not of interest for this comparison. Some species continued to contain multiple potential homologues even after this screening, thus all were included for completeness.

For alignment, M-Coffee was used for the PXY sequences, and Expresso for the CLE41 sequences. Following this, dendrograms were created from these alignments using R studio, using the packages phangorn, treeio, ggplot2 and ggtree. These packages were selected to create the desired appearance for the dendrogram, and to test multiple maximum likelihood models to obtain the best fit for the alignment data (Schliep, 2011; L.-G. Wang et al., 2020; Wilkinson, 2011; G. Yu et al., 2016).

DNA Extraction:

An extraction buffer was prepared including 2.55g d-Sorbitol, 11ml 2M Tris-HCl at pH8, 4.4ml 0.5M EDTA at pH8, 16ml 5M NaCl, 0.8g CTAB, and 1g n-Lauroylsarcosine, made up to 100ml with water. The tissue from which DNA was to be extracted was cut from the plant and immediately frozen with liquid nitrogen. The tissue was then ground in a pestle and mortar with 400µl of extraction buffer. The resulting solution was heated to 65°C for 5 minutes, then 400µl of chloroform was added and a vortex was used to mix. After this, the solution was spun for 20 minutes at 13000rpm, and the supernatant transferred to a new tube. 400µl isopropanol was added, and the solution vortexed again. The DNA was reprecipitated by adding 100µl 4.4M ammonium acetate at pH5.2, along with 700µl isopropanol. The solution was inverted several times until DNA precipitate could be seen. The solution was spun for 3 minutes at 10000rpm at 4°C, and the supernatant removed. The DNA pellet was washed with 300µl 80% ethanol, and spun again at 10000rpm for 2 minutes at 4°C. The pellet was then air dried before resuspension in 50µl TE buffer.

Cloning of *HvTDIF* and *HvPXY* for Complementation Experiments in *A. thaliana*

Table 8: Primers used in this method.

HvPXY_topo_F	caCCGACAATATTCCGCCTCGA
HvPXY_topo_R	TCTGGGGCGTATATCTGAGA
HvTDIF_topo_F	CaCCTGAGCGGGTTCTTGC
HvTDIF_topo_R	GAAACTTGAAAGCAGAGCAGC
HvPXY_2F	TCTGTCTCGTCGCAACCTAT
HvPXY_2R	ATACCCGATCTCAAGGCGTT
XhoI-PXYproF	CTCGAGCGACGCATGCCTCTATACATT
PXYproR-HindIII	AAGCTTTGTTCTTCTTTTTCATCGTAGCTTT

Using primers described above, *HvPXY* and *HvTDIF* full length genomic sequences were cloned into pENTR-D-Topo.

HvPXY was amplified from *H. vulgare* DNA using PCR in two reactions, one using BioULTRA polymerase and a second using VeriFi, according to the manufacturer's instructions (PCR Biosystems) and primers HvPXY_topo_F and R reactions were pooled prior to purification using the Ampure bead PCR clean-up method, included in this thesis. Two reactions were used due to insufficient BioULTRA polymerase requiring an alternative be used. A Topo reaction was performed according to the manufacturer's instructions (Thermo Fisher Scientific) to generate a gateway entry vector containing the *HvPXY* sequence. The Topo reaction was transformed into *Escherichia coli* using the transformation of *E. coli* method included later in this thesis.

E. coli colonies that carried a copy of *HvPXY* were identified using PCR. Approximately half the colony was used as template, and positive clones were identified using primers HvPXY2F and 2R using biomix red reaction mix (PCR Biosystems) according to the manufacturer's instructions. 4 positive clones were selected for further analysis. They were grown in 5ml cultures, and plasmids were purified using the NEB Monarch Plasmid Miniprep Kit. PCR products from clones were fully sequenced using the Durham University sequencing facility. One clone was identified with a 100% match to the *HvPXY* sequence.

HvTDIF entry clones were generated similarly. Primers HvTDIF_topo_F and R were used for both amplifying *HvTDIF* genomic sequence and for screening for positive clones. Rather than the Ampure bead clean-up method being used to clean-up the initial PCR amplification, gel extraction was performed using a Qiagen gel extraction kit according to the manufacturer's instructions.

To generate a *35S::HvTDIF* clone, an LR clonase™ II reaction was performed using the *HvTDIF* entry clone described above, and the gateway vector pK2GW7 (Karimi et al., 2002), according to the manufacturer's instructions. The LR clonase™ II reaction was transformed into *E. coli* using the previously mentioned transformation protocol included in this thesis. Positive colonies were identified using primers HvTDIF_topo_F and R, and Biomix red.

To generate an *AtPXYpro::HvPXY* clone, a gateway destination vector was first generated. The p3HSC vector (Atanassov et al., 2009) which contains a pCB1300 backbone carrying the *IRX3* promoter, STREP tag, and ccdB cassette was modified. The *IRX3* promoter and STREP tag sequences within p3HSC were excised as a XhoI-HindIII fragment. The *AtPXY* promoter was then inserted in its place. This was accomplished using primers that incorporated XhoI and HindIII sites (above), and Phusion polymerase (Thermo), to PCR amplify the *AtPXY* promoter.

This PCR product was subjected to digestion with XhoI and HindIII prior to ligation into the p3HSC backbone, yielding a AtPXYpro:ccdB plasmid, which was confirmed by DNA sequencing. *AtPXY:HvPXY* was subsequently generated using an LR reaction that included AtPXYpro:ccdB and the *HvPXY* entry vector. The LR clonase™ II reaction was transformed into *E. coli* and positive clones were selected by PCR screening using primers HvPXY2F and 2R using biomix red reaction mix.

Ampure Bead PCR Clean-Up

PCR products were transferred to an 8-well strip. Ampure magnetic beads were resuspended, then added to the PCR product at a ratio of 2:1 beads:PCR product. These were mixed by pipetting up and down approximately 8 times, then incubated at room temperature for 5 minutes. The samples were then placed onto a magnet for 3 minutes, or until the solutions became clear. Whilst still on the magnet, the supernatant was removed, and 180µl 80% ethanol was added to the remaining magnetic beads. This was repeated 2 more times. The ethanol was then removed, and the beads dried at room temperature on the magnet for 10-15 minutes. 35µl of Tris-EDTA buffer (TE) or water was then added to the beads, and the 8 well strip was removed from the magnet. The beads were resuspended in the new solution, and incubated at room temperature for 2 minutes. The 8-well strip was then returned to the magnet, left for 2 minutes, and the supernatant containing the purified PCR product was removed and placed into a new tube.

Transformation of *Escherichia coli*

100-150µl of competent *E. coli* cells were taken and put on ice to defrost. Once defrosted, the Topo reaction was added to the cells, and the mixture was chilled on ice for 30 minutes. Once done, the mixture was heat shocked at 42°C for 1.5 minutes, then returned to the ice for 1-2 minutes. 500µl of Super Optimal broth with Catabolite repression (SOC) medium was added, and the new mixture was incubated at 37°C on a shaker for 1 hour. The mixtures were then centrifuged at 5000rpm for 1 minute, and 500µl of the resulting supernatant was removed. The cells were resuspended in the remaining supernatant, then plated onto LB plates with kanamycin added at a concentration of 50µg/ml, and incubated at 37°C overnight.

Transformation of *A. thaliana*

100µl of a glycerol stock containing *Agrobacterium tumefaciens* strain GV3101 that harboured the plasmid to be transferred to plants was added to 10ml lysogeny broth (LB), along with 50µg/ml kanamycin. These mixtures were grown overnight on a shaker at 30°C, then added to 300ml LB and grown overnight on a shaker at 30°C again.

Once grown, the infiltration medium was made containing ½ Murashige and Skoog (MS) media (Sigma), 5% sucrose and 0.025% silwet L-77. The overnight cultures were centrifuged at 5000rpm for 15 minutes, and the resulting pellet resuspended in an equal volume of infiltration medium as the total overnight culture centrifuged.

A. thaliana plants are then dipped into the infiltration medium and left in the solution for 2 minutes, before being laid on their sides to allow excess infiltration medium to drain for 5 minutes. Plants were covered with a lid to maintain humidity for 48hrs, grown on to maturity, and seed collected.

To select transformed plants, seeds were sterilised with a 10 minute wash in 30% bleach, a 2 minute wash in 70% ethanol, which was repeated until no bleach scent remained. Sterilized seed were suspended in 0.1% agar and transferred to sterile MS plates containing 50µg/ml kanamycin for selection.

Embedding and Sectioning in JB-4®

100ml of FAA (formalin-acetic-alcohol) solution was prepared by mixing 50ml ethanol, 5ml glacial acetic acid, 10ml 37% formaldehyde, and 35ml distilled water. The tissue to be analysed was then dissected and immediately placed into the FAA solution for a minimum of 1 hour for fixation.

JB-4® infiltration solution was next prepared by mixing 1.25g of the catalyst (benzoyl peroxide, plasticized) with 100ml JB-4® solution A. This was mixed until dissolved. The tissue was then removed from the FAA solution and underwent a series of dehydration steps – 1 hour in 95% ethanol, then another hour in fresh 95% ethanol, followed by 1 hour in a mixture of 75% ethanol and 25% JB-4® infiltration solution, then 1 hour in a mixture of 50% ethanol and 50% JB-4® infiltration solution, then 1 hour in a mixture of 25% ethanol and 75% JB-4® infiltration solution, then 1 more hour in 100% JB-4® infiltration solution. After this, the tissue was left overnight in fresh 100% JB-4® infiltration solution, and this step was repeated the for the following night.

Prior to embedding, fresh JB-4® infiltration solution was made. The previous infiltration solution was replaced with this fresh batch and incubated at room temperature for 45 minutes. Immediately before beginning the embedding process, 25ml JB-4® infiltration solution was thoroughly mixed with 1ml JB-4® solution B. Directly after this, embedding began by flooding the mould with the new solution, and placing the samples into the wells of the flooded mould using tweezers. Once all samples were placed, the mould was covered with a layer of parafilm, ensuring no air bubbled remained between the parafilm and the solution. A petri dish was then placed on top of the parafilm, and a heavy weight placed on top of that, to ensure no air would enter. The solution was then allowed to harden

overnight, then was demoulded, and the samples placed into desiccant for 4-5 days to allow the blocks to fully harden.

Once hardened, the blocks were cut into 4 μ m sections via microtome. The resulting sections were stained by applying 0.05% toluidine blue for 10 seconds, and images were taken under a Zeiss Axioskop microscope with the 10x objective, using QCapture software.

H. vulgare Mutant Generation

CRISPR-Cas9 mutant generation was performed at the John Innes Centre, using the methods for generating gene knockouts described in Lawrenson & Harwood, 2019 and the methods for barley transformation described in Hinchliffe & Harwood, 2019. Once generated, plants were sent to Durham University in culture tubes. The plants were removed from the tubes, and their roots rinsed to remove any remaining culture medium. The plants were then planted into moist compost and covered with a propagator lid for the first week to maintain high humidity. The growth area was kept at a temperature of 15°C in the day, and 12°C at night. After the first week, the lid was removed, and the growth conditions were altered to standard greenhouse conditions (24°C; 16-8h light-dark cycle). Heterozygous lesions were detected in the M1 population by size polymorphism. M2 lines were tested for homozygosity and mutants were tested for loss of hygromycin resistance indicating that the editing cassette had been segregated out and thus the mutation was stable.

Barley Plant Growth

A solution was made by adding of 2 μ l gibberellic acid to 10ml water. *H. vulgare* seeds were added to this solution, and kept at 4°C for 3 days prior to sowing. Pots (10cm x 10cm x 20cm) were filled with a soil mixture containing a ratio of 6:1:1 potting compost:vermiculite:perlite, and 1 seed was sown into the centre of each pot. Plants were then grown in a greenhouse chamber conditions simulating long days (22hrs light, 2hrs dark) at 25°C. Pots were placed into large trays, able to store a maximum of 25 pots, and plants were watered regularly via these trays.

Lithograph X

Images of sections of *H. vulgare* vasculature were analysed using LithoGraphX v. 1.2.1, and was performed as previously described (de Reuille & Ragni, 2017; Wunderling et al., 2017). Sections were generated as per the method provided in this thesis. Images of vascular bundles were taken using a Leica 2500 microscope, using X5 and X10 objectives. Cell types were quantified within each vascular bundle by eye, and were identified based on visual assessment, anatomical features, and position within the vascular bundle (Crang et al., 2018; Esau, 1953). Following automatic segmentation, area was determined by calibrating pixel size to actual size within the LithographX program using graticule measurements. Total vascular bundle area was calculated by summing the cell areas of all vascular cells, plus the area of intercellular spaces.

Gross Morphological Measurements

All gross morphological measurements were done on mature (3 months old) *H. vulgare*, which had been allowed to dry completely to prevent differences due to water content variation. Measurements for tiller height were taken by cutting the tiller as close to the soil surface as possible, then measuring the length of the removed tiller using a tape measure. Measurements for tiller width were then done by using a pair of Vernier calipers just above the first node. Dry weight was measured by collecting all removed tillers and measuring their weight together on a set of scales. Number of internodes per tiller was recorded as each tiller was removed from the plant, and the number of tillers per plant was also recorded in this way.

Water Restriction

To investigate the role of water restriction, a set of plants were grown as per a modified version of the method described in the Barley Plant Growth section, including 25 pots being placed into each tray. The only alteration to this method was the frequency of watering and the amount of water given – plants which were to experience standard conditions were watered exactly twice a week, and given 4L of water per watering into the tray. Plants which were to experience water-restricted (termed “drought” as shorthand) conditions were watered exactly twice a week, and given 2L of water per watering into the tray. The higher value (used for the standard conditions) was chosen based on the approximate amount of water given to *H. vulgare* plants in other experiments contained in this thesis, with drought conditions then considered to be half of this. Measurements were performed as per the Gross Morphological Measurements section.

RNA Extraction:

Samples for RNA analysis were taken from *H. vulgare* plants which were approximately 3 months old, to gain insight into the impact of *HvPXY* on later stages of development. Node tissue was collected from the node 2nd from the top of the primary tiller of 4 separate individuals, and were frozen in liquid nitrogen.

Solutions were prepared in advance – lysis/binding buffer (LBB), washing buffer A (WBA), washing buffer B (WBB), and low salt buffer (LSB). For 50ml of LBB, 5ml of 1M pH 8 Tris-HCl, 6.25ml of 8M LiCl, 1ml of 500mM pH 8 EDTA, 5ml of 10% SDS, 250µl of 1M DTT, and 750µl of antifoam A were each added to 31.75ml RNase free water. For 50ml of WBA, 500µl of 1M pH 8 Tris-HCl, 940µl of 8M LiCl, 100µl of 500mM pH 8 EDTA, and 500µl of 10% SDS were each added to 47.60ml of RNase free water. For 50ml of WBB, 500µl of 1M pH 8 Tris-HCl, 940µl of 8M LiCl, and 100µl of 500mM pH 8 EDTA were added to 48.10ml of RNase free water. For 50ml of LSB, 1ml of 1M pH 8 Tris-HCl, 1.5ml of 5M NaCl, and 100µl of 500mM pH 8 EDTA were added to 47.40ml of RNase free water.

Before the RNA extraction, buffer LBB was prepared by adding 5µl of 2-mercaptoethanol per ml of buffer to be used. Samples were then ground under 200µl of the resulting LBB using a mortar and pestle for 1 minute. 200µl LBB was then added to the mortar and the samples were ground for a further minute. After this, another 200µl of LBB was added, or more if it was necessary, and the samples were ground for another minute. Samples were then centrifuged at maximum speed for 10 minutes, and the supernatant was collected. The supernatant was split into two equal portions, one to perform mRNA capture with, and the other to be frozen at -80°C as a backup.

For the mRNA capture, the sample lysate was heated to 65°C for 4 minutes, then was placed on ice. At this point a heat block was then turned on to 80°C in preparation for a later step. SeraMag Oligo (dT) Coated Magnetic particles were then vortexed and 40µl of the beads were distributed per prep. The samples were then placed on a magnet for 2-3 minutes, then removed and the supernatant was removed and replaced with 100µl LBB. The samples were then placed back onto the magnetic rack, the supernatant removed, and the beads then immediately resuspended with 200µl of sample lysate. The beads and lysate were mixed by pipetting, and the samples were placed on an agitator for 10 minutes at room temperature. The samples were again placed on a magnetic rack and the supernatant removed when clear. The beads were then washed with 200µl WBA, then the samples were removed from the magnet, mixed well by pipetting, then placed back onto the magnet before removing the supernatant. This process was repeated three times, once with a wash of 200µl WBB, and twice with a wash of 200µl LSB. The beads were then resuspended in 40µl TE and heated on the prepared heat block at 80°C for 2 minutes. The magnetic rack was heated to 60°C during this step, and once the step was completed the samples were transferred to the rack immediately and the supernatant transferred to new tubes. mRNA concentration was then quantified using a Qubit. Samples were then sent to and enriched and sequenced by Novogene in Cambridge, UK.

RNA Sequencing and Analysis:

As mentioned in the previous method, the steps in this section were performed by Novogene. All RNA samples were quality checked using a nanodrop to test the purity, with standard protocols from Novogene testing for an OD260/280 ratio of more than or equal to 2.0. All had agarose gel electrophoresis performed to test RNA degradation and contamination, and an Agilent 2100 to test RNA integrity, with standard protocols from Novogene seeking a value of more than or equal to 4.0. mRNA enrichment is done using dT oligo magnetic beads, as standard. 150 base pair, non-stranded, paired-end library construction was performed on cDNA synthesised from the mRNA. The library was then quality checked using a Qubit 2.0 fluorometer to test concentration, and an Agilent 2100 to test insert size. This was then quantified via qPCR. Libraries were then sequenced on the Illumina platform.

Raw data was transformed into sequenced reads via base calling, and recorded in FASTQ format. Error rates were calculated using the equation $Q_{\text{phred}} = -10\log_{10}e$. GC content distribution was evaluated to detect AT/GC separation. In sequencing for non-stranded libraries, it is typically expected that the number of G equals the number of C, and that the number of A equals the number of T, however AT/GC separation is typically observed in stranded libraries. Raw reads underwent data filtering to remove reads with adapter contamination or low quality, and read filtering was performed using FastQC (Available online at: <http://www.bioinformatics.babraham.ac.uk/projects/fastqc>). A summary of the data quality control can be found in Appendix H. Alignments were performed using HISAT2 (Kim et al., 2019) to the reference, and a summary of the mapping status can be found in Appendix I. The percentage of reads which mapped to exonic, intergenic and intronic regions

are shown in Appendix J. The reference genome used can be found at https://www.ebi.ac.uk/ena/browser/view/GCA_904849725.1. Quantification of gene expression level was done by measuring transcript abundance using FPKM (the expected number of Fragments Per Kilobase of transcript per Million base pairs sequenced), for which the software HTSeq (Putri et al., 2022) was used, using the union mode. The FPKM intervals, and specific examples of gene expression levels, can be found in Appendix K, and the reads per kilobase of transcript per million reads mapped (FKPM) distribution can be seen in Appendix L. Correlation between samples was determined using the Pearson correlation. Differential expression analysis was performed using DESeq2 (Love et al., 2014), using DESeq (Anders & Huber, 2010) as the normalization method, a negative binomial distribution as the p-value estimation model, and BH (Benjamini-Hochberg) procedure used as the FDR (false discovery rate) estimation method. Example differential expression analyses can be seen in Appendix M. Volcano plots of the differences between gene expression in WT and *pxy* samples were plotted, and cluster analysis of each gene was performed using FPKM cluster analysis. GO enrichment analysis was performed using Goseq (Young, n.d.). KEGG enrichment analysis was performed using Bioconductor (Gentleman et al., 2004). The GO database used was found on EnsemblPlants, and the collection of KEGG databases can be found at <https://www.genome.jp/kegg/pathway.html>.

Enrichnet Analysis:

A set of pathways was obtained using the BioMart section of the EnsemblPlants website (<https://plants.ensembl.org/index.html>), and a network obtained was from the STRING database (<https://string-db.org/>). EnsemblPlants was used to remain consistent with previous experiments, STRING was used to remain consistent with previous Enrichnet studies (Glaab et al., 2012). The pathways and network were then used with the Enrichnet R code included in Appendices B and C.

Embedding and Sectioning in Wax:

To make the fixative, first the required amount of 1x phosphate-buffered saline (PBS) was made up and set to pH 11 with NaOH. The solution was heated to between 60 and 70°C, then paraformaldehyde was added such that the end solution would be 4% paraformaldehyde. Once dissolved, the solution was placed on ice to cool to 4°C, then the pH of the solution was set to pH 7 with H₂SO₄. Dimethylsulfoxide (DMSO) was added to the solution such that that the end solution would be 4% DMSO.

The tissue to be embedded was collected into ice cold fixative. A vacuum was applied to the samples until the paraformaldehyde started to bubble. The vacuum was held for 15 minutes, then released slowly. This process was repeated until the tissue began to sink, or if the tissue was too light to sink the process was repeated 3 times. The fixative was replaced and the samples were shaken gently overnight at 4°C.

The next day, several solution changes took place, all at 4°C and with shaking. The first solution change was into 1x PBS for 30 minutes, then a 1 hour wash in 40% ethanol, then 1 hour in 50% ethanol, then 1 hour in 60% ethanol, then 1 hour in 70% ethanol, then 1 hour in 85% ethanol, then overnight in a mixture of 95% ethanol and 0.5g eosin B. The following day, further solution changes were made under the same conditions as previous. Two washes in a solution of 100% ethanol and 0.5g eosin were performed for 30 minutes each, followed by a 30 minute wash in 25% histoclear and 75% ethanol, then a 30 minute wash in 50% histoclear and 50% ethanol, a 30 minute wash in 75% histoclear and 25% ethanol, then two 1 hour washes in 100% histoclear, then an overnight wash overnight with no shaking in a mixture of 100% histoclear and enough paraplast wax chips to equal a half of the overall volume. The next day, the solution was placed at 55°C until the chips were melted

completely, then more paraplast chips were added equal to a quarter of the volume of the solution. The solution was moved to 60°C until the chips melted, then the solution was replaced completely with freshly melted wax and left overnight at 60°C. The next day, the solution was replaced twice with fresh molten wax, each replacement separated by several hours.

After these solution changes, the tissue was embedded using disposable embedding moulds and histology cassettes, and allowed to harden for at least 1 day at 4°C. Samples were unmoulded and excess wax was removed using a razor blade prior to sectioning.

Once the wax blocks had been prepared as above, they were cut into 8µm sections via microtome. The resulting sections were then prepared for *in situ* hybridisation.

In situ Probe Synthesis

Sequences for *HvPXY* and *HvHisH4* were identified using Gramene's BLAST function. Primers were then designed using Benchling, and ordered from Eurofins (Appendix D). PCR was performed using cDNA as the template, with each reaction containing 15µl 2x VeriFi™ Polymerase, 1µl each of the forward and reverse primers, 12µl of water, and 1µl of the template. The completed PCR reactions were run on a 1% agarose gel via gel electrophoresis to check the success of the PCR reactions. A PCR cleanup was performed using Ampure beads to the manufacturer's specifications, then a ligation reaction was performed on each reaction using 2.5µl of 2 x ligation buffer, 0.5µl of pGEM-T-easy, 0.5µl of DNA ligase, 1µl of the PCR product, and 1µl of water, and these reactions were left at 4°C overnight. Competent *E. coli* cells were then transformed with the ligation reaction and incubated overnight as per the Transformation of *E. coli* method in this thesis.

Colony PCR was performed on colonies obtained from the plates, using reactions containing 7.5µl 2x biomix red, 0.5µl each of M13 forward and reverse primers, 1µl of template, and 5.5µl water. The PCR products then underwent gel electrophoresis on a 1% agarose gel to determine which colonies contained the sequences desired, and these successful colonies were then resuspended in 3ml LB plus carbenicillin and left at 37°C overnight on a shaking plate. DNA was then isolated using a Monarch Plasmid Miniprep Kit, and the quality of the DNA tested via nanodrop. Samples were then sequenced using Applied Biosystems 3730 capillary instrumentation using the original primers, and the quality and orientation of the samples was checked via Benchling sequence comparison. PCR was performed again to linearise the sequence of interest, using 15µl 2 x VeriFi™ Polymerase, 12µl water, 1µl each of

M13 forward and reverse primers, and 1µl of template. The concentration and quality of the resulting DNA was tested again via nanodrop.

The linearised product was then cleaned with the Ampure bead cleanup mentioned previously, was mixed with enough DEPC-treated water to reach 300ng of DNA per reaction. 17.5µl of this DNA was then mixed with 2.5µl of 10x polymerase buffer, 1µl of RNase inhibitor, 2.5µl 10x NTP mix containing dioxigenin (DIG) -11-uridine triphosphate (UTP) for labelling, and 1µl of RNA polymerase (T7/SP6). These mixtures were incubated at 37°C for 1 hour. 75µl of water, 1µl of 100mg/ml tRNA, and 1µl RNase-free DNase was then added to each mixture, and incubated at 37°C for a further 10 minutes. 100µl of 4M ammonium acetate and 400µl ethanol were then added, and the mixtures were incubated overnight at -80°C. These were then centrifuged at maximum speed for 30 minutes, the supernatant removed, and the pellet dissolved in 100µl 50% deionised formamide in DEPC-treated water, and then stored at -80°C until needed.

A blot was then performed to check probe synthesis. 6µl of sample was mixed with 3µl of 50% de-ionised formamide and 50% formaldehyde. The mixtures were heated to 80°C for 3 minutes, and then these were run at 180V on a meniscus minigel made with equipment washed in 2M NaOH to remove possible RNase. The gel was then blotted by placing it upside down on a layer of cling film, then adding 1 wetted sheet of Hybond N, 1 wetted sheet of Whatman, 1 dry sheet of Whatman, and 3-4 layers of paper towel, all sheets cut to be slightly larger than the size of the gel beforehand. This parcel was then wrapped in cling film, and a dummy parcel of equal weight was made. The parcel was inverted and spun in a µtitre plate rotor at 3000rpm for 5 minutes. The Hybond N was then recovered and the RNA fixed in a Stratolinker. The sheet was then blocked for 15 minutes in 1% Boehringer block in

100mM Tris pH 7.5 and 150mM NaCl (Buffer 1). The sheet was washed briefly in more Buffer 1, then 5ml of Buffer 1 was mixed with 1 μ l anti-DIG antibody, and the sheet was left in this solution for 20 minutes. It was then washed twice for 10 minutes each in more Buffer 1, then incubated overnight in nitro blue tetrazolium/5-bromo-4-chloro-3-indolyl phosphate (NBT/BCIP).

In situ Hybridisation

Tissue samples on polysine slides were put through a variety of wash steps. First, two 10 minute washes in histoclear, followed by two 2 minute washes in 100% ethanol. They then a series of 2 minute washes in 95% ethanol, 90% ethanol, 80% ethanol, 60% ethanol, 30% ethanol, and water were performed. After this, they were washed for 5 minutes in 2x saline-sodium citrate (SSC), then for 30 minutes at 37°C in a proteinase K solution (15µl of 20mg/ml stock in 300ml DEPC-treated water). They were then transferred back to room temperature and placed into 2% glycine for 2 minutes, then had two 2 minute washes in PBS. This was followed by a 10 minute wash in 4% formaldehyde, then another two 2 minutes washes in PBS. In a fume hood, the slides were then placed into a triethanolamine buffer, which was being stirred vigorously by a stir bar. 3ml acetic anhydride was added dropwise to the solution, then the stirrer was slowed down and the slides remained in the solution for 10 minutes. There were then two 5 minute washes in PBS, followed by a 30 second wash in each of the previous ethanol series, from 30% to 100%. Slides were then stored in a rack over a small amount of 100% ethanol in a closed box while preparing the probes.

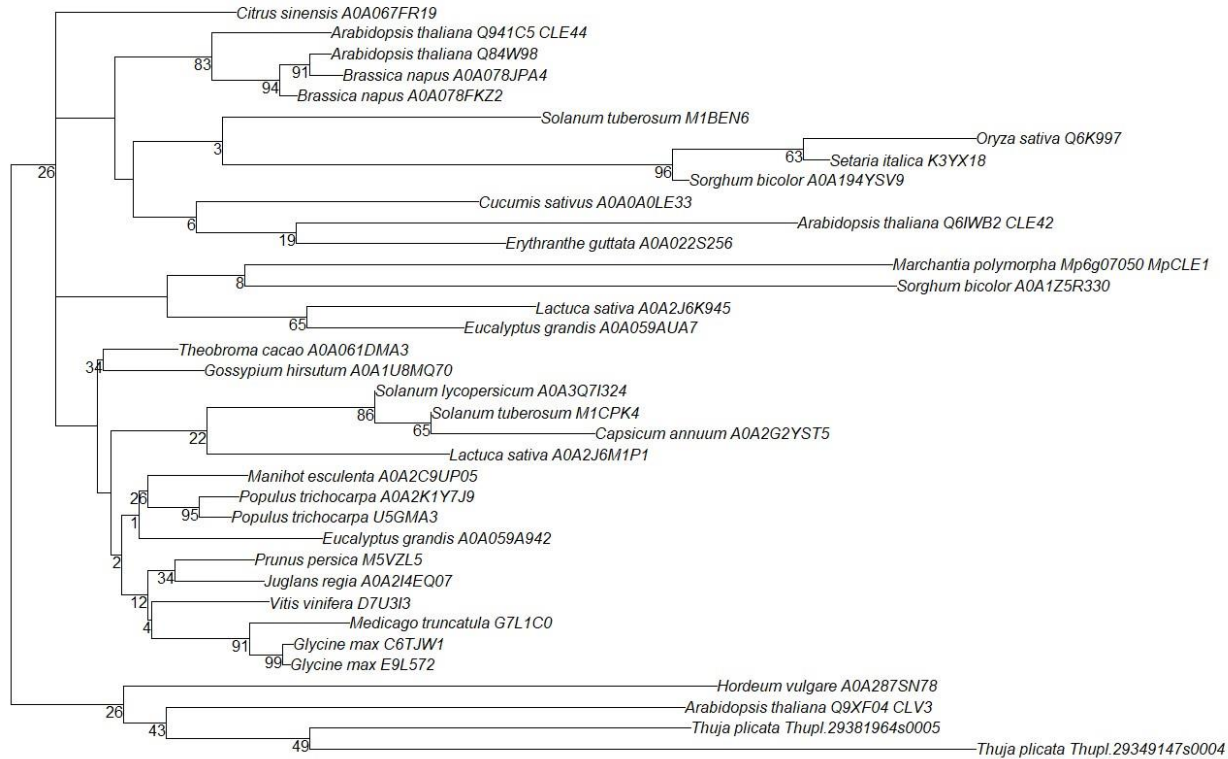
For a rack of 30 slides, a hybridisation mix containing 750µl 10x in situ salts, 594µl DEPC-treated water, 75µl 100x Denhardt's salts, 75µl 100mg/ml tRNA, 3000µl de-ionised formamide, and 6µl Triton X100 was made. Individual solutions were then be prepared for each probe to be used. The proportions sufficient for 1 slide were 1µl probe, 24µl DEPC-treated water, 24µl formamide, and 200µl hybridisation mix.

Four paper towels were then dampened with water and placed in the bottom of a long box. These towels were then covered with parafilm, and a rack added on top of the parafilm, such that the slides did not touch the towels when rested on the rack. The probe mix was

denatured by heating it to 80°C for 3 minutes, then placed on ice. One pair of slides at a time were removed from the slide rack, 250µl of probe mix was applied to each slide, and plastic hybridisation coverslips were placed over them. Once all slides were prepared, they were placed in the box and incubated at 55°C overnight. For a rack of 30 slides, a hybridisation mix containing 750µl 10x in situ salts, 594µl DEPC-treated water, 75µl 100x Denhardt's salts, 75µl 100mg/ml tRNA, 3000µl de-ionised formamide, and 6µl Triton X100 was made. Individual solutions were then prepared for each distinct probe to be used. The proportions sufficient for 1 slide are 1µl probe, 24µl DEPC-treated water, 24µl formamide, and 200µl hybridisation mix.

The next day, the coverslips were removed from the slides in a beaker filled with pre-warmed 0.2x SSC. The slides were then placed into a rack and kept in a box of warm 0.2x SSC. The slides were washed in another series of solutions, beginning with three 45 minute washes in 0.2x SSC at 55°C with gentle agitation. This was followed by a 5 minute wash in 1x Tris-buffered saline (TBS), then a 60 minute wash in 1% Roche block. Anti-DIG antibody was diluted in a ratio of 1:3000 in TBS-Tween[®] 20 (TBS-T), and the slides were then washed in this solution for 2 hours. They then had 4 10 minute washes in TBS-T, then they were immersed into NBT-BCIP premade solution and left in the dark for 1 to 3 days, until the signal developed. The slides were then rinsed in TE, then in water, and once dried they were mounted using Histomount. Slide images were then taken under a Zeiss Axioskop microscope with the 10x objective, using QCapture software.

Appendix B: CLE dendrogram with bootstrap values



Appendix C: Sequences and alignment of *HvPXY*, *Hvpxy-1* and *Hvpxy-2*

```
>HvPXY
MCMAHGKKLEQWRLLLSSRQSRFLFLSCMQSQACPTTAIITARSLSFSTPLSLSSSTTTTTTTPSSFRASHHDVHAPVQHRHYLSLLHFTIASPPH
TANTPTNTMAAQVPFHGLLLVLPLLTITAASSAPLPLLALLSLKSSLNDPAGALSPWYAAAAASAGATRSLSPPCAWPGVACDAATGDVVGVD
LSRRNLSGTVSPTAAALLAPTLASLNLSWNAFTGELPPAVFLLRRLVKLDISHNFFNSTFPDGITKLGSLAVLDAYSNCFVQQLPRGIRELHRL
EHLNLGGSFFNGSIPVEVQGLRQLRFLHLAGNALSGRLPKELGELPPLERLEIGYNGYNGGIPAEFGGLTQLQYLDIAAANASGPLPELGGLA
RLEYLFLFKNRLAGAIPPPWSRLRALQVLDLSDNHLAGVIPAGLGELANLTTLNVMNSFLSGTIPATIGELPNLEVLQWNNSLTGRLPELLGA
NGRLVRLDVSTNSLSGPIPSGLCAGHRLRLILFANRFDSAIPASLANCSSLWRVRLSNRLTGAI PSFGFVAVQNTLYMDLSSNELTGGIPADL
VISPSLEYLNVSGNPMGGTLPSTNTRAPKLQVLAASKCALDGEIPFFGTSGCANLYRLELAWNELSGAVPGDIGSCKRLVSLRLQHNNLSGEIP
AVLAALPSVTEVDLSWNGLTGSI PPGVANCTTLETFDVSFNHLAPVGTSPRSNPTEGESSARHAAAMWVSAVAVAFAGMVLALTAGWLQCLED
DSVAANGGGAGGARPNVVGWPRMTAFQRLSFTADDVVRCEVSDGIVGAGSSGTVYRAKMPNGEVI AVKKLWQAPGQKETAADHAAKQMDTQE
GGDGNERVLAEVEMLGHLRHRNIVRLGLCTNGETMMLLYEYMPNGSLDELLHGATAGKMPKARPEWDARYRIAVGVAQGVSYLHHDCLPAVAH
RDLKPSNILLDDMEARVADFGVAKALQGAAPMSVVAGSCGYIAPEYTYTLRVDEKSDVY SYGVVLEILTGRGSVEAEYGEESNIVDWVRCKV
AGGGGGLRDVMEHVGGSSAAAREEMALVLRVALLCTSRCPQDRPSMRDVLMSLQEARPRPSQKPAAKHVYGVPRS
```

```
>Hvpxy-1
MCMAHGKKLEQWRLLLSSRQSRFLFLSCMQSQACPTTAIITARSLSFSTPLSLSSSTTTTTTTPSSFRASHHDVHAPVQHRHYLSLLHFTIASPPH
TANTPTNTMAAQVPFHGLLLVLPLLTITAASSAPLPLLALLSLKSSLNDPAGALSPWYAAAAASAGATRSLSPPCAWPGVACDAATGDVVGVD
LSRRNLSGTVSPTAAALLAPTLASLNLSWNAFTGELPPAVFLLRRLVKLDISHNFFNSTFPDGITKLGSLAVLDAYSNCFVQQLPRGIHSTST
SVAVSSMGAFRSRLDSFGSYASCTSLGTPYRGGCRRSSASSRCSNALRSGIMATMVAYQRSSVG
```

```
>Hvpxy-2
MCMAHGKKLEQWRLLLSSRQSRFLFLSCMQSQACPTTAIITARSLSFSTPLSLSSSTTTTTTTPSSFRASHHDVHAPVQHRHYLSLLHFTIASPPH
TANTPTNTMAAQVPFHGLLLVLPLLTITAASSAPLPLLALLSLKSSLNDPAGALSPWYAAAAASAGATRSLSPPCAWPGVACDAATGDVVGVD
LSRRNLSGTVSPTAAALLAPTLASLNLSWNAFTGELPPAVFLLRRLVKLDISHNFFNSTFPDGITKLGSLAVLLHLAGNALSGRLPKELGELPL
LERLEIGYNGYNGGIPAEFGGLTQLQYLDIAAANASGPLPELGGGLARLEYLFLFKNRLAGAI PPPWSRLRALQVLDLSDNHLAGVIPAGLGEL
ANLTTLNVMNSFLSGTIPATIGELPNLEVLQWNNSLTGRLPELLGANGRLVRLDVSTNSLSGPIPSGLCAGHRLRLILFANRFDSAIPASLA
NCSSLWRVRLSNRLTGAI PSFGFVAVQNTLYMDLSSNELTGGIPADLVISPSLEYLNVSGNPMGGTLPSTNTRAPKLQVLAASKCALDGEIPFF
GTSGCANLYRLELAWNELSGAVPGDIGSCKRLVSLRLQHNNLSGEIPAVLAALPSVTEVDLSWNGLTGSI PPGVANCTTLETFDVSFNHLAPVG
TPSRNPTEGESSARHAAAMWVSAVAVAFAGMVLALTAGWLQCLEDSDVAANGGGAGGARPNVVGWPRMTAFQRLSFTADDVVRCEVSDGIVGAGSSGT
VYRAKMPNGEVI AVKKLWQAPGQKETAADHAAKQMDTQEGGDNERVLAEVEMLGHLRHRNIVRLGLCTNGETMMLLYEYMPNGS
LDELLHGATAGKMPKARPEWDARYRIAVGVAQGVSYLHHDCLPAVAHRDLKPSNILLDDMEARVADFGVAKALQGAAPMSVVAGSCGYIAPEY
TYTLRVDEKSDVY SYGVVLEILTGRGSVEAEYGEESNIVDWVRCKVAGGGGGLRDVMEHVGGSSAAAREEMALVLRVALLCTSRCPQDRPSMR
DVLMSLQEARPRPSQKPAAKHVYGVPRS
```

CLUSTAL O(1.2.4) multiple sequence alignment

		vUniprot start	
Hvpxy-1	MCMAHGKKLEQWRLLLSSRQSRFLFLSCMQSQACPTTAIITARSLSFSTPLSLSSSTTTTTTT	60	
HvPXY	MCMAHGKKLEQWRLLLSSRQSRFLFLSCMQSQACPTTAIITARSLSFSTPLSLSSSTTTTTTT	60	
Hvpxy-2	MCMAHGKKLEQWRLLLSSRQSRFLFLSCMQSQACPTTAIITARSLSFSTPLSLSSSTTTTTTT	60	

Hvpxy-1	TPSSFRASHHDVHAPVQHRHYLSLLHFTIASPPHTANTPTNTMAAQVPFHGLLLVLPLLT	120	
HvPXY	TPSSFRASHHDVHAPVQHRHYLSLLHFTIASPPHTANTPTNTMAAQVPFHGLLLVLPLLT	120	
Hvpxy-2	TPSSFRASHHDVHAPVQHRHYLSLLHFTIASPPHTANTPTNTMAAQVPFHGLLLVLPLLT	120	

Hvpxy-1	ITAASSAPLPLLALLSLKSSLNDPAGALSPWYAAAAASAGATRSLSPPCAWPGVACDAA	180	
HvPXY	ITAASSAPLPLLALLSLKSSLNDPAGALSPWYAAAAASAGATRSLSPPCAWPGVACDAA	180	
Hvpxy-2	ITAASSAPLPLLALLSLKSSLNDPAGALSPWYAAAAASAGATRSLSPPCAWPGVACDAA	180	

Hvpxy-1	TGDVVGVDLSRRNLSGTVSPTAAALLAPTLASLNLSWNAFTGELPPAVFLLRRLVKLDIS	240	
HvPXY	TGDVVGVDLSRRNLSGTVSPTAAALLAPTLASLNLSWNAFTGELPPAVFLLRRLVKLDIS	240	
Hvpxy-2	TGDVVGVDLSRRNLSGTVSPTAAALLAPTLASLNLSWNAFTGELPPAVFLLRRLVKLDIS	240	

Hvpxy-1	HNFFNSTFPDGITKLGSLAVLDAYSNCFVQQLPRGIHSTSTSVAVSSMGAFRSRL----	287	
HvPXY	HNFFNSTFPDGITKLGSLAVLDAYSNCFVQQLPRGIRELHRLHHLNLGGSFFNGSIPVEV	300	
Hvpxy-2	HNFFNSTFPDGITKLGSLAV-----	260	

Hvpxy-1	DSFGSYASCTSLGTPYRGGCRRSSASSRC-----SNALRSGIMATMV-----AYQ---	332	
HvPXY	GQLRQLRFLHLAGNALSGRLPKELGELPPLERLEIGYNGYNGGIPAEFGGLTQLQYLDIA	360	
Hvpxy-2	-----LLHLAGNALSGRLPKELGELPPLERLEIGYNGYNGGIPAEFGGLTQLQYLDIA	313	
	* . * : . . . * . . . * * :		

Hvpxy-1	-----RSSVG-----	337
HvPXY	AANASGPLPELGGGLARLEYLFLFKNRLAGAIPPPWSRLRALQVLDLSDNHLAGVIPAGL	420
Hvpxy-2	AANASGPLPELGGGLARLEYLFLFKNRLAGAIPPPWSRLRALQVLDLSDNHLAGVIPAGL	373
	. . *	
Hvpxy-1	-----	337
HvPXY	GELANLTTLVMSNFLSGTIPATIGELPNLEVLQWNNSLTGRLPELLGANGRLVRLDVS	480
Hvpxy-2	GELANLTTLVMSNFLSGTIPATIGELPNLEVLQWNNSLTGRLPELLGANGRLVRLDVS	433
Hvpxy-1	-----	337
HvPXY	TNSLSGPIPSGLCAGHRLRLILFANRFDSAIPASLANCSSLWRVRLESNRLTGAIPSGF	540
Hvpxy-2	TNSLSGPIPSGLCAGHRLRLILFANRFDSAIPASLANCSSLWRVRLESNRLTGAIPSGF	493
Hvpxy-1	-----	337
HvPXY	GAVQNLTYMDLSSNELTGGIPADLVISPSLEYLNVSGNPMGGTLPNTWRAPKLQVLAAS	600
Hvpxy-2	GAVQNLTYMDLSSNELTGGIPADLVISPSLEYLNVSGNPMGGTLPNTWRAPKLQVLAAS	553
Hvpxy-1	-----	337
HvPXY	KCALDGEIPPFGTSGCANLYRLELAWNELSGAVPGDIGSCKRLVSLRLQHNNLSGEIPAV	660
Hvpxy-2	KCALDGEIPPFGTSGCANLYRLELAWNELSGAVPGDIGSCKRLVSLRLQHNNLSGEIPAV	613
Hvpxy-1	-----	337
HvPXY	LAALPSVTEVDLSWNGLTGSI PPGVANCTTLETFDVSFNHLAPVGTPSRSPNTGEGSSAR	720
Hvpxy-2	LAALPSVTEVDLSWNGLTGSI PPGVANCTTLETFDVSFNHLAPVGTPSRSPNTGEGSSAR	673
Hvpxy-1	-----	337
HvPXY	HAAAMWVS AVAVAFAGMVV LALTAGWLQCLEDDSV AANGGGAGGARPNVVVGPWRMTAFQ	780
Hvpxy-2	HAAAMWVS AVAVAFAGMVV LALTAGWLQCLEDDSV AANGGGAGGARPNVVVGPWRMTAFQ	733
Hvpxy-1	-----	337
HvPXY	RLSFTADDVVRCEVSGDGI V GAGSSGT VYRAKMPNGEVI AVKKLWQAPGQKETAADHAAK	840
Hvpxy-2	RLSFTADDVVRCEVSGDGI V GAGSSGT VYRAKMPNGEVI AVKKLWQAPGQKETAADHAAK	793
Hvpxy-1	-----	337
HvPXY	QMDTQEGGDGNERVLA E V E M L G H L R H R N I V R L L G L C T N G E T T M L L Y E Y M P N G S L D E L L H G	900
Hvpxy-2	QMDTQEGGDGNERVLA E V E M L G H L R H R N I V R L L G L C T N G E T T M L L Y E Y M P N G S L D E L L H G	853
Hvpxy-1	-----	337
HvPXY	ATAGKMPKARPEWDARYRIA V G V A Q G V S Y L H H D C L P A V A H R D L K P S N I L L D D D M E A R V A D	960
Hvpxy-2	ATAGKMPKARPEWDARYRIA V G V A Q G V S Y L H H D C L P A V A H R D L K P S N I L L D D D M E A R V A D	913
Hvpxy-1	-----	337
HvPXY	FGVAKALQGAAPMSV V A G S C G Y I A P E Y T Y T L R V D E K S D V Y S Y G V V L L E I L T G R G S V E A E Y	1020
Hvpxy-2	FGVAKALQGAAPMSV V A G S C G Y I A P E Y T Y T L R V D E K S D V Y S Y G V V L L E I L T G R G S V E A E Y	973
Hvpxy-1	-----	337
HvPXY	GEGSNIVDWVRCKVAGGGGLRDVMEHVGGSS EAAREEMALVLRVALLCTSRCPQDRPSM	1080
Hvpxy-2	GEGSNIVDWVRCKVAGGGGLRDVMEHVGGSS EAAREEMALVLRVALLCTSRCPQDRPSM	1033
Hvpxy-1	----- 337	
HvPXY	RDVLSMLQEARPRPSQKPAAKHVYGVPRS 1109	
Hvpxy-2	RDVLSMLQEARPRPSQKPAAKHVYGVPRS 1062	
Hvpxy-2	ATGTGTATGGCACATGGAAAAAGCTAGAGCAATGGCGGCTGCTGCTCAGCAGCAGGCAA	60
HvPXY	ATGTGTATGGCACATGGAAAAAGCTAGAGCAATGGCGGCTGCTGCTCAGCAGCAGGCAA	60

Hvpxy-1	ATGTGTATGGCACATGGAAAAAGCTAGAGCAATGGCGGCTGCTGCTCAGCAGCAGGCAA *****	60
Hvpxy-2	AGTCGTCTCTTTCTTTCTTTCATGCAAAGCCAAGCCTGCCCGACCACGGCCATCATCACC	120
HvPXy	AGTCGTCTCTTTCTTTCTTTCATGCAAAGCCAAGCCTGCCCGACCACGGCCATCATCACC	120
Hvpxy-1	AGTCGTCTCTTTCTTTCTTTCATGCAAAGCCAAGCCTGCCCGACCACGGCCATCATCACC *****	120
Hvpxy-2	ACCGCGCGCTCTCTTCTTCTCCACTCCACTCTCCCTGTCCCTCCACCACCACCACCACC	180
HvPXy	ACCGCGCGCTCTCTTCTTCTCCACTCCACTCTCCCTGTCCCTCCACCACCACCACCACC	180
Hvpxy-1	ACCGCGCGCTCTCTTCTTCTCCACTCCACTCTCCCTGTCCCTCCACCACCACCACCACC *****	180
Hvpxy-2	ACCCCTCCTCCTTCCGAGCCTCTCATCATGATGTGCATGCACCAGTGCAACACCGCCAT	240
HvPXy	ACCCCTCCTCCTTCCGAGCCTCTCATCATGATGTGCATGCACCAGTGCAACACCGCCAT	240
Hvpxy-1	ACCCCTCCTCCTTCCGAGCCTCTCATCATGATGTGCATGCACCAGTGCAACACCGCCAT *****	240
Hvpxy-2	TACCTTTCTCTCCTCCATTTTACCATCGCCTCCCCTCCTCACACCGCCAACACCCCTACC	300
HvPXy	TACCTTTCTCTCCTCCATTTTACCATCGCCTCCCCTCCTCACACCGCCAACACCCCTACC	300
Hvpxy-1	TACCTTTCTCTCCTCCATTTTACCATCGCCTCCCCTCCTCACACCGCCAACACCCCTACC *****	300
Hvpxy-2	AATACCATGGCCGCACAGGTCCCCTTCCATGGCCTCCTGCTTGTGCTCCCGCTCCTCACC	360
HvPXy	AATACCATGGCCGCACAGGTCCCCTTCCATGGCCTCCTGCTTGTGCTCCCGCTCCTCACC	360
Hvpxy-1	AATACCATGGCCGCACAGGTCCCCTTCCATGGCCTCCTGCTTGTGCTCCCGCTCCTCACC *****	360
Hvpxy-2	ATCACAGCCGCGTCGTCGGCGCCGCTCCCCTGCTCGCGCTTCTCTCTCAAGTCTCCTCC	420
HvPXy	ATCACAGCCGCGTCGTCGGCGCCGCTCCCCTGCTCGCGCTTCTCTCTCAAGTCTCCTCC	420
Hvpxy-1	ATCACAGCCGCGTCGTCGGCGCCGCTCCCCTGCTCGCGCTTCTCTCTCAAGTCTCCTCC *****	420
Hvpxy-2	CTGAACGACCCGGCCGGCGCGCTGAGCCCATGGACGTACGCCGCCGGCCCTCCGCAGGC	480
HvPXy	CTGAACGACCCGGCCGGCGCGCTGAGCCCATGGACGTACGCCGCCGGCCCTCCGCAGGC	480
Hvpxy-1	CTGAACGACCCGGCCGGCGCGCTGAGCCCATGGACGTACGCCGCCGGCCCTCCGCAGGC *****	480
Hvpxy-2	GCCACTCGGTGCGTCTCCCCTCCGTGGTGCGCATGGCCCGGTGTCGCGTGCGACGCGGCC	540
HvPXy	GCCACTCGGTGCGTCTCCCCTCCGTGGTGCGCATGGCCCGGTGTCGCGTGCGACGCGGCC	540
Hvpxy-1	GCCACTCGGTGCGTCTCCCCTCCGTGGTGCGCATGGCCCGGTGTCGCGTGCGACGCGGCC *****	540
Hvpxy-2	ACAGGTGACGTCGTCGGGGTTGATCTGTCTCGTCGCAACCTATCCGGTACCGTCTCCCC	600
HvPXy	ACAGGTGACGTCGTCGGGGTTGATCTGTCTCGTCGCAACCTATCCGGTACCGTCTCCCC	600
Hvpxy-1	ACAGGTGACGTCGTCGGGGTTGATCTGTCTCGTCGCAACCTATCCGGTACCGTCTCCCC *****	600
Hvpxy-2	ACGGCCGCCGCGCTGCTCGCACCAGCCTGGCTTCGCTCAACCTCAGCTGGAACGCCTTC	660
HvPXy	ACGGCCGCCGCGCTGCTCGCACCAGCCTGGCTTCGCTCAACCTCAGCTGGAACGCCTTC	660
Hvpxy-1	ACGGCCGCCGCGCTGCTCGCACCAGCCTGGCTTCGCTCAACCTCAGCTGGAACGCCTTC *****	660
Hvpxy-2	ACGGGGGAGCTCCCGCCGGCGGTGTTCTTGCTCCGTCGCTTGTGAAGCTTGACATCAGC	720
HvPXy	ACGGGGGAGCTCCCGCCGGCGGTGTTCTTGCTCCGTCGCTTGTGAAGCTTGACATCAGC	720
Hvpxy-1	ACGGGGGAGCTCCCGCCGGCGGTGTTCTTGCTCCGTCGCTTGTGAAGCTTGACATCAGC *****	720
Hvpxy-2	CACAATTCTTCAACTCCACCTTCCCCGACGGCATTACCAAGCTCGGCTCTCTCGCCGTC	780
HvPXy	CACAATTCTTCAACTCCACCTtccccgacggcattaccaagctcggtctctctcgccgtc	780
Hvpxy-1	CACAATTCTTCAACTCCACC----- *****	741
Hvpxy-2	CTCC-----	784
HvPXy	TTCCCCGACGGCATTACCAAGCTCGGCTCTCTCGCCGTCCTCGACGCTACAGCAACTGT	840
Hvpxy-1	-----	741

Hvpxy-2	-----	784
HvPXY	TTCGTGGGCCAGCTTCCCCGCGGCATCCGGGAGCTCCACAGACTCGAGCACCTCAACCTC	900
Hvpxy-1	-----TACTCGAGCACCTCAACCTC	761
Hvpxy-2	-----	784
HvPXY	GGTGGCAGTTTCTTCAATGGGAGCATTCGGTTCGAGGTTGGACAGCTTCGGCAGCTACGC	960
Hvpxy-1	GGTGGCAGTTTCTTCAATGGGAGCATTCGGTTCGAGGTTGGACAGCTTCGGCAGCTACGC	821
Hvpxy-2	----TGCACCTCGCTGGGAACGCCCTATCGGGGCGGCTGCCGAAGGAGCTCGGCGAGCTC	840
HvPXY	TTCTTGCACCTCGCTGGGAACGCCCTATCGGGGCGGCTGCCGAAGGAGCTCGGCGAGCTC	1020
Hvpxy-1	TTCTTGCACCTCGCTGGGAACGCCCTATCGGGGCGGCTGCCGAAGGAGCTCGGCGAGCTC	881

Hvpxy-2	CCGCTGCTCGAACGCCTTGAGATCGGGTATAATGGCTACAATGGTGGCATAACCAGCGGAG	900
HvPXY	CCGCTGCTCGAACGCCTTGAGATCGGGTATAATGGCTACAATGGTGGCATAACCAGCGGAG	1080
Hvpxy-1	CCGCTGCTCGAACGCCTTGAGATCGGGTATAATGGCTACAATGGTGGCATAACCAGCGGAG	941

Hvpxy-2	TTCGGTGGGCTAACGCAGCTCCAGTACCTCGACATCGCCGCGGCAAACGCGTCCGGCCCG	960
HvPXY	TTCGGTGGGCTAACGCAGCTCCAGTACCTCGACATCGCCGCGGCAAACGCGTCCGGCCCG	1140
Hvpxy-1	TTCGGTGGGCTAACGCAGCTCCAGTACCTCGACATCGCCGCGGCAAACGCGTCCGGCCCG	1001

Hvpxy-2	CTTCCGCCGGAGCTCGGCGGGCTCGCGCGGCTCGAATATCTGTTTCTGTTCAAGAACAGG	1020
HvPXY	CTTCCGCCGGAGCTCGGCGGGCTCGCGCGGCTCGAATATCTGTTTCTGTTCAAGAACAGG	1200
Hvpxy-1	CTTCCGCCGGAGCTCGGCGGGCTCGCGCGGCTCGAATATCTGTTTCTGTTCAAGAACAGG	1061

Hvpxy-2	CTAGCCGGCGCGATACCGCCGCCGTGGTTCGCGCCTCCGAGCGCTGCAGGTTCTTGACCTG	1080
HvPXY	CTAGCCGGCGCGATACCGCCGCCGTGGTTCGCGCCTCCGAGCGCTGCAGGTTCTTGACCTG	1260
Hvpxy-1	CTAGCCGGCGCGATACCGCCGCCGTGGTTCGCGCCTCCGAGCGCTGCAGGTTCTTGACCTG	1121

Hvpxy-2	TCCGACAACCATCTCGCCGGAGTTATCCCCGCCGGTCTCGGCGAACTCGCGAATCTCAGC	1140
HvPXY	TCCGACAACCATCTCGCCGGAGTTATCCCCGCCGGTCTCGGCGAACTCGCGAATCTCAGC	1320
Hvpxy-1	TCCGACAACCATCTCGCCGGAGTTATCCCCGCCGGTCTCGGCGAACTCGCGAATCTCAGC	1181

Hvpxy-2	ACGCTGAATGTCATGAGCAACTTCCTCTCCGGCACGATCCCGGCGACGATCGGTGAGCTT	1200
HvPXY	ACGCTGAATGTCATGAGCAACTTCCTCTCCGGCACGATCCCGGCGACGATCGGTGAGCTT	1380
Hvpxy-1	ACGCTGAATGTCATGAGCAACTTCCTCTCCGGCACGATCCCGGCGACGATCGGTGAGCTT	1241

Hvpxy-2	CCCAATCTCGAGGTGCTGCAATTGTGGAACAACCTCGCTCACTGGGAGGCTGCCGGAGTTG	1260
HvPXY	CCCAATCTCGAGGTGCTGCAATTGTGGAACAACCTCGCTCACTGGGAGGCTGCCGGAGTTG	1440
Hvpxy-1	CCCAATCTCGAGGTGCTGCAATTGTGGAACAACCTCGCTCACTGGGAGGCTGCCGGAGTTG	1301

Hvpxy-2	CTCGGAGCGAACGGGCGGCTCGTTCGCTTGACGTGTCGACTAACTCCCTCTCCGGCCCG	1320
HvPXY	CTCGGAGCGAACGGGCGGCTCGTTCGCTTGACGTGTCGACTAACTCCCTCTCCGGCCCG	1500
Hvpxy-1	CTCGGAGCGAACGGGCGGCTCGTTCGCTTGACGTGTCGACTAACTCCCTCTCCGGCCCG	1361

Hvpxy-2	ATCCCGTCCGGACTCTGCGCCGGCCACCGTCTCCTCCGCTCATCCTATTCCGCAACCGA	1380
HvPXY	ATCCCGTCCGGACTCTGCGCCGGCCACCGTCTCCTCCGCTCATCCTATTCCGCAACCGA	1560
Hvpxy-1	ATCCCGTCCGGACTCTGCGCCGGCCACCGTCTCCTCCGCTCATCCTATTCCGCAACCGA	1421

Hvpxy-2	TTTGACTCCGCCATCCCGGCGAGCCTCGCCAACCTGCTCGTTCGCTGTGGCGGCTTCGGCTC	1440
HvPXY	TTTGACTCCGCCATCCCGGCGAGCCTCGCCAACCTGCTCGTTCGCTGTGGCGGCTTCGGCTC	1620
Hvpxy-1	TTTGACTCCGCCATCCCGGCGAGCCTCGCCAACCTGCTCGTTCGCTGTGGCGGCTTCGGCTC	1481

Hvpxy-2	GAGTCCAACCGGCTCACCGGCGCGATTCGGTCCGGCTTCGGAGCGGTGCAGAATCTGACG	1500
HvPXY	GAGTCCAACCGGCTCACCGGCGCGATTCGGTCCGGCTTCGGAGCGGTGCAGAATCTGACG	1680
Hvpxy-1	GAGTCCAACCGGCTCACCGGCGCGATTCGGTCCGGCTTCGGAGCGGTGCAGAATCTGACG	1541

Hvpxy-2	TACATGGACTTGAGCTCCAACGAGCTCACCGGCGGCATTCGGCTGATCTGGTAATTTCC	1560
HvPXY	TACATGGACTTGAGCTCCAACGAGCTCACCGGCGGCATTCGGCTGATCTGGTAATTTCC	1740
Hvpxy-1	TACATGGACTTGAGCTCCAACGAGCTCACCGGCGGCATTCGGCTGATCTGGTAATTTCC	1601

Hvpxy-2	CCGAGCCTCGAGTACCTCAACGTCTCCGGCAACCCGATGGGCGGTACGCTTCCGAGCAAT	1620
HvPXY	CCGAGCCTCGAGTACCTCAACGTCTCCGGCAACCCGATGGGCGGTACGCTTCCGAGCAAT	1800
Hvpxy-1	CCGAGCCTCGAGTACCTCAACGTCTCCGGCAACCCGATGGGCGGTACGCTTCCGAGCAAT	1661

Hvpxy-2	ACGTGGCGGGCACC GAAGCTGCAAGTCTTGGCGGCGAGCAAGTGCCTCTGGACGGCGAA	1680
HvPXY	ACGTGGCGGGCACC GAAGCTGCAAGTCTTGGCGGCGAGCAAGTGCCTCTGGACGGCGAA	1860
Hvpxy-1	ACGTGGCGGGCACC GAAGCTGCAAGTCTTGGCGGCGAGCAAGTGCCTCTGGACGGCGAA	1721

Hvpxy-2	ATCCCGCGTTTGGCACCTCCGGGTGCGCAAAC TTGTACAGGCTGGAGCTGGCCTGGAAT	1740
HvPXY	ATCCCGCGTTTGGCACCTCCGGGTGCGCAAAC TTGTACAGGCTGGAGCTGGCCTGGAAT	1920
Hvpxy-1	ATCCCGCGTTTGGCACCTCCGGGTGCGCAAAC TTGTACAGGCTGGAGCTGGCCTGGAAT	1781

Hvpxy-2	GAGCTGAGCGGCGCGGTCCCCGGCGACATTGGCAGCTGCAAGCGGCTGGTGAGCTTGAGG	1800
HvPXY	GAGCTGAGCGGCGCGGTCCCCGGCGACATTGGCAGCTGCAAGCGGCTGGTGAGCTTGAGG	1980
Hvpxy-1	GAGCTGAGCGGCGCGGTCCCCGGCGACATTGGCAGCTGCAAGCGGCTGGTGAGCTTGAGG	1841

Hvpxy-2	CTGCAGCACAACAACCTGAGTGGCGAGATCCCAGCGGTGCTCGCGGCGCTGCCGTCCGGTC	1860
HvPXY	CTGCAGCACAACAACCTGAGTGGCGAGATCCCAGCGGTGCTCGCGGCGCTGCCGTCCGGTC	2040
Hvpxy-1	CTGCAGCACAACAACCTGAGTGGCGAGATCCCAGCGGTGCTCGCGGCGCTGCCGTCCGGTC	1901

Hvpxy-2	ACCGAGGTGCACCTCTCCTGGAACGGCCTCACCGGCAGCATCCC GCCGGGCGTCGCCAAC	1920
HvPXY	ACCGAGGTGCACCTCTCCTGGAACGGCCTCACCGGCAGCATCCC GCCGGGCGTCGCCAAC	2100
Hvpxy-1	ACCGAGGTGCACCTCTCCTGGAACGGCCTCACCGGCAGCATCCC GCCGGGCGTCGCCAAC	1961

Hvpxy-2	TGTACTACGCTGGAGACCTTCGACGTGTCTTTCAACCATTTAGCACC GGTTGGGACGCC	1980
HvPXY	TGTACTACGCTGGAGACCTTCGACGTGTCTTTCAACCATTTAGCACC GGTTGGGACGCC	2160
Hvpxy-1	TGTACTACGCTGGAGACCTTCGACGTGTCTTTCAACCATTTAGCACC GGTTGGGACGCC	2021

Hvpxy-2	TCGCGGTCTCCGAATACCGGCGAGGGCAGTT CAGCGCGGCACGCCGCTGCAATGTGGGTG	2040
HvPXY	TCGCGGTCTCCGAATACCGGCGAGGGCAGTT CAGCGCGGCACGCCGCTGCAATGTGGGTG	2220
Hvpxy-1	TCGCGGTCTCCGAATACCGGCGAGGGCAGTT CAGCGCGGCACGCCGCTGCAATGTGGGTG	2081

Hvpxy-2	TCAGCCGTGGCAGTGGCGTTCGCCGGGATGGTGGTGTGGCGCTCACCGGGGCTGGCTG	2100
HvPXY	TCAGCCGTGGCAGTGGCGTTCGCCGGGATGGTGGTGTGGCGCTCACCGGGGCTGGCTG	2280
Hvpxy-1	TCAGCCGTGGCAGTGGCGTTCGCCGGGATGGTGGTGTGGCGCTCACCGGGGCTGGCTG	2141

Hvpxy-2	CAGTGTCTGGAGGACGACTCGGTGGCGGCGAACGGCGGCGGAGCGGGAGGGGCACGCCCT	2160
HvPXY	CAGTGTCTGGAGGACGACTCGGTGGCGGCGAACGGCGGCGGAGCGGGAGGGGCACGCCCT	2340
Hvpxy-1	CAGTGTCTGGAGGACGACTCGGTGGCGGCGAACGGCGGCGGAGCGGGAGGGGCACGCCCT	2201

Hvpxy-2	AACGTAGTCGTCGGGCCGTGGAGGATGACCGCGTTTCAGAGGCTGAGCTTACAGCGGAC	2220
HvPXY	AACGTAGTCGTCGGGCCGTGGAGGATGACCGCGTTTCAGAGGCTGAGCTTACAGCGGAC	2400
Hvpxy-1	AACGTAGTCGTCGGGCCGTGGAGGATGACCGCGTTTCAGAGGCTGAGCTTACAGCGGAC	2261

Hvpxy-2	GACGTGGTACGGTGCCTCGAGGGGAGCGACGGCATCGTCGGCGCCGGGTCGTCGGGAACG	2280
HvPXY	GACGTGGTACGGTGCCTCGAGGGGAGCGACGGCATCGTCGGCGCCGGGTCGTCGGGAACG	2460
Hvpxy-1	GACGTGGTACGGTGCCTCGAGGGGAGCGACGGCATCGTCGGCGCCGGGTCGTCGGGAACG	2321

Hvpxy-2	GTGTACCGGGCGAAGATGCCAATGGCGAGGTCATCGCCGTGAAGAAGCTATGGCAAGCG	2340

HvPXY	GTGTACCGGGCGAAGATGCCGAATGGCGAGGTCATCGCCGTGAAGAAGCTATGGCAAGCG	2520
Hvpxy-1	GTGTACCGGGCGAAGATGCCGAATGGCGAGGTCATCGCCGTGAAGAAGCTATGGCAAGCG *****	2381
Hvpxy-2	CCCGGGCAAAGGAGACAGCCGCAGATCACGCGGCGAAGCAAATGGACACACAAGAAGGC	2400
HvPXY	CCCGGGCAAAGGAGACAGCCGCAGATCACGCGGCGAAGCAAATGGACACACAAGAAGGC	2580
Hvpxy-1	CCCGGGCAAAGGAGACAGCCGCAGATCACGCGGCGAAGCAAATGGACACACAAGAAGGC *****	2441
Hvpxy-2	GGCGACGGCAACGAGAGGGTGCTCGCCGAGGTGGAGATGCTCGGCCACCTCCGCCACCGT	2460
HvPXY	GGCGACGGCAACGAGAGGGTGCTCGCCGAGGTGGAGATGCTCGGCCACCTCCGCCACCGT	2640
Hvpxy-1	GGCGACGGCAACGAGAGGGTGCTCGCCGAGGTGGAGATGCTCGGCCACCTCCGCCACCGT *****	2501
Hvpxy-2	AACATCGTCCGGCTGCTCGGGTTGTGCACAAACGGCGAGACGACGATGCTGCTGTACGAG	2520
HvPXY	AACATCGTCCGGCTGCTCGGGTTGTGCACAAACGGCGAGACGACGATGCTGCTGTACGAG	2700
Hvpxy-1	AACATCGTCCGGCTGCTCGGGTTGTGCACAAACGGCGAGACGACGATGCTGCTGTACGAG *****	2561
Hvpxy-2	TACATGCCCAACGGCAGCCTCGACGAGCTCCTGCACGGCGCCACCGGGGAAGATGCC	2580
HvPXY	TACATGCCCAACGGCAGCCTCGACGAGCTCCTGCACGGCGCCACCGGGGAAGATGCC	2760
Hvpxy-1	TACATGCCCAACGGCAGCCTCGACGAGCTCCTGCACGGCGCCACCGGGGAAGATGCC *****	2621
Hvpxy-2	AAGGCGCGCCGGAGTGGGACGCGCGGTACAGAATCGCCGTGGGCGTGGCGCAAGGCGTG	2640
HvPXY	AAGGCGCGCCGGAGTGGGACGCGCGGTACAGAATCGCCGTGGGCGTGGCGCAAGGCGTG	2820
Hvpxy-1	AAGGCGCGCCGGAGTGGGACGCGCGGTACAGAATCGCCGTGGGCGTGGCGCAAGGCGTG *****	2681
Hvpxy-2	AGTTACCTCCACCAGACTGCCTGCCCGGTTGGCGCACCGCGACCTCAAGCCCAGCAAC	2700
HvPXY	AGTTACCTCCACCAGACTGCCTGCCCGGTTGGCGCACCGCGACCTCAAGCCCAGCAAC	2880
Hvpxy-1	AGTTACCTCCACCAGACTGCCTGCCCGGTTGGCGCACCGCGACCTCAAGCCCAGCAAC *****	2741
Hvpxy-2	ATCCTCCTCGACGACGACATGGAGGCCCGGTGCGCCGACTTCGGCGTCGCCAAGGCTCTC	2760
HvPXY	ATCCTCCTCGACGACGACATGGAGGCCCGGTGCGCCGACTTCGGCGTCGCCAAGGCTCTC	2940
Hvpxy-1	ATCCTCCTCGACGACGACATGGAGGCCCGGTGCGCCGACTTCGGCGTCGCCAAGGCTCTC *****	2801
Hvpxy-2	CAGGGAGCCGCGCCTATGTCCGTGCTGCGCGGCTCCTGCGGCTACATCGCACCAGAGTAC	2820
HvPXY	CAGGGAGCCGCGCCTATGTCCGTGCTGCGCGGCTCCTGCGGCTACATCGCACCAGAGTAC	3000
Hvpxy-1	CAGGGAGCCGCGCCTATGTCCGTGCTGCGCGGCTCCTGCGGCTACATCGCACCAGAGTAC *****	2861
Hvpxy-2	ACGTACACACTTCGCGTGGACGAGAAGAGCGACGTGTACAGCTACGGCGTGGTGTCTGCTG	2880
HvPXY	ACGTACACACTTCGCGTGGACGAGAAGAGCGACGTGTACAGCTACGGCGTGGTGTCTGCTG	3060
Hvpxy-1	ACGTACACACTTCGCGTGGACGAGAAGAGCGACGTGTACAGCTACGGCGTGGTGTCTGCTG *****	2921
Hvpxy-2	GAGATCCTGACCGGGCGGGGTCGGTGGAGGCGGAGTACGGAGAGGGCAGCAACATTGTA	2940
HvPXY	GAGATCCTGACCGGGCGGGGTCGGTGGAGGCGGAGTACGGAGAGGGCAGCAACATTGTA	3120
Hvpxy-1	GAGATCCTGACCGGGCGGGGTCGGTGGAGGCGGAGTACGGAGAGGGCAGCAACATTGTA *****	2981
Hvpxy-2	GACTGGGTGAGATGCAAGGTCGCCGCGCGGGGGCGGCTTGCGCGACGTGATGGAGCAC	3000
HvPXY	GACTGGGTGAGATGCAAGGTCGCCGCGCGGGGGCGGCTTGCGCGACGTGATGGAGCAC	3180
Hvpxy-1	GACTGGGTGAGATGCAAGGTCGCCGCGCGGGGGCGGCTTGCGCGACGTGATGGAGCAC *****	3041
Hvpxy-2	GTCGGCGGTAGCAGCGAGGCAGCGCGGGAGGAAATGGCGCTGGTGTCTGCGGGTGGCGCTG	3060
HvPXY	GTCGGCGGTAGCAGCGAGGCAGCGCGGGAGGAAATGGCGCTGGTGTCTGCGGGTGGCGCTG	3240
Hvpxy-1	GTCGGCGGTAGCAGCGAGGCAGCGCGGGAGGAAATGGCGCTGGTGTCTGCGGGTGGCGCTG *****	3101
Hvpxy-2	CTGTGCACGAGCCGGTGCCTCGCAGGACCGGCCGTCGATGAGGGACGTGCTGTCCATGCTG	3120
HvPXY	CTGTGCACGAGCCGGTGCCTCGCAGGACCGGCCGTCGATGAGGGACGTGCTGTCCATGCTG	3300
Hvpxy-1	CTGTGCACGAGCCGGTGCCTCGCAGGACCGGCCGTCGATGAGGGACGTGCTGTCCATGCTG *****	3161

Hvpxy-2	CAGGAGGCCAGGCCCAGGCCAGCCAGAAGCCGGCGGCGAAACATGTGTACGGTGTACCG	3180
HvPXY	CAGGAGGCCAGGCCCAGGCCAGCCAGAAGCCGGCGGCGAAACATGTGTACGGTGTACCG	3360
Hvpxy-1	CAGGAGGCCAGGCCCAGGCCAGCCAGAAGCCGGCGGCGAAACATGTGTACGGTGTACCG	3221

Hvpxy-2	CGTAGTTAA	3189
HvPXY	CGTAGTTAA	3369
Hvpxy-1	CGTAGTTAA	3230

Appendix D: R code for dendrogram construction

```
myalign<-phangorn::read.phyDat("FILE.fas",type="AA",format="fasta") #load the alignment

mtestalign<-phangorn::modelTest(myalign,model="all") #test all available evolutionary models for proteins

mtestalign[which.min(mtestalign$AIC),] #show the best model according to AIC score

mtestalign[which.min(mtestalign$BIC),] #show the best model according to BIC score (usually the same as AIC)

mdist<-phangorn::dist.ml(myalign,model="JTT") #build a pairwise maximum likelihood distance matrix with
the JTT model (choose a different model if indicated in the previous steps)

tree.ini<-phangorn::NJ(mdist) #build a starting tree (neighbour-joining)

fit.ini<-pml(tree.ini, myalign, k=4) #build a starting maximum likelihood tree from the first tree

fitJTT <- update(fit.ini, k=4, inv=0.2) #improve this tree further

fitJTT <- optim.pml(fitJTT, model="JTT", optInv=TRUE, optGamma=TRUE, rearrangement = "NNI", control =
pml.control(trace = 0)) #explore similar trees by swapping nearest neighbours, the optGamma and optInv
options correspond to the JTT+G+I model if that was the best model for you

logLik(fitJTT) #a measure of how good this tree is, smaller values are better

plot(midpoint(fitJTT$tree)) #plot the tree, rooting to the longest branch

fitJTT <- optim.pml(fitJTT, model="JTT", optInv=TRUE, optGamma=TRUE, rearrangement = "stochastic", control
= pml.control(trace = 0)) #explore similar trees with stochastic rearrangements

logLik(fitJTT) #measure how much your tree has improved, view it with plot(midpoint(fitJTT$tree)) if you wish.

fitJTT <- optim.pml(fitJTT, model="JTT", optInv=TRUE, optGamma=TRUE, rearrangement = "ratchet", control =
pml.control(trace = 0)) #explore similar trees with ratchet rearrangements (go back to the previous best tree if
no improvement)

logLik(fitJTT) #measure how much your tree has improved, view it with plot(midpoint(fitJTT$tree)) if you wish.

write.tree(fitJTT$tree, file="TREE.tre") #save the tree file so you don't have to repeat the previous analysis
steps again

atree<-read.newick(file="TREE.tre") #import the tree file
```

```

bstree = bootstrap.pml(fitJTT, bs=100, model="JTT", optInv=TRUE, optGamma=TRUE, rearrangement =
"ratchet", control = pml.control(trace = 0)) #build 100 bootstrap trees to get percentage support for each
branch (this takes a while)

plotBS(midpoint(fitJTT$tree), bstree, p = 0, type="p") #plot the tree with bootstrap supports added

cnettree <- consensusNet(bstree, p=0.2) #plot a network tree (visually shows the support for each branch)

plot(cnettree, "2D", show.edge.label=F)

pbstree<-plotBS(midpoint(fitJTT$tree), bstree, p = 50, type="p") #plot tree with bootstrap supports over 50%

write.tree(bstree, file="bootstrapree.tre") #save the bootstrap file for later

importedtree<-read.newick(file="bootstrapree.tre") #import the bootstrap file

seqnames<-importedtree$tip.label #extract the sample names. You can modify them if necessary and put
them back with aamltree$tip.label <- newseqnames

plotTree(importedtree, node.numbers = T) #plot the tree with internal branch (node) numbers

rtr<-reroot(importedtree, node.number=X) #reroot tree at node X

plotTree(rtr, node.numbers = T)

testtree<-root(rtr,node=169) #root the tree at this branch number

testtree<-rotateNodes(rtr,node=223) #rotate the clade leading off from this branch number

X <- c("pxy")

dotTree(testtree,X, ftype="i",fsize=0.9) #adds blank dots to tree

```

Appendix E: enrichnet_stat.R.

```
enrichnet <- function(genelist, pathwaylist=c("kegg", "biocarta", "go", "reactome", "pid"),
network="human_ensembl", minsize = 10)

{

  if(!require('igraph'))

  {

    stop("Error: You first need to install the igraph package to use enrichnet")

  }

  net <- NULL

  curdir <- getwd()

  # load network

  if(typeof(network) == "character")

  {

    if(network == "human_ensembl")

    {

      net <- read.graph("string600con.txt", format="ncol")

      setwd(curdir)

    } else {

      if (data.class(result<- try( net <- read.graph(network, format="ncol") , TRUE))=="try-error") {

        stop("Error: Could not parse the user-defined network file. Please make sure that you use a
two-column tab- or space-delimited input file.")

      }

    }

  }

}
```

```

} else {

  net = network

}

# read labels

nodelabels <- V(net)$name

# load pathway data

if(typeof(pathwaylist) == "character")

{

  if(all(pathwaylist == c("kegg","biocarta","go","reactome","pid")))

    pathwaylist = "kegg"

  if(pathwaylist %in% c("kegg","biocarta","go","reactome","pid"))

  {

    setwd("C:/xampp/htdocs/geneconversion/")

    load(file=paste(pathwaylist,"ens_smc.Rdata",sep=""))

    setwd(curdir)

  } else {

    readGenesetFile <- function(filename)

    {

      dat <- sapply(readLines(filename), function(x) strsplit(x, "\t"))

      smclst = sapply(dat, function(x) x[2:length(x)])

      smcnames = sapply(dat, function(x) x[1])

      names(smclst) <- smcnames

```

```

        return(smclst)
    }

    if (data.class(result<- try( smclst <- readGenesetFile(file.path(getwd()), pathwaylist)) ,
TRUE))=="try-error") {

        stop("Error: Could not parse the user-defined pathway file.")

    }

}

pathwaylist = smclst

}

set_indices <- NULL

    set_names <- NULL

set_names = names(pathwaylist)

set_indices = sapply(pathwaylist, function(x) match(x,nodelabels)[x %in% nodelabels])

# filter by minsize

path_sizes = sapply(set_indices, length)

set_indices = set_indices[which(path_sizes >= minsize)]

set_names = set_names[which(path_sizes >= minsize)]

    # get indices of geneset of interest

    ind <- match(genelist, nodelabels)

    genes <- ind[which(!is.na(ind))]

# start Random Walk with Restart (RWR) algorithm

if(!require('Matrix'))

```

```

{

  stop("Error: You first need to install the Matrix package to use enrichnet")

}

if(!require('lattice'))

{

  stop("Error: You first need to install the lattice package to use enrichnet")

}

if(network == "human_ensembl")

{

  load(file="columnnorm_adj_string.Rdata") # load adjacency matrix netadj

  setwd(curdir)

} else #if (network == "own")

{

  # compute adjacency matrix

netadj <- get.adjacency(net, type="both", sparse=T)

  for(j in 1:ncol(netadj))

    netadj[,j] <- netadj[,j]/sum(netadj[,j])

  save(netadj, file="columnnorm_adj_user.Rdata")

}

v <- rep(0, length(V(net)))

v[genes] <- rep(1, length(genes))

u = v

```

```

restartprob = 0.95

uold = rep(1, length(v))

print("Random Walk till convergence...")

while(sum(abs(u-uold)) >= 1e-06)

{

  uold = u

  u = (1-restartprob) * netadj %*% uold + restartprob * v

  print(sum(abs(u-uold)))

}

print("converged.")

# extract scores for all pathways

# compare continuous scores for target pathway against all other pathways

final_pvals <- numeric(length(set_indices))

path_scores = list()

# foreground distributions

gene2path_hash <- matrix(0, nrow=length(set_indices), ncol=7)

for(j in 1:length(set_indices)) # iterate over reference DB

{

  gene_ids <- set_indices[[j]]

  # get RWR scores for this pathway

  rwr_scores <- u[gene_ids]

  # convert similarity scores into distance scores (max score = 1)

```

```

    path_scores[[j]] = 1 - rwr_scores

}

# foreground distributions

gene2path_hash <- matrix(0, nrow=length(path_scores), ncol=10)

for(j in 1:length(path_scores))

{

    splitscores <- cut(path_scores[[j]], breaks=seq(0.0,1,0.1))

    freqs <- table(splitscores)

    gene2path_hash[j,] <- as.numeric(freqs)

}

path2path_hash <- apply(gene2path_hash, 2, sum)/nrow(gene2path_hash) # mean used here:
median better

# compute pairwise distances: gene set vs. reference pathways

xd_vec <- numeric(length(set_indices))

# number of distance bins minus 1

diam <- 9

xd_distance <- function(distrib1, distrib2, diam)

{

    # compute Xd-distance

    sum_xd <- 0.0

    total_real <- sum(distrib1)

```

```

total_rand <- sum(distrib2)

for(xd_iter in 1:(diam+1))

{

    # prevent division by zero

    term1 <- distrib1[xd_iter]/total_real

    if(distrib1[xd_iter] == 0)

        term1 <- 0

    term2 <- distrib2[xd_iter]/total_rand

    if(distrib2[xd_iter] == 0)

        term2 <- 0

    # convert counts to percentages

    sum_xd <- sum_xd + (100*term1 - 100*term2) / (xd_iter * (diam+1))

}

return (sum_xd)

}

for(j in 1:length(set_indices))

{

    xd_dist <- xd_distance(gene2path_hash[j,], path2path_hash, diam)

    xd_vec[j] <- xd_dist

}

}

overlap_ids <- sapply(set_indices, function(x) nodelabels[intersect(x, genes)])

```

```

overlaps <- sapply(overlap_ids, function(x) length(x))

path_lengths <- sapply(set_indices, length)

resmat <- data.frame(set_names, xd_vec, rep(length(genes),length(set_indices)), path_lengths,
overlaps) # no compactness

names(resmat) <- c("path_names", "xd_scores", "upload_sizes", "pathway_sizes", "overlap_sizes")

o <- order(xd_vec, decreasing=T)

# optional: output including overlapping gene ids

# return (list(resmat[o,], overlap_ids[o]))

# compact output (no overlapping gene ids)

return (resmat[o,])

}

```

Appendix F: R code for using enrichnet with gene sets of interest

```
source('enrichnet_stat.R')
```

```
genelist1 = c() #insert list of genes into the brackets
```

```
result <- enrichnet(genelist1, pathwaylist="eseemblplant50_IBSC_v2_mart_GO_export_gmtlike.txt",
```

```
    network="barley_string_network_IBSC_v2_GeneID.txt", minsize = 10) # show the 10 top-ranked  
pathways + the enrichnet statistics
```

```
#note that pathwaylist should be pathways relevant to your species of interest, and network should likewise be  
the appropriate STRING network
```

Appendix G: The genomic locations of identified *H. vulgare* genes, and the primers generated for them.

Gene	Genomic Location	Forward Primer	Reverse Primer
<i>HvPXY</i>	chr7H:407834402-407835037	5' ATGGACACACAAGAAGGCGGCG 3'	5' ATGTTGCTGGGCTTGAGGTCGC 3'
<i>HvHistoneH4</i>	chr5H:577037303-577037548	5' ATCAGCCACAGCAGCAACCCAC 3'	5' GATGAGCCCCGAGATGCGCTTC 3'

Appendix H: An overview of the data production quality during RNA sequencing. Sample = sample name, raw reads = the original sequencing reads count, clean reads = the number of reads after filtering, raw data = raw reads number multiply read length (saved in G unit), clean data = clean reads number multiply read length (saved in G unit), error rate = average sequencing error rate (calculated by $Q_{\text{phred}} = -10\log_{10}^e$), Q20 = percentages of bases whose correct base recognition rates are greater than 99% in total bases, Q30 = percentage of bases whose correct base recognition rates are greater than 99.9% in total bases, GC content = percentages of G and C in total bases.

Sample	Raw Reads	Clean Reads	Raw Data (G)	Clean Data (G)	Error Rate (%)	Q20 (%)	Q30 (%)	GC Content (%)
A9WT	87036061	86001142	26.1	25.8	0.02	98.09	94.46	52.46
A10WT	88761651	87462709	26.6	26.2	0.02	98.07	94.38	52.38
A11WT	92191332	90776184	27.7	27.2	0.02	98.04	94.22	52.44
A12WT	87458243	86375879	26.2	25.9	0.03	97.97	94.16	52.37
A21pxy	89793949	88404142	26.9	26.5	0.03	97.96	94.05	52.36
A22pxy	81884520	80847819	24.6	24.3	0.03	97.97	94.19	52.31
A23pxy	91608543	90168279	27.5	27.1	0.02	98.02	94.31	52.56
A24pxy	89736774	88266718	26.9	26.5	0.02	98.06	94.34	52.46

Appendix I: Overview of mapping status. Total reads = total number of filtered reads (clean data), total mapped = total number of reads that can be mapped to the reference genome, multiple mapped = number of reads that can be mapped to multiple sites in the reference genome, uniquely mapped = number of reads that can be uniquely mapped to the reference genome, read-1 = number of left read that can be mapped to the reference genome, read-2 = number of right read that can be mapped to the reference genome, reads map to '+' = number of reads that can be mapped to the positive strand, reads map to '-' = number of reads that can be mapped to the negative strand, non-splice reads = number of reads that can be mapped entirely to a single exon, splice reads = number of reads that can be segmented and mapped to two exons.

Sample Name	A9WT	A10WT	A11WT	A12WT	A21pxy	A22pxy	A23pxy	A24pxy
Total Reads	1720022 84	1749254 18	1815523 68	1727517 58	1768082 84	1616956 38	1803365 58	1765334 36
Total Mapped	1600429 83 (93.05%)	1622726 59 (92.77%)	1688484 48 (93.00%)	1609251 26 (93.15%)	1641004 83 (92.81%)	1496973 01 (92.58%)	1674577 91 (92.86%)	1647709 26 (93.34%)
Multiple Mapped	1415518 3 (8.23%)	1399000 5 (8.00%)	1498649 6 (8.25%)	1425255 9 (8.25%)	1429357 7 (8.08%)	1299316 7 (8.04%)	1454869 3 (8.07%)	1474206 2 (8.35%)
Uniquely Mapped	1458878 00 (84.82%)	1482826 54 (84.77%)	1538619 52 (84.75%)	1466725 67 (84.90%)	1498069 06 (84.73%)	1367041 34 (84.54%)	1529090 98 (84.79%)	1500288 64 (84.99%)
Read-1	7309946 2 (42.50%)	7431388 0 (42.48%)	7716321 3 (42.50%)	7358405 4 (42.60%)	7509343 5 (42.47%)	6856652 9 (42.40%)	7667675 8 (42.52%)	7523322 9 (42.62%)
Read-2	7278833 8 (42.32%)	7396877 4 (42.29%)	7669873 9 (42.25%)	7308851 3 (42.31%)	7471347 1 (42.26%)	6813760 5 (42.14%)	7623234 0 (42.27%)	7479563 5 (42.37%)
Reads Map to '+'	7305645 4 (42.47%)	7422281 2 (42.43%)	7703278 7 (42.43%)	7349377 4 (42.54%)	7505317 8 (42.45%)	6840127 6 (42.30%)	7656298 0 (42.46%)	7518652 6 (42.59%)
Reads Map to '-'	7283134 6 (42.34%)	7405984 2 (42.34%)	7682916 5 (42.32%)	7317879 3 (42.36%)	7475372 8 (42.28%)	6830285 8 (42.24%)	7634611 8 (42.34%)	7484233 8 (42.40%)
Non-Splice Reads	9454613 0 (54.97%)	9688260 9 (55.39%)	9999228 8 (55.08%)	9546823 6 (55.26%)	9780322 9 (55.32%)	8844214 2 (54.70%)	1011553 30 (56.09%)	9642894 0 (54.62%)

Splice Reads	5134167 0 (29.85%)	5140004 5 (29.38%)	5386966 4 (29.67%)	5120433 1 (29.64%)	5200367 7 (29.41%)	4826199 2 (29.85%)	5175376 8 (28.70%)	5359992 4 (30.36%)
---------------------	--------------------------	--------------------------	--------------------------	--------------------------	--------------------------	--------------------------	--------------------------	--------------------------

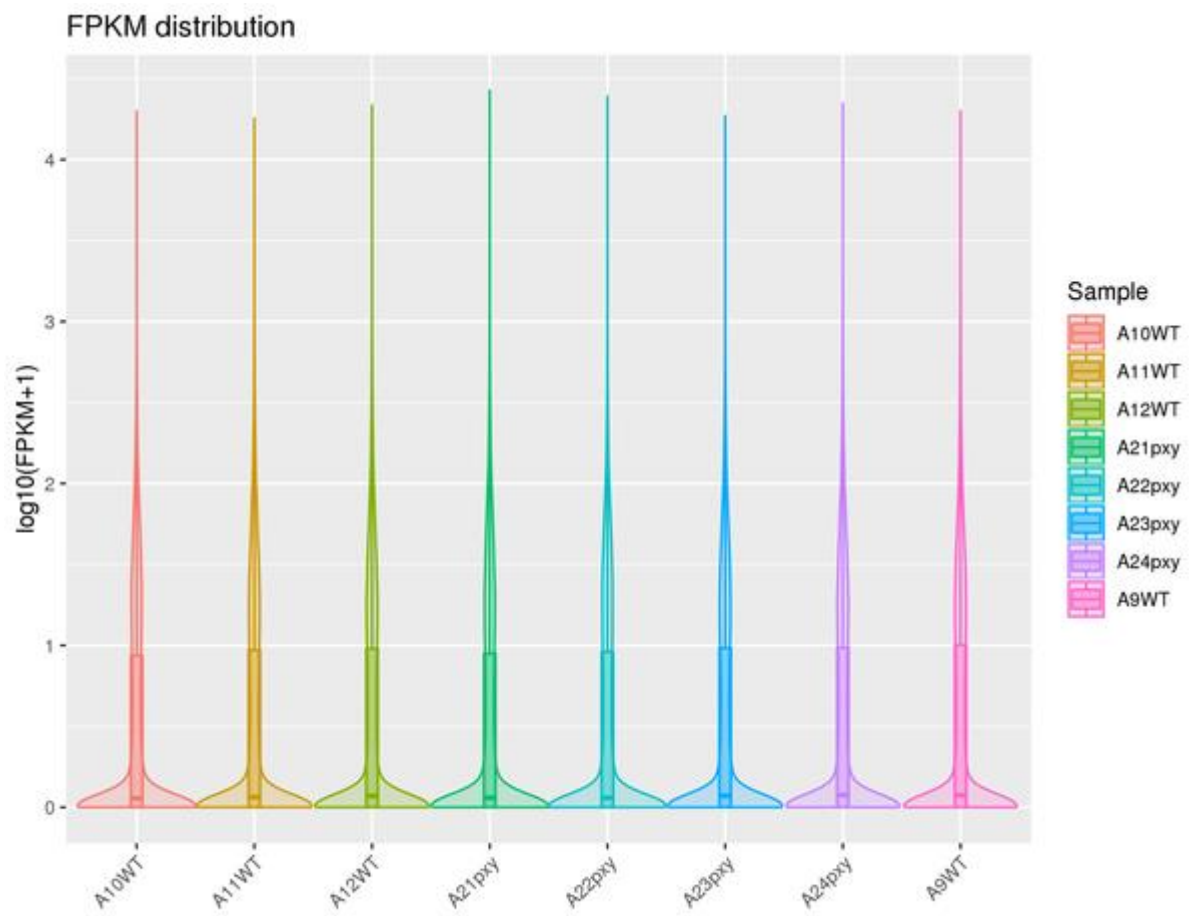
Appendix J: The percentage of reads from each sample which mapped to exonic, intergenic and intronic regions.

Sample Name	A9WT	A10WT	A11WT	A12WT	A21pxy	A22pxy	A23pxy	A24pxy
Exonic (%)	88.25	87.37	88.18	88.75	87.8	86.91	87.34	88.49
Intergenic (%)	10.22	10.94	10.37	9.96	10.62	11.30	10.86	10.04
Intronic (%)	1.53	1.68	1.45	1.29	1.57	1.79	1.79	1.47

Appendix K: FPKM intervals for the reads of each sample, and example expression levels of specific genes.

FPKM Interval	A9WT	A10WT	A11WT	A12WT	A21pxy	A22pxy	A23pxy	A24pxy
0~1	25198 (58.53%)	26225 (60.92%)	25617 (59.51%)	25462 (59.15%)	26053 (60.52%)	26039 (60.49%)	25610 (59.49%)	25404 (59.01%)
1~3	3015 (7%)	2931 (6.81%)	3014 (7%)	3021 (7.02%)	2946 (6.84%)	2947 (6.85%)	3039 (7.06%)	3097 (7.19%)
3~15	6450 (14.98%)	5923 (13.76%)	6274 (14.57%)	6361 (14.78%)	6010 (13.96%)	5947 (13.81%)	6154 (14.3%)	6301 (14.64%)
15~60	5848 (13.58%)	5538 (12.86%)	5565 (12.93%)	5658 (13.14%)	5516 (12.81%)	5681 (13.2%)	5714 (13.27%)	5712 (13.27%)
>60	2539 (5.9%)	2433 (5.65%)	2580 (5.99%)	2548 (5.92%)	2525 (5.87%)	2436 (5.66%)	2533 (5.88%)	2536 (5.89%)
Gene	A9WT	A10WT	A11WT	A12WT	A21pxy	A22pxy	A23pxy	A24pxy
HORVU6Hr1 G093570	104.151 8	41.3888 9	45.1606 9	73.1329 3	50.8417 3	51.8842	106.161 3	87.2051 9
HORVU5Hr1 G075260	2.04407 3	2.61547 2	2.08718 3	2.05225 7	2.22779 7	2.31616	8.29676 2	3.38029
HORVU5Hr1 G037160	30.2592 4	18.9045 4	28.0759 1	31.2830 8	21.9042 7	21.7908 3	23.8328 8	28.1781
HORVU6Hr1 G048290	63.9380 4	56.9155 2	61.9451 5	61.2360 3	57.2620 4	53.0822 2	64.2276 9	76.7947 9

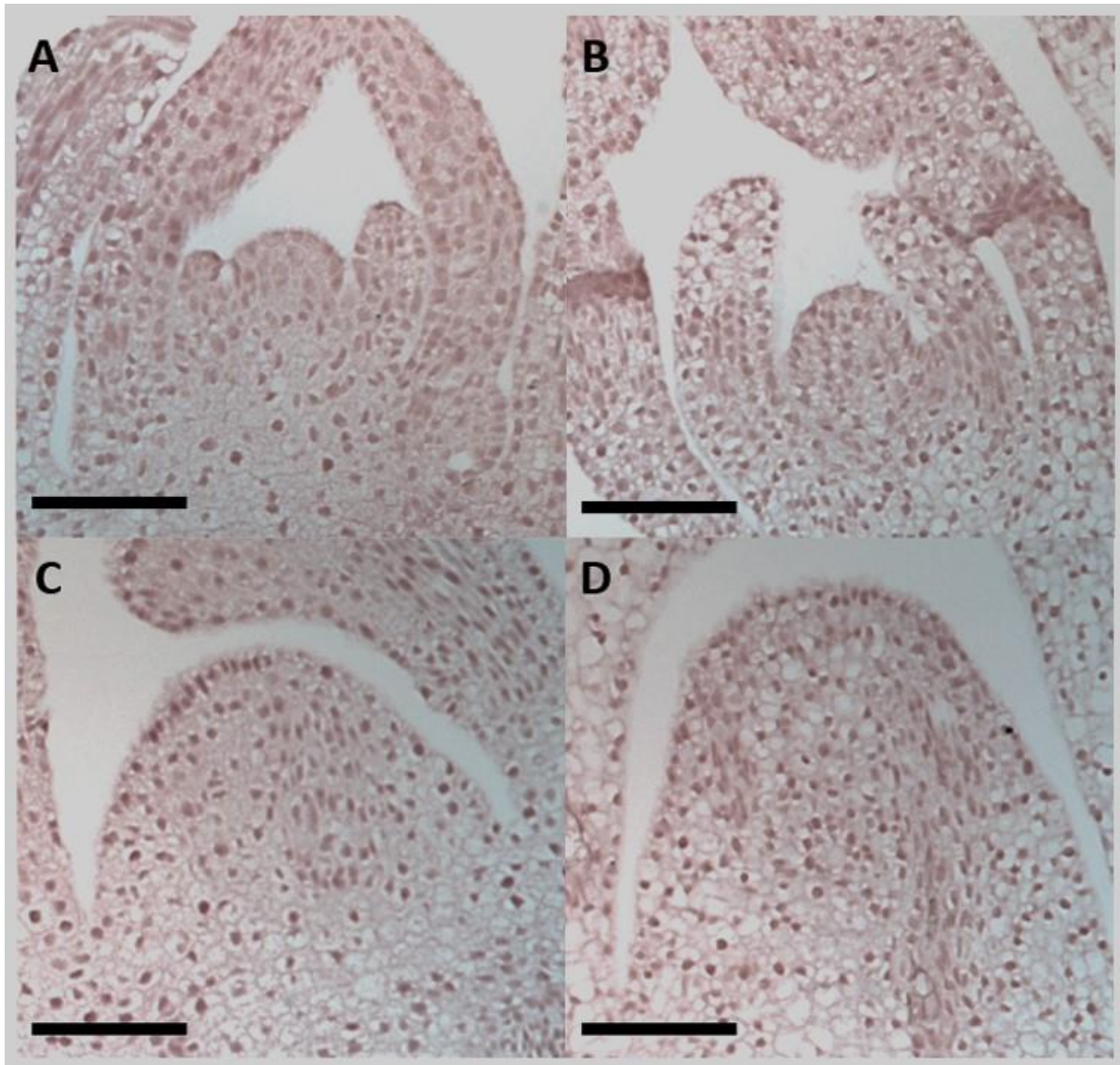
Appendix L: A violin plot depicting the FPKM distribution of each sample. Figure generated by Novogene.



Appendix M: Example differential gene analysis. Gene ID = gene ID, *pxy* value = the mean of the normalised FPKMs in the *pxy* group, WT value = the mean of the normalised FPKMs in the wild type group, \log_2 fold change = $\log_2(\text{pxy}/\text{WT})$, p-value = p-value, p adjust = the adjusted p-value after normalisation.

Gene ID	<i>pxy</i> Value	WT Value	\log_2 Fold Change	P-Value	P Adjust
HORVU5Hr1G120060	0.097416	4.399625	-5.49708	9.73E-72	2.47E-67
HORVU7Hr1G006630	1.445425	0.082559	4.129917	1.76E-61	2.24E-57
HORVU7Hr1G103710	26.54594	0.026403	9.97355	1.02E-49	8.62E-46
HORVU6Hr1G018030	0.835795	82.4123	-6.62356	2.43E-49	1.55E-45

Appendix N: *In situ* images using sense and antisense probes. (A) *HvHistoneH4* antisense probe, (B) *HvPXY* antisense probe, (C) *HvHistoneH4* sense probe, (D) *HvPXY* sense probe. Scale bars represent 100 μ m.



References

- Agustí, J., & Blázquez, M. A. (2020). Plant vascular development: Mechanisms and environmental regulation. *Cellular and Molecular Life Sciences*, *77*, 3711–3728.
<https://doi.org/10.1007/s00018-020-03496-w>
- Ali, O., Cheddadi, I., Landrein, B., & Long, Y. (2022). Revisiting the relationship between turgor pressure and plant cell growth. *New Phytologist*, *238*(1), 62–69.
<https://doi.org/10.1111/nph.18683>
- Amack, S. C., & Antunes, M. S. (2020). CaMV35S promoter – A plant biology and biotechnology workhorse in the era of synthetic biology. *Current Plant Biology*, *24*, 100179.
<https://doi.org/10.1016/j.cpb.2020.100179>
- Anders, S., & Huber, W. (2010). Differential expression analysis for sequence count data. *Genome Biology*, *11*, R106. <https://doi.org/10.1186/gb-2010-11-10-r106>
- Atanassov, I. I., Pittman, J. K., & Turner, S. R. (2009). Elucidating the Mechanisms of Assembly and Subunit Interaction of the Cellulose Synthase Complex of Arabidopsis Secondary Cell Walls. *Journal of Biological Chemistry*, *284*(6), 3833–3841.
<https://doi.org/10.1074/jbc.M807456200>
- Averof, M., & Patel, N. H. (1997). Crustacean appendage evolution associated with changes in Hox gene expression. *Nature*, *388*, 682–686. <https://doi.org/10.1038/41786>
- Avramova, V., AbdElgawad, H., Zhang, Z., Fotschki, B., Casadevall, R., Vergauwen, L., Knapen, D., Taleisnik, E., Guisez, Y., Asard, H., & Beemster, G. T. S. (2015). Drought Induces Distinct Growth Response, Protection, and Recovery Mechanisms in the Maize Leaf Growth Zone. *Plant Physiology*, *169*(2), 1382–1396. <https://doi.org/10.1104/pp.15.00276>
- Bagdassarian, K. S., Etchells, J. P., & Savage, N. S. (2022). A mathematical model integrates diverging PXY and MP interactions in cambium development.
<https://doi.org/10.48550/ARXIV.2208.10985>

- Barkley, G. (1924). Secondary Stellar Structures of *Yucca*. *Botanical Gazette*, 78(4), 433–439.
- Bartlett, J. G., Alves, S. C., Smedley, M., Snape, J. W., & Harwood, W. A. (2008). High-throughput *Agrobacterium*-mediated barley transformation. *Plant Methods*, 4.
<https://doi.org/10.1186/1746-4811-4-22>
- Barton, M. K. (2010). Twenty years on: The inner workings of the shoot apical meristem, a developmental dynamo. *Developmental Biology*, 341(1), 95–113.
<https://doi.org/10.1016/j.ydbio.2009.11.029>
- Begum, T., Reuter, R., & Schöffl, F. (2013). Overexpression of AtHsfB4 induces specific effects on root development of *Arabidopsis*. *Mechanisms of Development*, 130(1), 54–60.
<https://doi.org/10.1016/j.mod.2012.05.008>
- Beier, S., Himmelbach, A., Colmsee, C., Zhang, X.-Q., Barrero, R. A., Zhang, Q., Li, L., Bayer, M., Bolser, D., Taudien, S., Groth, M., Felder, M., Hastie, A., Šimková, H., Staňková, H., Vrána, J., Chan, S., Muñoz-Amatriaín, M., Ounit, R., ... Mascher, M. (2017). Construction of a map-based reference genome sequence for barley, *Hordeum vulgare* L. *Scientific Data*, 4, 170044.
<https://doi.org/10.1038/sdata.2017.44>
- Berckmans, B., Kirschner, G., Gerlitz, N., Stadler, R., & Simon, R. (2020). CLE40 Signaling Regulates Root Stem Cell Fate. *Plant Physiology*, 182(4), 1776–1792.
<https://doi.org/10.1104/pp.19.00914>
- Botha, C. E. J. (2005). 6—Interaction of Phloem and Xylem During Phloem Loading: Functional Symplasmic Roles for Thin- and Thick-Walled Sieve Tubes in Monocotyledons. In *Vascular Transport in Plants* (1st ed., pp. 115–130). Academic Press.
- Bowman, J. L., Kohchi, T., Yamato, K. T., Jenkins, J., Shu, S., Ishizaki, K., Yamaoka, S., Nishihama, R., Nakamura, Y., Berger, F., Adam, C., Shiori, S. A., Althoff, F., Araki, T., Arteaga-Vazquez, M. A., Balasubramanian, S., Barry, K., Bauer, D., Boehm, C. R., ... Schmutz, J. (2017). Insights into Land Plant Evolution Garnered from the *Marchantia polymorpha* Genome. *50 Cell*, 171(2), 287–304.E15. <https://doi.org/10.1016/j.cell.2017.09.030>

- Brakefield, P. M., & French, V. (1999). Butterfly wings: The evolution of development of colour patterns. *BioEssays*, 21(5), 391–401. [https://doi.org/10.1002/\(SICI\)1521-1878\(199905\)21:5%3C391::AID-BIES6%3E3.0.CO;2-Q](https://doi.org/10.1002/(SICI)1521-1878(199905)21:5%3C391::AID-BIES6%3E3.0.CO;2-Q)
- Chandler, J. W. (2008). Cotyledon organogenesis. *Journal of Experimental Botany*, 59(11), 2917–2931. <https://doi.org/10.1093/jxb/ern167>
- Chen, K., Li, G.-J., Bressan, R. A., Song, C.-P., Zhu, J.-K., & Zhao, Y. (2019). Abscisic acid dynamics, signaling, and functions in plants. *Journal of Integrative Plant Biology*, 62(1), 25–54. <https://doi.org/10.1111/jipb.12899>
- Chen, X.-Y., & Kim, J.-Y. (2009). Callose synthesis in higher plants. *Plant Signalling & Behavior*, 4, 489–492. <https://doi.org/10.4161/psb.4.6.8359>
- Coumou, D., & Rahmstorf, S. (2012). A decade of weather extremes. *Nature Climate Change*, 2(7), 491–496. <https://doi.org/10.1038/nclimate1452>
- Crang, R., Lyons-Sobaski, S., & Wise, R. (2018). *Plant Anatomy: A Concept Based Approach to the Structure of Seed Plants* (1st ed.). Springer International Publishing.
- Cunningham, C. (2019, July 16). Harvest 2019: Barley yield prospects rise with 10t/ha in Wales. *Farmers Weekly*.
- Davenport, D., & Kohanzadeh, Y. (1982). Orchids, bilateral symmetry and insect perception. *Journal of Theoretical Biology*, 94(2), 241–252. [https://doi.org/10.1016/0022-5193\(82\)90311-3](https://doi.org/10.1016/0022-5193(82)90311-3)
- de Reuille, P. B., & Ragni, L. (2017). Vascular Morphodynamics During Secondary Growth. *Methods in Molecular Biology*, 103–125. https://doi.org/10.1007/978-1-4939-6722-3_10
- DEFRA. (2019). *Farming Statistics—Final crop areas, yields, livestock populations and agricultural workforce At June 2019*. DEFRA.
- El Khoury, D., Cuda, C., Luhovyy, B. L., & Anderson, G. H. (2012). Beta Glucan: Health Benefits in Obesity and Metabolic Syndrome. *Journal of Nutrition and Metabolism*, 2012, 851362. <https://doi.org/10.1155/2012/851362>
- Esau, K. (1953). *Plant Anatomy* (2nd ed.). John Wiley & Sons, Ltd.

- Etchells, J. P., Mishra, L. S., Kumar, M., Campbell, L., & Turner, S. R. (2015). Wood Formation in Trees Is Increased by Manipulating PXY-Regulated Cell Division. *Current Biology*, *25*(8), 1050–1055. <https://doi.org/10.1016/j.cub.2015.02.023>
- Etchells, J. P., Provost, C. M., Mishra, L., & Turner, S. R. (2013). WOX4 and WOX14 act downstream of the PXY receptor kinase to regulate plant vascular proliferation independently of any role in vascular organisation. *Development*, *140*(10), 2224–2234. <https://doi.org/10.1242/dev.091314>
- Etchells, J. P., Provost, C. M., & Turner, S. R. (2012). Plant Vascular Cell Division Is Maintained by an Interaction between PXY and Ethylene Signalling. *PLoS Genetics*, *8*(11), e1002997. <https://doi.org/10.1371/journal.pgen.1002997>
- Etchells, J. P., Smit, M. E., Gaudinier, A., Williams, C. J., & Brady, S. M. (2016). A brief history of the TDIF-PXY signalling module: Balancing meristem identity and differentiation during vascular development. *New Phytologist*, *209*(2), 474–484. <https://doi.org/10.1111/nph.13642>
- Etchells, J. P., & Turner, S. R. (2010). The PXY-CLE41 receptor ligand pair defines a multifunctional pathway that controls the rate and orientation of vascular cell division. *Development*, *137*(5), 767–774. <https://doi.org/10.1242/dev.044941>
- Evans, P. S. (1968). Intercalary growth in the aerial shoot of *Eleocharis acuta* R. BR. *New Zealand Journal of Botany*, *7*(1), 36–42. <https://doi.org/10.1080/0028825X.1969.10429100>
- Ferrari, C., Shivhare, D., Hansen, B. O., Pasha, A., Esteban, E., Provart, N. J., Kragler, F., Fernie, A., Tohge, T., & Mutwil, M. (2020). Expression Atlas of *Selaginella moellendorffii* Provides Insights into the Evolution of Vasculature, Secondary Metabolism, and Roots. *The Plant Cell*, *32*(4), 853–870. <https://doi.org/10.1105/tpc.19.00780>
- Fisher, K., & Turner, S. (2007). PXY, a receptor-like kinase essential for maintaining polarity during plant vascular-tissue development. *Current Biology*, *17*(12), 1061–1066. <https://doi.org/10.1016/j.cub.2007.05.049>

- Furumizu, C., & Sawa, S. (2021). Insight into early diversification of leucine-rich repeat receptor-like kinases provided by the sequenced moss and hornwort genomes. *Plant Molecular Biology*, 107, 337–353. <https://doi.org/10.1007/s11103-020-01100-0>
- Gentleman, R. C., Carey, V. J., Bates, D. M., Bolstad, B., Dettling, M., Dudoit, S., Ellis, B., Gautier, L., Ge, Y., Gentry, J., Hornik, K., Hothorn, T., Huber, W., Iacus, S., Irizarry, R., Leisch, F., Li, C., Maechler, M., Rossini, A. J., ... Zhang, J. (2004). Bioconductor: Open software development for computational biology and bioinformatics. *Genome Biology*, 5, R80. <https://doi.org/10.1186/gb-2004-5-10-r80>
- Glaab, E., Baudot, A., Krasnogor, N., Schneider, R., & Valencia, A. (2012). EnrichNet: Network-based gene set enrichment analysis. *Bioinformatics*, 28(18), i451–i457. <https://doi.org/10.1093/bioinformatics/bts389>
- Groover, A., & Robischon, M. (2006). Developmental mechanisms regulating secondary growth in woody plants. *Current Opinion in Plant Biology*, 9(1), 55–58. <https://doi.org/10.1016/j.pbi.2005.11.013>
- Haberer, G., Mayer, K. F., & Spannagl, M. (2016). The big five of the monocot genomes. *Current Opinion in Plant Biology*, 30, 33–40. <https://doi.org/10.1016/j.pbi.2016.01.004>
- Handakumbura, P. P., & Hazen, S. P. (2012). Transcriptional Regulation of Grass Secondary Cell Wall Biosynthesis: Playing Catch-Up with *Arabidopsis thaliana*. *Frontiers in Plant Science*, 3(74). <https://doi.org/10.3389/fpls.2012.00074>
- Hazak, O., & Hardtke, C. S. (2016). CLAVATA 1-type receptors in plant development. *Journal of Experimental Botany*, 67(16), 4827–4833. <https://doi.org/10.1093/jxb/erw247>
- Hinchliffe, A., & Harwood, W. A. (2019). Agrobacterium-Mediated Transformation of Barley Immature Embryos. In *Barley: Methods in Molecular Biology* (Vol. 1900). Humana Press.
- Hirakawa, Y., Kondo, Y., & Fukuda, H. (2010). Regulation of Vascular Development by CLE Peptide-receptor Systems. *Journal of Integrative Plant Biology*, 52(1), 8–16. <https://doi.org/10.1111/j.1744-7909.2010.00904.x>

- Hirakawa, Y., Uchida, N., Yamaguchi, Y. L., Tabata, R., Ishida, S., Ishizaki, K., Nishihama, R., Kohchi, T., Sawa, S., & Bowman, J. L. (2019). Control of proliferation in the haploid meristem by CLE peptide signaling in *Marchantia polymorpha*. *PLoS Genetics*, *15*(3), e1007997.
- Hoad, S. (2019). *Cereal varieties: Summer 2019 update—Winter wheat, winter barley and spring barley*. *SRUC Cereal Variety Update*. Scotland's Rural College, CSS: Crop Improvement and Agronomy.
- Hochholdinger, F., & Zimmerman, R. (2008). Conserved and diverse mechanisms in root development. *Current Opinion in Plant Biology*, *11*(1), 70–74.
<https://doi.org/10.1016/j.pbi.2007.10.002>
- Horiguchi, G., & Tsukaya, H. (2011). Organ Size Regulation in Plants: Insights from Compensation. *Frontiers in Plant Science*, *2*. <https://doi.org/10.3389/fpls.2011.00024>
- Jha, P., Ochatt, S. J., & Kumar, V. (2020). WUSCHEL: a master regulator in plant growth signaling. *Plant Cell Reports*, 431–444. <https://doi.org/10.1007/s00299-020-02511-5>
- Ji, J., Strable, J., Shimizu, R., Koenig, D., Sinha, N., & Scanlon, M. J. (2010). WOX4 Promotes Procambial Development. *Plant Physiology*, *152*(3), 1346–1356.
<https://doi.org/10.1104/pp.109.149641>
- Jones, A. R., Band, L. R., & Murray, J. A. H. (2019). Double or Nothing? Cell Division and Cell Size Control. *Trends in Plant Science*, *24*(12), 1083–1093.
<https://doi.org/10.1016/j.tplants.2019.09.005>
- Jose, J., Ghantasala, S., & Choudhury, S. R. (2020). Arabidopsis Transmembrane Receptor-Like Kinases (RLKs): A Bridge between Extracellular Signal and Intracellular Regulatory Machinery. *International Journal of Molecular Sciences*, *21*(11), 4000.
<https://doi.org/10.3390/ijms21114000>
- Karimi, M., Inzé, D., & Depicker, A. (2002). GATEWAY vectors for *Agrobacterium*-mediated plant transformation. *Trends in Plant Science*, *7*(5), 193–195. [https://doi.org/10.1016/S1360-1385\(02\)02251-3](https://doi.org/10.1016/S1360-1385(02)02251-3)

- Kim, D., Paggi, J. M., Park, C., Bennett, C., & Salzberg, S. L. (2019). Graph-based genome alignment and genotyping with HISAT2 and HISAT-genotype. *Nature Biotechnology*, *37*, 907–915.
<https://doi.org/10.1038/s41587-019-0201-4>
- Kondo, Y. (2022). Competitive action between Brassinosteroid and tracheary element differentiation inhibitory factor in controlling xylem cell differentiation. *Plant Biotechnology*, *39*(1), 59–64.
<https://doi.org/10.5511/plantbiotechnology.21.1109a>
- Kondo, Y., & Fukuda, H. (2015). The TDIF signaling network. *Current Opinion in Plant Biology*, *28*, 106–110. <https://doi.org/10.1016/j.pbi.2015.10.002>
- Lawrenson, T., & Harwood, W. A. (2019). Creating Targeted Gene Knockouts in Barley Using CRISPR/Cas9. *Methods in Molecular Biology*, *1900*, 217–232. https://doi.org/10.1007/978-1-4939-8944-7_14
- Laxmi, M. (2016). *The Role of the PXY-CLE Signalling Pathway in Regulating Cell Division During Wood Formation in Poplar*.
<https://www.proquest.com/docview/2047442236?fromopenview=true&pq-origsite=gscholar>
- Leegood, R. C. (2008). Roles of the bundle sheath cells in leaves of C3 plants. *Journal of Experimental Botany*, *59*(7), 1663–1673. <https://doi.org/10.1093/jxb/erm335>
- Li, Q., Fu, C., Liang, C., Ni, X., Zhao, X., Chen, M., & Ou, L. (2022). Crop Lodging and The Roles of Lignin, Cellulose, and Hemicellulose in Lodging Resistance. *Agronomy*, *12*(8), 1795.
<https://doi.org/10.3390/agronomy12081795>
- Li, X., Ahmad, S., Guo, C., Yu, J., Cao, S., Gao, X., Li, W., Li, H., & Guo, Y. (2018). Identification and Characterization of LRR-RLK Family Genes in Potato Reveal Their Involvement in Peptide Signaling of Cell Fate Decisions and Biotic/Abiotic Stress Responses. *Cells*, *7*(9), 120.
<https://doi.org/10.3390/cells7090120>

- Liu, Z., Yang, N., Lv, Y., Pan, L., Lv, S., Han, H., & Guodong, W. (2016). The CLE gene family in *Populus trichocarpa*. *Plant Signalling & Behavior*, *11*(6).
<https://doi.org/10.1080/15592324.2016.1191734>
- Lopez, F. B., & Barclay, G. F. (2017). Plant Anatomy and Physiology. In *Pharmacognosy* (1st ed.). Academic Press.
- Love, M., Anders, S., & Huber, W. (2014). Moderated estimation of fold change and dispersion for RNA-seq data with DESeq2. *15*, 550. <https://doi.org/10.1186/s13059-014-0550-8>
- Mangan, S., & Alon, U. (2003). Structure and function of the feed-forward loop network motif. *Physical Sciences*, *100*(21), 11980–11985. <https://doi.org/10.1073/pnas.2133841100>
- Manghwar, H., Hussain, A., Ali, Q., & Liu, F. (2022). Brassinosteroids (BRs) Role in Plant Development and Coping with Different Stresses. *International Journal of Molecular Sciences*, *23*(3), 1012. <https://doi.org/10.3390/ijms23031012>
- McKim, S. M. (2020). Moving on up – controlling internode growth. *New Phytologist*, *226*(3), 672–678. <https://doi.org/10.1111/nph.16439>
- Miralles, D. J., Abeledo, L. G., Prado, S. A., Chenu, K., Serrago, R. A., & Savin, R. (2021). Chapter 4—Barley. In V. O. Sadras & D. F. Calderini (Eds.), *Crop Physiology Case Histories for Major Crops* (pp. 164–195). Academic Press. <https://doi.org/10.1016/B978-0-12-819194-1.00004-9>
- Mou, S., Zhang, X., Han, Z., Wang, J., Gong, X., & Chai, J. (2017). CLE42 binding induces PXL2 interaction with SERK2. *Protein & Cell*, *8*(8), 612–617. <https://doi.org/10.1007/s13238-017-0435-1>
- Nelissen, H., Gonzalez, N., & Inzé, D. (2016). Leaf growth in dicots and monocots: So different yet so alike. *Current Opinion in Plant Biology*, *33*, 72–76. <https://doi.org/10.1016/j.pbi.2016.06.009>
- Putri, G. H., Anders, S., Pyl, P. T., Pimanda, J. E., & Zanini, F. (2022). Analysing high-throughput sequencing data in Python with HTSeq 2.0. *Bioinformatics*, *38*(10), 2943–2945. <https://doi.org/10.1093/bioinformatics/btac166>

- Qiang, Y., Wu, J., Han, H., & Wang, G. (2013). CLE Peptides in Vascular Development. *Journal of Integrative Plant Biology*, *55*(4), 389–394. <https://doi.org/10.1111/jipb.12044>
- Rensing, S. A., Goffinet, B., Meyberg, R., Wu, S.-Z., & Bezanilla, M. (2020). The Moss *Physcomitrium* (*Physcomitrella*) patens: A Model Organism for Non-Seed Plants. *The Plant Cell*, *32*(5), 1361–1376. <https://doi.org/10.1105/tpc.19.00828>
- Roodt, D., Li, Z., Van de Peer, Y., & Mizrachi, E. (2019). Loss of Wood Formation Genes in Monocot Genomes. *Genome Biology and Evolution*, *11*(7), 1986–1996. <https://doi.org/10.1093/gbe/evz115>
- Rudall, P. J., & Bateman, R. M. (2004). Evolution of zygomorphy in monocot flowers: Iterative patterns and developmental constraints. *New Phytologist*, *162*(1), 25–44. <https://doi.org/10.1111/j.1469-8137.2004.01032.x>
- Sage, R. F. (2003). The evolution of C4 photosynthesis. *New Phytologist*, *161*(2), 341–370. <https://doi.org/10.1111/j.1469-8137.2004.00974.x>
- Sage, R. F. (2016). A portrait of the C4 photosynthetic family on the 50th anniversary of its discovery: Species number, evolutionary lineages, and Hall of Fame. *Journal of Experimental Botany*, *67*(14), 4039–4056. <https://doi.org/10.1093/jxb/erw156>
- Saito, M., Kondo, Y., & Fukuda, H. (2018). BES1 and BZR1 Redundantly Promote Phloem and Xylem Differentiation. *Plant and Cell Physiology*, *59*(3), 590–600. <https://doi.org/10.1093/pcp/pcy012>
- Scarpella, E., & Meijer, A. H. (2004). Pattern formation in the vascular system of monocot and dicot plant species. *New Phytologist*, *164*(2), 209–242. <https://doi.org/10.1111/j.1469-8137.2004.01191.x>
- Schliep, K. P. (2011). phangorn: Phylogenetic analysis in R. *Bioinformatics*, *27*(4), 592–593. <https://doi.org/10.1093/bioinformatics/btq706>
- Schreiber, M., Mascher, M., Wright, J., Padmarasu, S., Himmelbach, A., Heavens, D., Milne, L., Clavijo, B. J., Stein, N., & Waugh, R. (2020). A Genome Assembly of the Barley ‘Transformation

- Reference' Cultivar Golden Promise. *G3 Genes/Genomes/Genetics*, 10(6), 1823–1827.
<https://doi.org/10.1534/g3.119.401010>
- Setter, T. L., & Flannigan, B. A. (2001). Water deficit inhibits cell division and expression of transcripts involved in cell proliferation and endoreduplication in maize endosperm. *Journal of Experimental Botany*, 52(360), 1401–1408. <https://doi.org/10.1093/jexbot/52.360.1401>
- Shah, L., Yahya, M., Shah, S. M. A., Nadeem, M., Ali, A., Ali, A., Wang, J., Riaz, M. W., Rehman, S., Wu, W., Khan, R. M., Abbas, A., Riaz, A., Anis, G. B., Si, H., Jiang, H., & Ma, C. (2019). Improving Lodging Resistance: Using Wheat and Rice as Classical Examples. *International Journal of Molecular Sciences*, 20(17), 4211. <https://doi.org/10.3390/ijms20174211>
- Shen-Orr, S. S., Milo, R., Mangan, S., & Alon, U. (2002). Network motifs in the transcriptional regulation network of Escherichia coli. *Nature Genetics*, 31, 64–68.
<https://doi.org/10.1038/ng881>
- Sieburth, L. E. (2007). Plant development: PXY and polar cell division in the procambium. *Current Biology*, 17(15), R594-6. <https://doi.org/10.1016/j.cub.2007.05.066>
- Smit, M. E., McGregor, S. R., Sun, H., Gough, C., Bågman, A.-M., Soyars, C. L., Kroon, J. T., Gaudinier, A., Williams, C. J., Yang, X., Nimchuk, Z. L., Weijers, D., Turner, S. R., Brady, S. M., & Etchells, J. P. (2020). A PXY-Mediated Transcriptional Network Integrates Signaling Mechanisms to Control Vascular Development in Arabidopsis. *The Plant Cell*, 32(2), 319–335.
<https://doi.org/10.1105/tpc.19.00562>
- Spicer, R., & Groover, A. (2010). Evolution of development of vascular cambia and secondary growth. *New Phytologist*, 186(3), 577–592. <https://doi.org/10.1111/j.1469-8137.2010.03236.x>
- Stahl, Y., Wink, R. H., Ingram, G. C., & Simon, R. (2009). A signaling module controlling the stem cell niche in Arabidopsis root meristems. *Current Biology*, 19(11), 909–914.
<https://doi.org/10.1016/j.cub.2009.03.060>

- Suer, S., Agusti, J., Sanchez, P., Schwarz, M., & Greb, T. (2011). WOX4 Imparts Auxin Responsiveness to Cambium Cells in Arabidopsis. *The Plant Cell*, *23*(9), 3247–3259.
<https://doi.org/10.1105/tpc.111.087874>
- Sullivan, P., Arendt, E., & Gallagher, E. (2013). The increasing use of barley and barley by-products in the production of healthier baked goods. *Trends in Food Science & Technology*, *29*(2), 124–134. <https://doi.org/10.1016/j.tifs.2012.10.005>
- Takahashi, G., Betsuyaku, S., Okuzumi, N., Kiyosue, T., & Hirakawa, Y. (2021). An Evolutionarily Conserved Coreceptor Gene Is Essential for CLAVATA Signaling in *Marchantia polymorpha*. *Frontiers in Plant Science*, *12*, 1–12. <https://doi.org/10.3389/fpls.2021.657548>
- Taylor, N. G., Scheible, W.-R., Cutler, S., Somerville, C. R., & Turner, S. R. (1999). The irregular xylem3 Locus of Arabidopsis Encodes a Cellulose Synthase Required for Secondary Cell Wall Synthesis. *The Plant Cell*, *11*(5), 769–779. <https://doi.org/10.1105/tpc.11.5.769>
- Tilman, D., Balzer, C., Hill, J., & Befort, B. L. (2011). Global food demand and the sustainable intensification of agriculture. *Proceedings of the National Academy of Sciences*, *108*(50), 20260–20264. <https://doi.org/10.1073/pnas.1116437108>
- Uchida, N., & Tasaka, M. (2013). Regulation of plant vascular stem cells by endodermis-derived EPFL-family peptide hormones and phloem-expressed ERECTA-family receptor kinases. *Journal of Experimental Botany*, *64*(17), 5335–5343. <https://doi.org/10.1093/jxb/ert196>
- Wang, F., Yu, Z., Zhang, M., Wang, M., Lu, X., Liu, X., Li, Y., Zhang, X., Tan, B., Li, C., & Ding, Z. (2021). ZmTE1 promotes plant height by regulating intercalary meristem formation and internode cell elongation in maize. *Plant Biotechnology Journal*, *20*(3), 526–537.
<https://doi.org/10.1111/pbi.13734>
- Wang, G., Long, Y., Thomma, B. P. H. J., de Wit, P. J. G. M., Angenent, G. C., & Fiers, M. (2010). Functional Analyses of the CLAVATA2-Like Proteins and Their Domains That Contribute to CLAVATA2 Specificity. *Plant Physiology*, *152*(1), 320–331.
<https://doi.org/10.1104/pp.109.148197>

- Wang, L.-G., Lam, T. T.-Y., Xu, S., Dai, Z., Zhou, L., Feng, T., Guo, P., Dunn, C. W., Jones, B. R., Bradley, T., Zhu, H., Guan, Y., Jiang, Y., & Yu, G. (2020). Treeio: An R Package for Phylogenetic Tree Input and Output with Richly Annotated and Associated Data. *Molecular Biology and Evolution*, *37*(2), 599–603. <https://doi.org/10.1093/molbev/msz240>
- Wang, N., Bagdassarian, K. S., Doherty, R. E., Kroon, J. T., Connor, K. A., Wang, X. Y., Wang, W., Jermyn, I. H., Turner, S. R., & Etchells, J. P. (2019). Organ-specific genetic interactions between paralogues of the PXY and ER receptor kinases enforce radial patterning in *Arabidopsis* vascular tissue. *Development*, *146*(10), dev177105. <https://doi.org/10.1242/dev.177105>
- Whitewoods, C. (2021). Evolution of CLE peptide signalling. *Seminars in Cell & Developmental Biology*, *109*, 12–19. <https://doi.org/10.1016/j.semcd.2020.04.022>
- Whitewoods, C. D., Cammarata, J., Venza, Z. N., Sang, S., Crook, A. D., Aoyama, T., Wang, X. Y., Waller, M., Kamisugi, Y., Cuming, A. C., Szövényi, P., Nimchuk, Z. L., Roeder, A. H. K., Scanlon, M. J., & Harrison, C. J. (2018). CLAVATA Was a Genetic Novelty for the Morphological Innovation of 3D Growth in Land Plants. *Current Biology*, *28*(15), 2365-2376.E5. <https://doi.org/10.1016/j.cub.2018.05.068>
- Wilkinson, L. (2011). ggplot2: Elegant Graphics for Data Analysis by WICKHAM, H. *Biometrics*, *67*(2), 678–679. <https://doi.org/10.1111/j.1541-0420.2011.01616.x>
- Wolfe, K. H., Gouy, M., Yang, Y. W., Sharp, P. M., & Li, W. H. (1989). Date of the monocot-dicot divergence estimated from chloroplast DNA sequence data. *Proceedings of the National Academy of Sciences*, *86*(16), 6201–6205. <https://doi.org/10.1073/pnas.86.16.6201>
- Wu, G., Tian, N., She, F., Cao, A., Wu, W., Zheng, S., & Yang, N. (2022). Characteristics analysis of Early Responsive to Dehydration genes in *Arabidopsis thaliana* (AtERD). *Plant Signalling & Behavior*, *18*(1), 2105021. <https://doi.org/10.1080/15592324.2022.2105021>

- Wunderling, A., Targem, M. B., de Reuille, P. B., & Ragni, L. (2017). Novel tools for quantifying secondary growth. *Journal of Experimental Botany*, *68*, 89–95.
<https://doi.org/10.1093/jxb/erw450>
- Xu, N., Meng, L., Tang, F., Du, S., Xu, Y., Kuang, S., Lv, Y., Song, W., Li, Y., Qi, W., & Zhang, Y. (2023). Plant Spacing Effects on Stem Development and Secondary Growth in *Nicotiana tabacum*. *Agronomy*, *13*(8), 2142. <https://doi.org/10.3390/agronomy13082142>
- Yaginuma, H., Hirakawa, Y., Kondo, Y., Ohashi-Ito, K., & Fukuda, H. (2011). A Novel Function of TDIF-Related Peptides: Promotion of Axillary Bud Formation. *Plant and Cell Physiology*, *52*(8), 1354–1364. <https://doi.org/10.1093/pcp/pcr081>
- Yamaguchi, Y. L., Ishida, T., Yoshimura, M., Imamura, Y., Shimaoka, C., & Sawa, S. (2017). A Collection of Mutants for CLE-Peptide-Encoding Genes in Arabidopsis Generated by CRISPR/Cas9-Mediated Gene Targeting. *Plant and Cell Physiology*, *58*(11), 1848–1856.
<https://doi.org/10.1093/pcp/pcx139>
- Yang, J. H., Lee, K.-H., Du, Q., Yang, S., Yuan, B., Qi, L., & Wang, H. (2019). A membrane-associated NAC domain transcription factor XVP interacts with TDIF co-receptor and regulates vascular meristem activity. *New Phytologist*, *226*(1), 59–74. <https://doi.org/10.1111/nph.16289>
- Young, M. (n.d.). Gene Ontology analyser for RNA-seq and other length biased data. *Bioconductor*.
<https://doi.org/doi:10.18129/B9.bioc.goseq>
- Yu, G., Smith, D. K., Zhu, H., Guan, Y., & Lam, T. T.-Y. (2016). ggtree: An r package for visualization and annotation of phylogenetic trees with their covariates and other associated data. *Methods in Ecology and Evolution*, *8*(1), 28–36. <https://doi.org/10.1111/2041-210X.12628>
- Yu, Y., Song, W., Zhai, N., Zhang, S., Wang, J., Wang, S., Liu, W., Huang, C.-H., Ma, H., Chai, J., & Chang, F. (2023). PXL1 and SERKs act as receptor–coreceptor complexes for the CLE19 peptide to regulate pollen development. *Nature Communications*, *14*. <https://doi.org/10.1038/s41467-023-39074-4>

- Yu, Z., Zhang, D., Xu, Y., Jin, S., Zhang, L., Zhang, S., Yang, G., Huang, J., Yan, K., Wu, C., & Zheng, C. (2019). CEPR2 phosphorylates and accelerates the degradation of PYR/PYLs in Arabidopsis. *Journal of Experimental Botany*, *70*(19), 5457–5469. <https://doi.org/10.1093/jxb/erz302>
- Yuan, F., Yang, H., Xue, Y., Kong, D., Ye, R., Li, C., Zhang, J., Theprungsirikul, L., Shrift, T., Krichilsky, B., Johnson, D. M., Swift, G. B., He, Y., Siedow, J. N., & Pei, Z.-M. (2014). OSCA1 mediates osmotic-stress-evoked Ca²⁺ increases vital for osmosensing in Arabidopsis. *Nature*, *514*, 367–371. <https://doi.org/10.1038/nature13593>
- Zhang, H., Lin, X., Han, Z., Qu, L.-J., & Chai, J. (2016). Crystal structure of PXY-TDIF complex reveals a conserved recognition mechanism among CLE peptide-receptor pairs. *Cell Research*, *26*, 543–555. <https://doi.org/10.1038/cr.2016.45>
- Zhang, H., Lin, X., Han, Z., Wang, J., Qu, L.-J., & Chai, J. (2016). SERK Family Receptor-like Kinases Function as Co-receptors with PXY for Plant Vascular Development. *Molecular Plant*, *9*(10), 1406–1414. <http://dx.doi.org/10.1016/j.molp.2016.07.004>
- Zhang, J., Serra, J. A. A., & Helariutta, Y. (2015). Wood development: Growth through knowledge. *Nature Plants*, *1*, 15060. <https://doi.org/10.1038/nplants.2015.60>
- Zhang, S., Hu, W., Wang, L., Lin, C., Cong, B., Sun, C., & Luo, D. (2005). TFL1/CEN-like genes control intercalary meristem activity and phase transition in rice. *Plant Science*, *168*(6), 1393–1408. <https://doi.org/10.1016/j.plantsci.2004.10.022>
- Zhang, Y., Wang, C., Wang, C., Yun, L., Song, L., Idrees, M., Liu, H., Zhang, Q., Yang, J., Zheng, X., Zhang, Z., & Gao, J. (2022). OsHsfB4b Confers Enhanced Drought Tolerance in Transgenic Arabidopsis and Rice. *International Journal of Molecular Sciences*, *23*(18), 10830. <https://doi.org/10.3390/ijms231810830>
- Zhou, M. (2010). *Genetics and Improvement of Barley Malt Quality* (G. Zhang & C. Li, Eds.). Springer Berlin Heidelberg. <https://doi.org/10.1007/978-3-642-01279-2>

Zinkgraf, M., Gerttula, S., & Groover, A. (2017). Transcript profiling of a novel plant meristem, the monocot cambium. *Journal of Integrative Plant Biology*, 59(6), 436–449.

<https://doi.org/10.1111/jipb.12538>